INVESTIGATING THE ROLES OF HLA-DO IN THE IMMUNE RESPONSE IN HUMANS AND MICE

By

AUSTIN M. GRAVES

A dissertation submitted to the

School of Graduate Studies

Rutgers, the State University of New Jersey

In partial fulfillment of the requirements

For the degree of

Doctor of Philosophy

Graduate Program in Microbiology and Molecular Genetics

Written under the direction of

Lisa Denzin

And approved by

_____

_____

_____

_____

New Brunswick, New Jersey

January 2021

ABSTRACT OF THE DISSERTATION

Investigating the Roles of HLA-DO in the Immune Response in Humans and Mice

by AUSTIN M. GRAVES

Dissertation Director:

Lisa Denzin

The MHC class II antigen presentation pathway acts as a bridge between the innate and adaptive immune responses. HLA molecules of the MHC class II (MHCII) bind and present pathogen-derived peptides for CD4 T cell activation. Peptide loading of MHCII in the endosomes of cells is controlled by the interplay of the nonclassical MHCII molecules, HLA-DM (DM) and HLA-DO (DO). DM catalyzes peptide loading, whereas DO, an MHCII substrate mimic, prevents DM from interacting with MHCII, resulting in an altered MHCII-peptide repertoire and increased MHCII-CLIP. Previous studies from our lab revealed that the mouse homolog of DO, H2-O, blocks a neutralizing antibody response to a retrovirus. We investigated the effect of H2-O deficiency on immune function in mice. Interestingly, we found an increase in immune cell activation in the small intestines of H2-O deficient mice. These changes appeared to dissipate as the mice aged. Our previous study also found naturally occurring variants of the gene that encodes the beta chain of DO, *DOB*, that altered DO function. A more functional variant of *DOB* was linked to individuals who struggle to neutralize Hepatitis C virus. We have now analyzed naturally occurring variants of the gene

that encodes the alpha chain of DO, *DOA*, and found several with altered function. In fact, 52% of the variants analyzed altered DO function, two of which were linked to Hepatitis B viral immune responses. A more functional variant, *DOA*0102*, was linked to Hepatitis B viral persistence. A functionally null variant, DOα F114L, was conversely linked to Hepatitis B viral clearance. Further characterization of the gain-of-function variants identified in this study suggests that the mechanism of DO's inhibitory function of DM is more complex than previously understood. DO binding to DM may permanently alter DM's functional capability, even if DO is no longer bound to DM.

ACKNOWLEDGEMENTS

This dissertation represents original work performed by Austin Graves. The dissertation has been adapted from the following manuscripts:

Graves AM, Virdis F, Morrison E, Alvaro-Benito M, Khan AA, Freund C, Golovkina TV, and Denzin LK. Human Hepatitis B Viral Infection Outcomes Are Linked to Naturally Occurring Variants of *HLA-DOA* That Have Altered Function. *The Journal of Immunology*. July 20, 2020.

My experience as a graduate student at Rutgers has been extremely challenging and enriching both in and out of the lab. This dissertation is the culmination of all that I have accomplished in my life thus far, but I certainly did not accomplish this on my own. Every step of the way, I have had others who supported and challenged me. This is their accomplishment just as much as it is mine.

I first have to thank my mentor, Dr. Lisa Denzin. When I came to Rutgers, I was dead set on studying non-coding RNAs. Unfortunately (or I suppose, in hindsight, fortunately), I was not able to find a lab in that field that was a good fit for me. Armed with little to no immunology experience, I asked Lisa if I could rotate with her in the spring of 2016. I am very grateful to her for taking me in as her student and being so supportive of me as a burgeoning scientist. Lisa has always pushed me to think very critically about each experiment I performed, and

never hesitated to be tough when necessary if I became complacent. I will take all of her many lessons with me as I continue my scientific career.

I next have to acknowledge the other members of the Denzin/Sant'Angelo labs, to whom I am so grateful for welcoming me into their lab and fostering my growth as a scientist and as a person. Derek has provided invaluable feedback and guidance in lab meeting and for that I am grateful. Josh taught me everything I know about flow cytometry and without his help, I would not be near the scientist I am now. Lou is the most dependable and considerate person I have ever had the pleasure of working with. I was extremely spoiled to have him as a lab manager and will miss having him as a coworker. Without him, this lab would grind to a screeching halt.

Then there are my fellow graduate students, Victor Tan, Brandon Schweibenz, Jenna Newman, Eve Reilly, Agata Krzyzanowska, Larry Chang, Vrushank Bhatt, Vaidhy Mahaganapathy, and Christen Attia. From discussions in first year fundamentals, to arguing in the library about prelim papers, to our periodic dinners together, to our virtual game nights, they all have been there as a source of support and guidance. I will miss each and every one of them, and hope that someday I can return to New Brunswick to properly celebrate this achievement with them when the time is right.

I also must express my gratitude to the other mentors that I had on my way through high school and college. In particular I want to acknowledge Dr. Ashton Powell at the North Carolina School of Science and Mathematics, and Dr. Susan Carson at North Carolina State University. I took several biology courses

from Dr. Powell at NCSSM, and through his course and conversations with him I formed a greater appreciation for the biological sciences, and for the proper ethics involved when doing science. I spent a lot of time as a nervous 17 year old speaking getting advice from him about planning for my future, and his friendship and guidance were appreciated. Dr. Susan Carson helped to guide me through my first ever true research experience. When I entered the Phage Hunters course at NC State, my plan was still to go to medical school after college. The experience gained in this course, and the opportunity to present our class' finding at the annual SEA-PHAGES symposium sparked my passion for academic research. Dr. Carson had a large role in my success in that course and continued to be a source of support and guidance long after the class had ended.

I would also like to acknowledge NCSSM as a whole. It is hard for me to think about the mental state I was in when I first moved onto my hall at 16 years old. I was deeply depressed and could not see a way out while attending the high school in my hometown. My 2 years at NCSSM were a struggle compared to where I had come from, and there were many instances in which I thought I could not make it. Thankfully, there were many resources available to me that kept me on track and moving forward. One in particular was my counselor, Lori Hackney, who provided much needed support when I was at my lowest. NCSSM probably saved my life, but it definitely changed my life in so many ways. It taught me how to learn from my mistakes and shortcomings, to accept failure and grow because of it. It gave me a sense of self-worth, and lifelong

friendships. Most importantly, it is where I met the love of my life. For all of this, I am forever grateful.

Next, I have to thank my family. I was extremely fortunate to have grown up with a loving and nurturing family. I have many cherished memories with my grandmothers, LaDona and Ruth. I am also grateful to thank grandfather, Harley, for allowing me to work for a summer on his farm, which was instrumental in teaching me the value of hard work. I must also mention my sister, Kayli, whose selflessness and compassion are an inspiration. Then there are my parents, Randy and Sondra Graves. All my parents ever wanted from me was my best. They did not put pressure on to be something I did not want to be or push me in a direction of study that I did not want to go. In fact, I would say that they frequently temper the lofty expectations that I had set for myself. I am so grateful to them for all of their love, support, and encouragement from the very beginning.

Finally, I am so grateful to my dear wife Christy. Through our time together in high school, college, and now graduate school, she has always encouraged, supported, and inspired me. Graduate school was, at times, exhausting and discouraging, and I would struggle to pull myself out of the mental ruts I would find myself in. She was always a ray of light to help pull me out of these slumps. Her belief in me has never wavered, especially when I did not believe in myself. This dissertation is dedicated to her.

TABLE OF CONTENTS

TABLE OF FIGURES

TABLE OF TABLES

CHAPTER 1: INTRODUCTION

Innate vs. Adaptive Immunity

Innate immunity is a feature of the majority of multicellular organisms that acts as a general defense against pathogens. This type of immunity consists of a series of physical barriers, secretions of antimicrobial compounds, and membrane bound or cytoplasmic receptors that recognize pathogen associated molecular patterns (PAMPs) expressed on the surface of, or within invading microbes. While these mechanisms are quite effective at dealing with a plethora of challenges, many microbes have evolved ways of evading the innate immune system and infecting the host. Clearing such an infection requires a much more robust and specific response, a feature offered by the adaptive immune system.

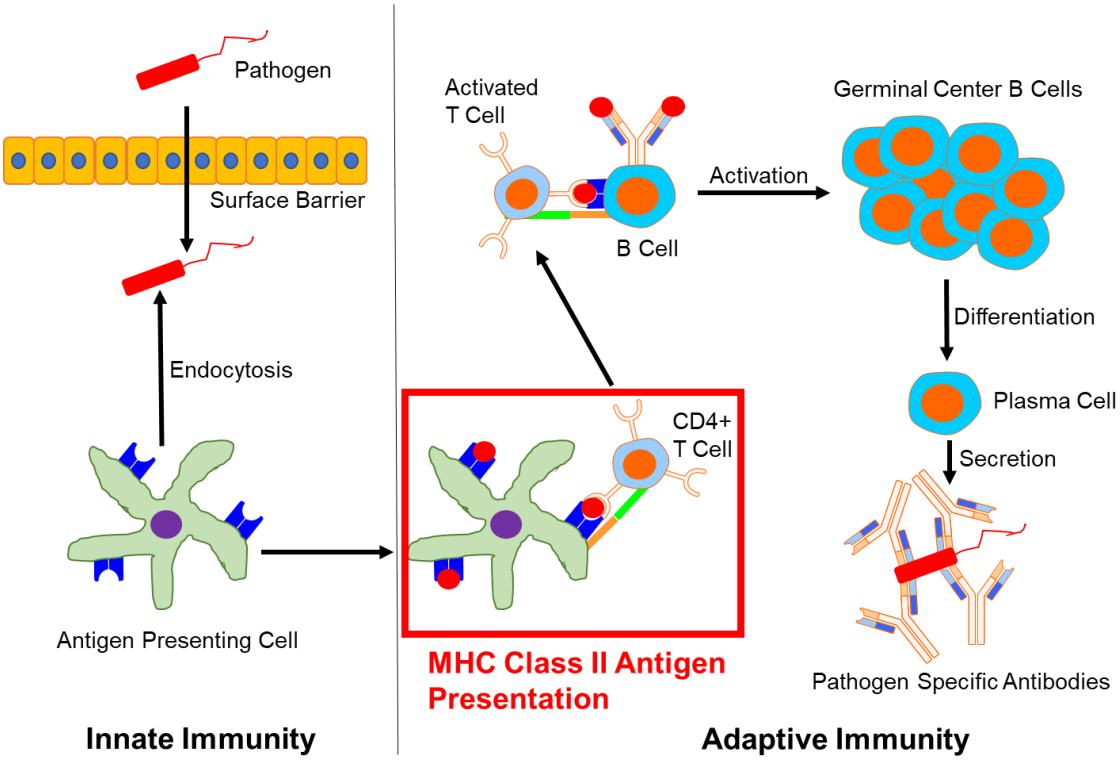

Figure 1.1 MHC class II antigen presentation bridges the innate and adaptive immune responses. An invading organism is met by an antigen presenting cell

which endocytoses and presents pieces of said organism to antigen specific CD4+ T cells. Activated T cells then traffic to secondary lymphoid tissues where they help activate antigen specific B cells. These activated B cells form germinal centers, which differentiate into plasma cells which secrete antigen specific antibodies. Antibody-coated pathogen is eliminated from the body.

Antigen presentation is a process that acts as a bridge from the innate to the adaptive immune response (Fig. 1.1). Specialized cells known as antigen presenting cells (APCs) act in an innate fashion by using their innate immune receptors to detect foreign entities and endocytose either whole, parts, or by products of the invading organism (antigens). These antigens are further processed and presented on the surface of APCs by either major histocompatibility complex (MHC) class I or MHC class II, which activates CD8+ and CD4+ T lymphocytes, respectively. The activated T cells go on to generate an adaptive immune response by activating other lymphocytes, secreting cytokines that recruit more immune cells, or directly killing pathogen infected cells. Activated CD4+ T cells assist B lymphocytes in their activation and differentiation into germinal centers. It is in these germinal centers that CD4+ T follicular helper cells assist germinal center B cells in further differentiating into plasma cells, which secrete high affinity, antigen specific antibodies. These antibodies are necessary for neutralization and clearance of pathogens[1].

Deficiencies in antigen presentation are the cause of a type of immunodeficiency known as bare lymphocyte syndrome (BLS). BLS type II is recessive genetic disorder caused by a disruption in the transcription factors that regulate expression of the MHC class II genes, and patients with the disease experience chronic respiratory and gastrointestinal infections. The only

treatment for this form of BLS is blood transplantation, and individuals who do not receive treatment do not survive early childhood[2]. In addition, polymorphisms in the MHCII genes have been well documented in their association with infectious and autoimmune diseases. For example, variants of MHC class II have been identified as risk factors for the development of autoimmune disorders like type 1 diabetes[3]. Furthermore, the progression of these diseases has been traced back to the presentation of self-antigen by MHCII[4, 5]. MHCII presentation is also known to be important for anti-tumor immunity. In fact, mutant peptides which do not bind well to MHCII are positively selected for during tumorigenesis[6]. Studies like these accentuate the need for a more complete understanding of the MHC class II antigen presentation pathway, and the potential for harnessing it in the future to improve the prognosis of these conditions.

MHC Class II Antigen Presentation

MHC class II antigen presentation is the process by which extracellular antigens are endocytosed by specialized cells called antigen presenting cells (APCs), degraded into short peptides, and presented on the cell membrane for recognition by other immune cells (Fig. 1.2)[7]. Early studies of transplantation biology and graft rejection between different inbred strains of mice led to the discovery of the MHC, which was dubbed the histocompatibility-2 (H-2) locus in mice[8, 9, 10]. Mixed leukocyte cultures[11] performed with human blood samples led to the discovery of the human MHC, dubbed the human leukocyte antigen (HLA) locus[10, 12, 13]. The mouse H-2 complex was later determined to have a role in controlling specific antibody responses[14, 15] and cooperation between T and B

lymphocytes[16]. Furthermore, recognition of antigen by CD4+ T cells was found to require processing and presentation of antigen by macrophages[17]. The HLA class II molecules exist in three different forms known as, HLA-DP, HLA-DQ, and HLA-DR[18]. Each of these molecules are expressed on the surface of antigen presenting cells, and each are highly polymorphic[19]. Each protein is encoded by at least two genes, which code for α and β chain proteins. For example, HLA-DP is encoded by *HLA-DPA1* and *HLA-DPB1*, but HLA-DQ is expressed as a combination of *HLA-DQA1* and *HLA-DQB1* or *HLA-DQA2* and *HLA-DQB2*[18, 19]. This feature results in an increased variability in the expression of these proteins, which greatly widens the breadth of peptides that these molecules can bind to and present.

MHC class II assembles as an obligate $\alpha\beta$ heterodimer in the endoplasmic reticulum (ER) bound to invariant chain (Ii). Ii binds to MHCII in the peptide binding groove which keeps the complex stable as it is trafficked out of the ER. The MHCII-Ii complex is trafficked through the trans-Golgi network to the plasma membrane, and then moved to the late endo/lysosomes via targeting motifs contained within the cytoplasmic tail of Ii. The late endosome compartments are very acidic and are inhabited by proteases, an environment necessary for degradation of antigen into antigen-derived peptide[20, 21]. These proteases cleave Ii into class II-associated invariant chain peptides (CLIP) through stepwise proteolysis, which is later removed via interaction with HLA-DM (DM)[22, 23]. DM is a non-classical MHC class II-like molecule that is synthesized and assembled as an obligate heterodimer of DMα and DMβ. DM binds to MHCII in the late

endosomes and lysosomes and releases CLIP, which allows MHC class II to bind to short peptides generated from degraded antigen (Fig. 1.2). As stated above, MHCII is unstable when not bound by peptide, so DM stays bound to MHCII until it is bound by its peptide. DM also edits during peptide loading and ensures that MHCII binds to higher affinity peptides, a process known as DM mediated peptide editing[24]. Once MHCII is bound to peptide, the complex is then trafficked to the plasma membrane for potential recognition by CD4+ T cells[7]. Much evidence has accumulated that this process is influenced by another MHCII-like molecule, HLA-DO.

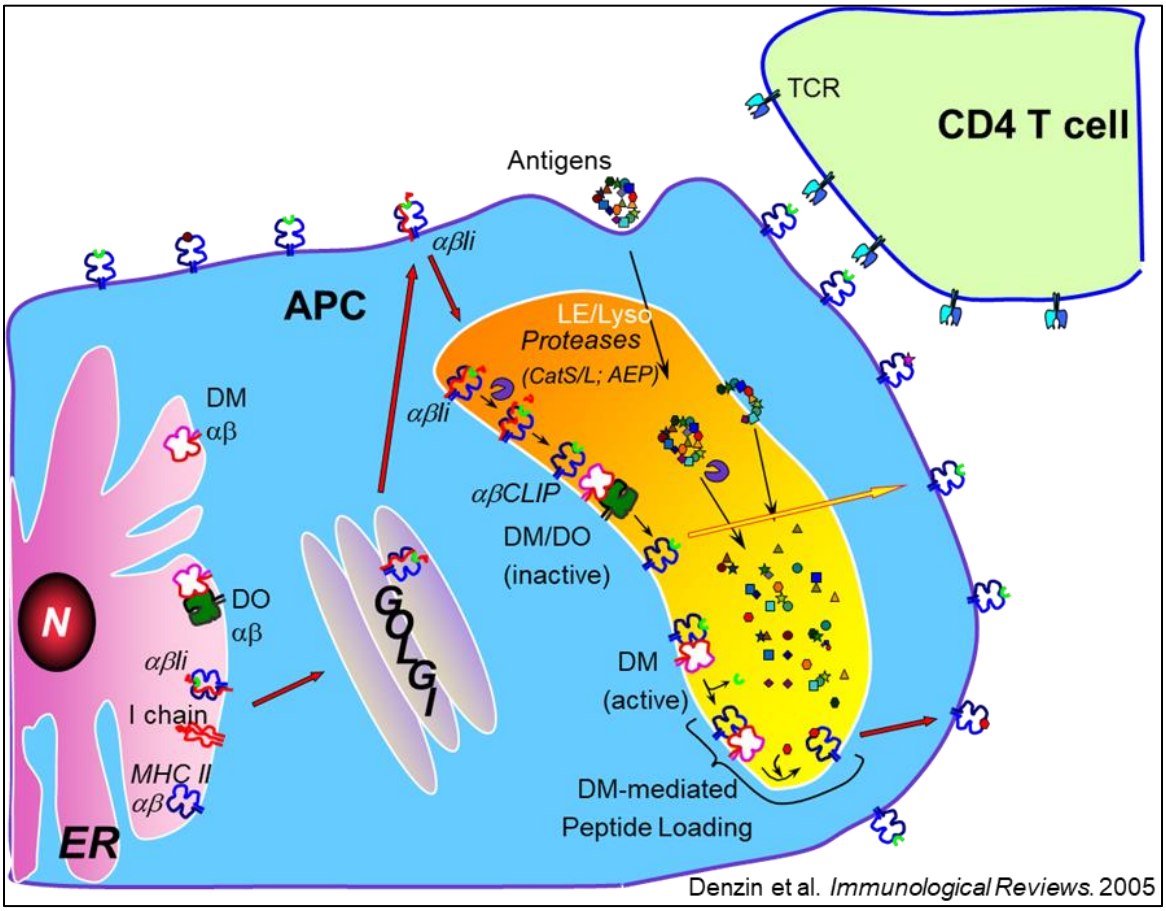

Figure 1.2 Overview of MHC class II antigen presentation. MHCII assembles in the endoplasmic reticulum (ER) bound to invariant chain (Ii). MHCII-Ii moves

through the trans-Golgi network to the cell surface, and then the late endosome/lysosome. Ii is cleaved into CLIP by proteases, and CLIP is removed from the MHCII binding groove via DM binding. DM ensures MHCII stability while MHCII is loaded with a high affinity antigen derived peptide. MHCII-peptide complex is then trafficked to the cell surface. DO binds to DM in the ER and inhibits DM from binding to MHCII.

HLA-DO

HLA-DO (DO) is a non-classical MHCII-like molecule which is known to modulate MHCII antigen presentation in APCs[25, 26, 27]. DO is encoded by two separate genes, *HLA-DOA* and *HLA-DOB*, which code for an α and a β chain. *HLA-DOA* was the first of these two genes to be described[28, 29], and *HLA-DOB* was identified a short time later[30]. The mouse homolog of HLA-DO, H2-O, was later identified and found to be expressed in B cells and thymic medullary epithelial cells[31], and DO expression in dendritic cells was later confirmed[32]. Expression of the genes in the HLA region is controlled by the transcription factor, Class II Transactivator (CIITA)[33]. While the expression of *HLA-DOA* is indeed controlled by CIITA activity, *HLA-DOB* expression is not[34]. Although expression of *DOB* is known to be enhanced by CIITA activity[35]. DO expression in B cells begins as B cells leave the bone marrow as immature transitional B cells and continues in mature B cells[36, 37]. DO expression levels in dendritic cells (DCs) has been shown to be variable between different subsets of DCs[32, 38]. DO expression in these cells is now known to fluctuate as these cells become activated. DO expression is downregulated as B cells differentiate into germinal center B cells[39], and dendritic cells downregulate DO expression upon activation[40].

DO assembles as a DOα and DOβ obligate heterodimer. DO binds to DM as a competitive inhibitor that is structurally similar to MHC class II, and thus DO mimics MHC class II when inhibiting DM[22] (Fig 1.3). DO is synthesized and assembled in the ER with its binding partner, DM, and the two are transported to endosomes (Fig. 1.2). DO is unable to traffic out of the ER on its own and requires interaction with DM to exit the ER. The cytoplasmic tail of DM contains a targeting sequence for trafficking to the late endosomes, and DM traffics to the endosomes either alone, or bound to DO[41]. Interestingly, the cytoplasmic tail of DOβ also contains a dileucine motif that may be used for targeting. In fact, adding the DOβ dileucine motif to CD8, a protein that does not normally traffic to the lysosome, is sufficient to target CD8 to the lysosome[42]. This indicates that the DO heterodimer should be able to traffic out of the ER, but it does not. DO's inability to traffic on its own is due to instability in the MHCII-like domain of DO caused by a proline at amino acid position 11 in DOα[43]. Mutating this proline residue to a valine resulted in a DO heterodimer that successfully trafficked out of the ER without DM interaction. DM:DO interactions are known to be influenced by pH, and while the DM:DO complex does not easily dissociate, DO has been shown to be destabilized and degraded at lower pH found in the late endo/lysosome compartments[44].

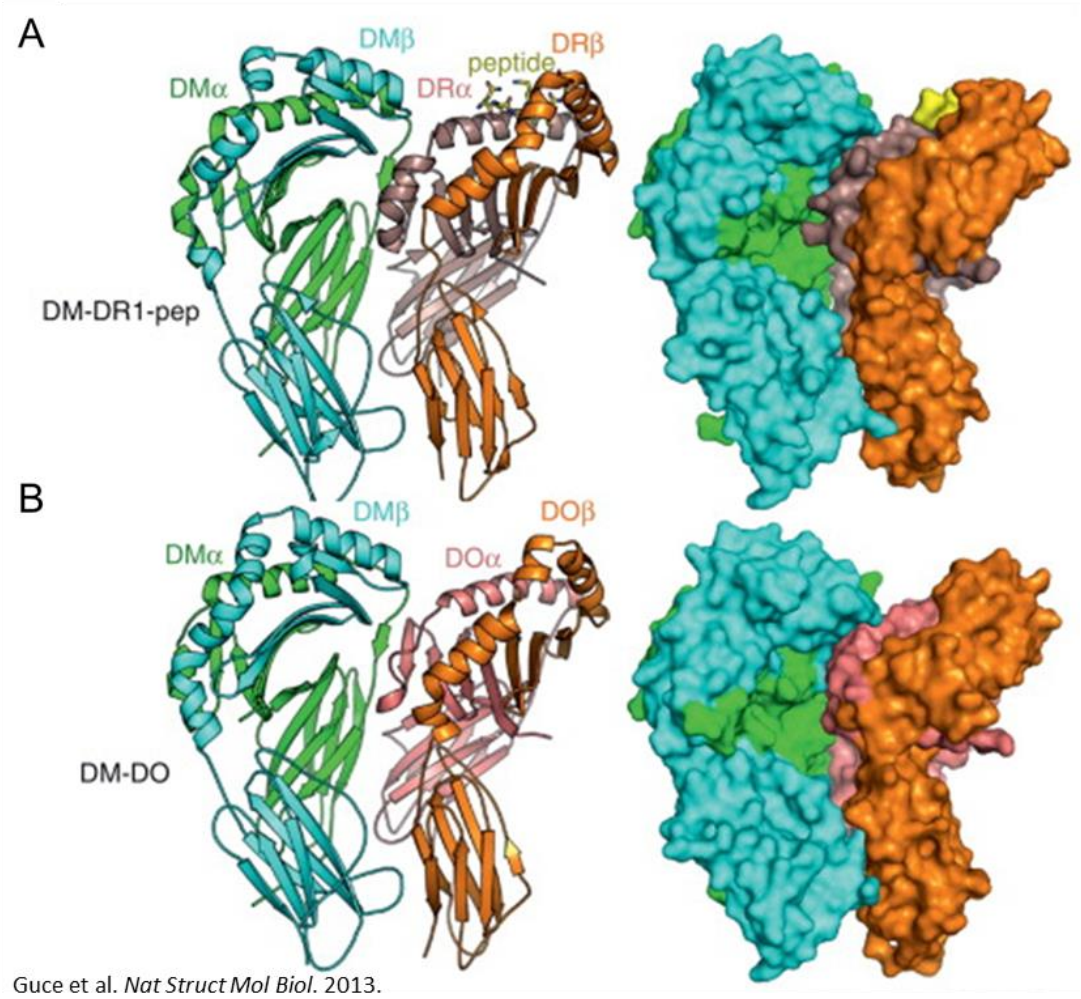

Figure 1.3 HLA-DO binds to HLA-DM as a substrate mimic. **(A)** Crystal structure of HLA-DM bound to the MHCII molecule HLA-DR1. **(B)** Crystal structure of HLA-DM bound to HLA-DO.

One of the key unanswered questions in the study of DO is, why is an inhibitor of DM mediated peptide loading necessary for proper immune function? Numerous studies have demonstrated the effect that DO expression has on the peptide repertoire on the surface of APCs. Mass spectrometric analysis of the peptide repertoire of DO/H2-O deficient and sufficient APCs revealed that the pool of peptides found on the surface of DO/H2-O expressing cells is slightly

larger than that of cells without DO/H2-O[27] (Fig. 1.4). It is possible that peptides only found on DO/H2-O expressing cells are peptides with lower affinity for MHCII, and would be edited out of the repertoire by DM/H2-M. This idea is supported by the finding that MHCII complexes loaded in the absence of H2-M are less stable than those loaded in the presence of H2-M[45]. Additionally, most peptides presented on the surface of resting APCs are self-peptides[26]. DO activity may be expanding the peptide repertoire to lower affinity self-peptides which further promotes self-tolerance. DO has been shown to have implications for autoimmunity, as our lab previously published a study in which NOD mice, which are predisposed to development of type 1 diabetes (T1D), do not develop the disease if DO is overexpressed in dendritic cells[46]. Pathogenic CD4+ T cell activation was reduced as a result of DO expression in NOD dendritic cells, indicating that DO altered the peptide repertoire away from the T1D generating peptide(s). Our lab is currently investigating the connection between DO and T1D by screening alleles of DO from T1D patients. Other groups have shown that while deficiencies in DO are not sufficient to cause autoimmunity, mouse studies suggest that loss of H2-O leads to increased antibodies to self-antigens[47].

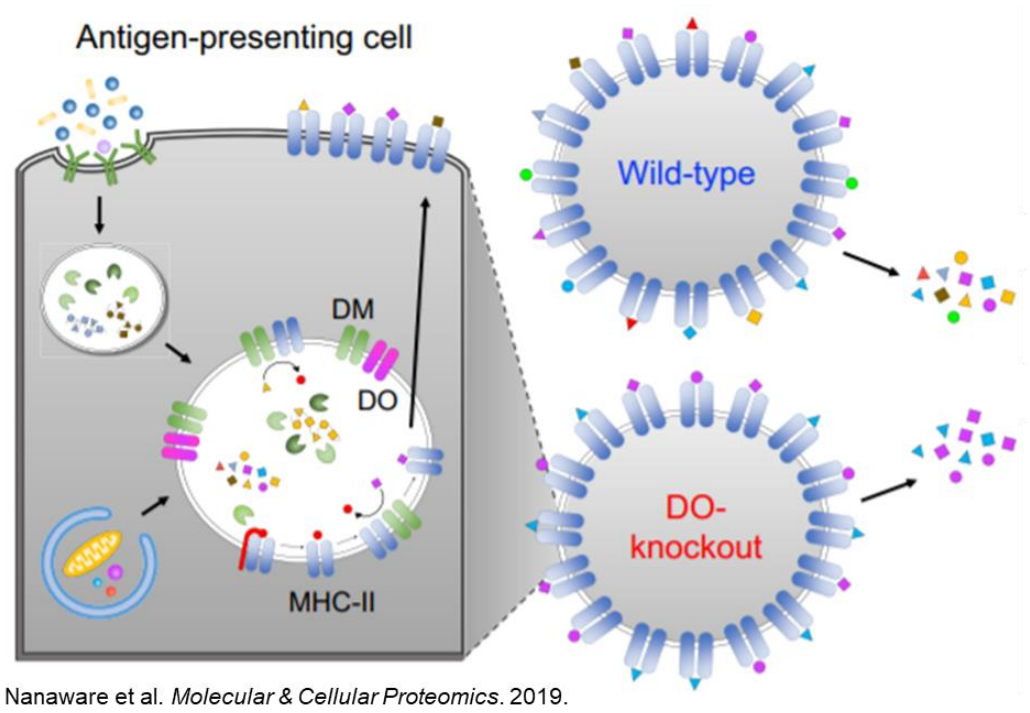

Figure 1.4 HLA-DO expression results in a more diverse repertoire of peptides on the surface of antigen presenting cells. Mass spectrometric analysis of peptides isolated from the surface of DO deficient and sufficient antigen presenting cells showed a broader pool of peptides isolated from DO sufficient cells.

H2-O and Mouse Mammary Tumor Virus

Mouse mammary tumor virus (MMTV) is an endogenous murine retrovirus that infects dendritic cells, B cells, and mammary cells where it induces tumor formation. Upon integration, MMTV expresses a superantigen that is expressed on the cell surface, binds to MHC class II, and induces a strong T cell-dependent response that leads to further B cell activation and proliferation. In B6 mice, this superantigen activates CD4+ T cells which express either TCR Vβ6 or Vβ14, but since this response is non-specific, it protects the virus from the generation of a viral-specific antibody response. This non-specific immune response aids in viral replication as the infected host cells rapidly proliferate. In addition, the

continuous T cell stimulation results in rapid expansion of reactive T cells which eventually die off. This leaves a hole in the T cell population that further protects MMTV from an immune response. As the host essentially ignores the viral infection, the virus is eventually able to transmit to pups through milk secretions from the mammary glands[48].

It was discovered that the I/LnJ mouse strain displays an unusual response after infection with MMTV[49, 50, 51, 52]. In the majority of mouse strains, MMTV does not illicit a neutralizing antibody response[49, 50]. However, I/LnJ mice generate a neutralizing antibody response to MMTV due to a recessive mutation. The recessive mutation was mapped to a region of Chromosome 17 containing the MHC genes and was given the name virus infectivity controller 1 (*vic1*)[49, 52]. The identity of *vic1* was narrowed down by cloning pieces of the I/LnJ MHC locus into B6 mice and checking for MMTV susceptibility. These studies eventually led the investigators to a region containing the full sequence of the gene encoding the β chain of H2-O, *H2-Ob*. Whole genome sequencing of I/LnJ, BALBc/J, and C3H/HeN mice revealed several mutations in I/LnJ Ob compared to the two MMTV susceptible mouse strains[53]. Four of these mutations lead to amino acid substitutions, S154N, V174I, and L193H located in the immunoglobulin domain, and E265K located in the cytoplasmic tail. Investigations into each of these mutations has found that all three mutations in the immunoglobulin domain are necessary to copy the phenotype of I/LnJ mice. In fact, these same three mutations in the immunoglobulin domain were found in the *H2-Ob* gene of CAST/EiJ mice. Mutant Ob in I/LnJ mice has been determined to be functionally

null. Deletion of either *H2-Oa* or *H2-Ob* in B6 mice showed reduced MHCII-CLIP expression on APCs, and generated neutralizing antibody responses to MMTV. What remains unclear is how I/LnJ is null, as it has been shown to successfully associate with H2-M[53].

The following works constitute an effort to better understand the role of DO in the immune response in both mice and humans. We identified naturally occurring variants of *HLA-DOA* with altered function and were able to link these altered functions to human disease phenotypes. In studying these variants function, we have potentially identified a new mechanism for how DO inhibits DM activity. We also investigated the role of mouse H2-O in the innate immune system. This included characterizing H2-O regulation in response to TLR7 stimulation, as well as the innate immune response of H2-O deficient B cells. Finally, we characterized the intestinal immune landscape of H2-O deficient mice and how it changes in response to MMTV infection.

CHAPTER 2: HUMAN HEPATITS B VIRAL OUTCOMES ARE LINKED TO NATURALLY OCCURRING VARIANTS OF HLA-DOA THAT HAVE ALTERED FUNCTION

Introduction

A previous study published by our lab found that I/LnJ mice are able to mount a neutralizing antibody response to MMTV due to a functionally null variant of *H2-Ob*, the gene encoding the β chain of H2-O. This finding led us to investigate the presence of naturally occurring variants of *HLA-DOA* and *HLA-DOB* with the potential to alter DO protein function[53]. We searched the Exome

Aggregation Consortium database[54] and identified several naturally occurring variants of *HLA-DOA* and *HLA-DOB* with potentially interesting phenotypes. Our previous study analyzed the naturally occurring variants of *HLA-DOB* selected for further analysis[53]. Functional analysis of these *DOB* variants identified several which altered DO function. In particular, we identified a variant of *DOB* (DOβ G77V) which resulted in a more functional form of DO protein. This variant was found to be linked to individuals with chronic Hepatitis C infection. Following this study, we turned to the naturally occurring variants of *DOA* we previously identified. The DOα-chain contributes the majority of contacts between DM and DO[22, 43, 55], suggesting that genetic variation in *DOA* may also confer altered DO function. Similar to *DOB*, the *DOA* gene is also mostly nonpolymorphic, and over 99% of all individuals (ALL) express the four known common alleles. Using an in vitro cell line transfection-based screen to measure DO function, we showed that three of the four common *DOA* alleles, when paired with the most common *DOB* allele, had altered function. Two were gain-of-function variants, whereas one was a loss-of-function allele and made no detectable protein because of a frameshift mutation. Using bioinformatic approaches, we determined the naturally occurring haplotypic combinations of the *DOA* and *DOB* common allele genes. Functional analyses of the haplotypic pairs showed that polymorphisms in the *DOA* common alleles altered the ability of DO to modify DM activity; however, changes in the *DOB* common alleles did not. Extension of the functional analysis to 21 rare *DOA* missense variants showed that two variants produced no detectable heterodimeric DO protein, seven variants were gain-of-function

mutations, and one variant had reduced function, despite producing more DO protein. Interestingly, a single-nucleotide polymorphism (SNP) in one of the common alleles, *DOA*0102*, a gain-of-function variant, was shown to be linked to an allele of HLA-DP that was previously associated with persistent hepatitis B virus (HBV) infection. Conversely, an SNP in one of the *DOA* null alleles was linked to an HLA-DP allelic SNP that was associated with resistance to HBV. Thus, a specific *DOA* allele generated a DO protein with enhanced function that may be detrimental to HBV immunity, whereas a nonfunctional allele of *DOA* produced no protein and thus might have been beneficial with respect to HBV infection outcomes.

Results

Assay Measuring DO Function

DM induces the dissociation of CLIP from the MHCII peptide binding groove[56, 57]. DO has been shown to be a substrate mimic of MHCII, thereby preventing DM from functionally interacting with MHCII–CLIP[22]. DO expression in cells resulted in increased MHCII–CLIP levels[25]. Thus, the ability of DO to functionally interact with and inhibit DM activity can be monitored by measuring the level of cell surface MHCII–CLIP[25, 37, 39, 53]. Therefore, we took advantage of the direct relationship between DO expression levels and MHCII–CLIP levels to determine if amino acid changes encoded by *DOA* gene variants resulted in DO proteins with altered function. For these studies, we established and used an in vitro assay to monitor surface MHCII–CLIP levels after expression of *DOA* gene variants coexpressed with the most commonly expressed *DOB* allele,

*DOB*0101*. For this assay, *DOA* and *DOB* expression constructs were cotransfected into DO-negative HeLa cells that had been previously stably transfected with the class II MHC transactivator (HeLa.CIITA)[58]. Previous studies have shown that CIITA drives the expression of MHCII, DM, Ii, and *DOA* but not *DOB* in B cell lines[58]. However, others have shown that expression of CIITA in B cell lines and HeLa can also turn on *DOB* expression[35, 58]. In our hands, HeLa.CIITA cells expressed MHCII, DM, and Ii but only (very) low levels of *DOA* mRNA and no *DOB* mRNA, providing a recipient cell in which we could express and functionally test *DOA* and *DOB* gene variants[53]. To allow for the identification of cells that had been cotransfected with both genes, the *DOA* gene was followed by an IRES sequence and the mRuby gene, and the *DOB* gene was followed by an IRES sequence and the *AcGFP* gene. Seventy-two hours after transfection, one half of the cells were surface stained with Abs specific for total MHCII and MHCII–CLIP[57], the other half were fixed and permeabilized to allow for intracellular staining for DO and DM using heterodimer-specific Abs[39, 59], and the levels of these proteins were measured by flow cytometry. Only mRuby and AcGFP double-expressing cells that marked the coexpression of DOα and DOβ were analyzed (Fig. 2.1). The mRuby+ AcGFP+ cells were gated for MHCII high cells before measuring MHCII–CLIP levels (Fig. 2.1A) and, for the measurement of DO, cells were first gated for DM (Fig. 2.1B) to ensure that any HeLa cells that had lost CIITA were excluded from the analyses. HeLa.CIITA cells transfected with vectors encoding only *mRuby* and *AcGFP* (i.e., empty vectors), with the vector encoding only *DOA* (*DOA*0101-mRuby*) or the vector

encoding only *DOB* (*DOB*0101-AcGFP*), resulted in no detectable DO protein and low levels of MHCII–CLIP (Fig. 2.1). However, when HeLa.CIITA cells were transfected with vectors encoding both the *DOA* and *DOB* genes, DO protein was produced and resulted in increased MHCII–CLIP levels (Fig. 2.1). DM and MHCII levels were similar in all transfection conditions (Fig. 2.1). These control experiments showed that DM function was inhibited, and MHCII–CLIP levels increased only after expression of both chains of the DO $\alpha\beta$ heterodimer in HeLa.CIITA cells. These experiments validated the use of the in vitro transient transfection system to measure if natural *DOA* gene variation in humans results in DO proteins with altered function.

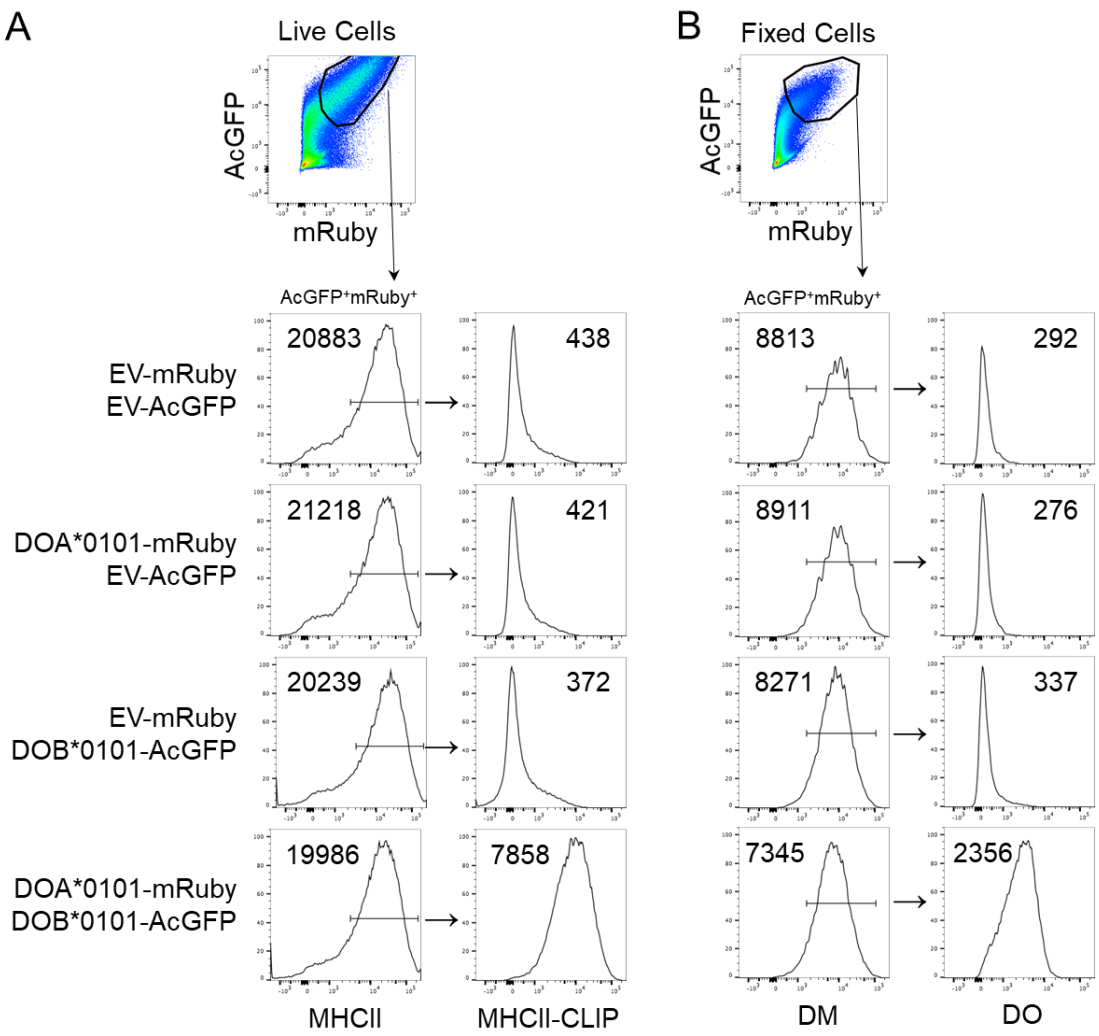

Figure 2.1 Approach used to measure DO function. **(A)** HeLa.CIITA cells (MHCII+, Ii+, and DM+) were transiently transfected with an EV-mRuby and EV-AcGFP, a vector expressing *DOA*0101* mRuby and EV-AcGFP, EV-mRuby and a vector expressing *DOB*0101*-AcGFP, or *DOA*0101*-mRuby and *DOB*0101*-AcGFP. Cells were analyzed 72 h later by flow cytometry after staining for cell surface MHCII and MHCII–CLIP expression. Live cells were gated for the expression of both mRuby, which reports DOA expression, and AcGFP, which reports *DOB* expression as shown. MHCII levels in the mRuby+ AcGFP+ cells are shown (left), and after gating for the MHCII+ cells, MHCII–CLIP levels are shown (right). gMFI values for MHCII and MHCII–CLIP are shown on each histogram. **(B)** HeLa.CIITA cells transfected as in **(A)** were fixed, permeabilized, and stained for intracellular DM and DO prior to analysis by flow cytometry. Fixed cells were gated on AcGFP+ mRuby+ cells (fixation of cells results in decreased mRuby and AcGFP fluorescence) and the DM levels determined (left). After gating for DM+ cells, the level of DO was determined (right). gMFI values for DM and DO are shown on each histogram. DO expression and increased

MHCII–CLIP levels were observed only after transfection of vectors expressing both DOA and DOB. Data are representative of five similar experiments.

Three of four DOA common alleles have altered function

DOA, like *DOB* and the *DMA* and *DMB* genes, is considered to be a nonpolymorphic gene[60]. Currently, there are four common *DOA* alleles, *DOA*0101*, **0102*, **0103*, and **0104*, according to the Immuno Polymorphism Database–IMGT for HLA[61]. *DOA*0101* is the most common allele and is present in ~98% of the population. *DOA*0102* (R80C), *DOA*0103* (L74V), and *DOA*0104* (P11 del FS) account for ~1.7% of the rest of the DOA alleles found in humans (Fig. 2A). The frameshift mutation in DOA*0104 is inserted at amino acid residue 11 and results in the addition of 25 aa before ending in an early stop codon. Therefore, *DOA*0104* is predicted to produce a frameshift protein that terminates after only 36 aa (Fig. 2A), resulting in a null protein.

To determine if *DOA*0102*, **0103*, or **0104* produced DO proteins with altered function compared with the most common *DOA* allele, *DOA*0101*, HeLa.CIITA cells were transfected with each of the individual four common *DOA* alleles and *DOB*0101*. Note that unless otherwise specifically stated, the individual DOA alleles and variants analyzed in this paper were coexpressed in HeLa.CIITA cells with *DOB*0101*, the most frequently expressed DOB allele. Seventy-two hours post-transfection, the cells were stained and analyzed by flow cytometry as described above. Representative flow cytometry plots obtained for MHCII, MHCII–CLIP, DM, and DO are shown in Fig. 2B. To allow for quantification of the results obtained from multiple independent experiments, the

levels obtained from at least four independent experiments were normalized to the levels obtained after expression of *DOA*0101* (Fig. 2.2C). The expression of the four DOA common alleles had no impact on the levels of MHCII, and DM levels were only minimally impacted. MHCII–CLIP levels were uniformly high for *DOA*0101*, **0102*, and **0103*, despite *DOA*0102* and **0103* expressing only half the amount of DO protein when compared with *DOA*0101* (Fig. 2.2B, 2.2C). The DO Ab used to measure DO levels (Mags.DO5) recognizes a conformational epitope on the DO heterodimer; however, the epitope is on the DOβ-chain[39, 43]. Thus, mutations in DOα are unlikely to impact Mags.DO5 recognition of DO proteins produced after transfection of *DOB*0101* with *DOA* gene variants. As expected, *DOA*0104* expressed no detectable DO protein because of the frameshift mutation and thus is a null allele. As expected, expression of the *DOA*0104* null allele resulted in no increase in MHCII–CLIP (Fig. 2.2B, 2.2C).

MHCII–CLIP levels directly correlate with DO protein levels[25, 37, 39, 53]. Therefore, to determine if the three *DOA* alleles that produced DO protein (*DOA*0101*, **0102*, and **0103*) had differential function, the ratio of MHCII–CLIP to DO was determined. Compared with *DOA*0101*, expression of *DOA*0102* and **0103* resulted in increased MHCII–CLIP/DO ratios showing that these two DO proteins had enhanced function (Fig. 2.2D). In our previous work, we identified two rare *DOB* gene variants with increased function that had amino acid mutations that mapped to the MHCII β-like, membrane distal domain[53]. Like the two DOβ variants, the polymorphisms in *DOA*0102* and **0103* similarly mapped to the MHCII α-like membrane distal domain (Fig. 2.2A). Collectively,

these analyses show that the *DOA*0102*, **0103*, and **0104 DOA* common alleles either produce no DO protein or DO proteins with altered function when compared with *DOA*0101*.

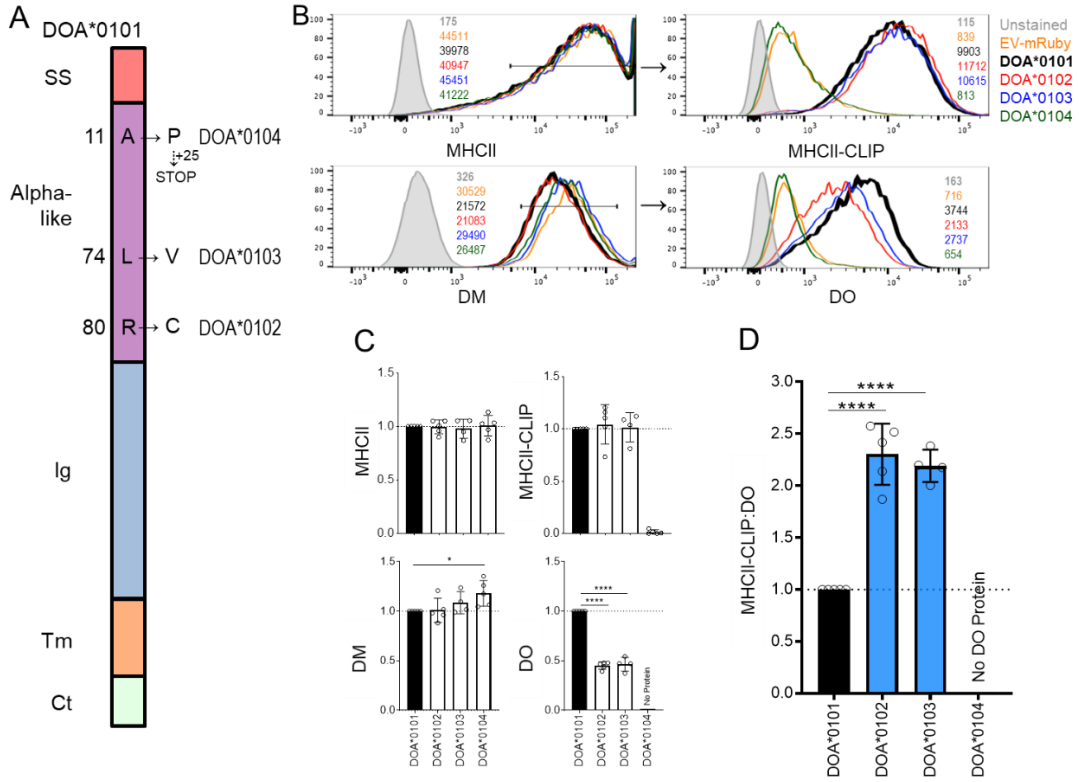

Figure 2.2 Three of the four common *DOA* alleles have altered function. **(A)** Schematic of the *DOA* common alleles relative to the *DOA*0101* gene. *DOA* contains the following domains as indicated: a signal sequence (SS), an MHCII α-like (α-like), an Ig-like (Ig), a transmembrane (TM), and a cytoplasmic tail (Ct). The other three common alleles have single missense mutations that result in single amino acid changes, which are shown. Numbering indicates amino acid number starting after SS cleavage, and the amino acid encoded by the *DOA*0101* gene is shown in the rectangle domains followed by an arrow showing amino acid changes for *DOA*0102*, *DOA*0103*, and *DOA*0104* alleles. For *DOA*0104*, a frameshift mutation results in the addition of 25 random amino acids prior to a stop codon (see Fig. 4). **(B)** HeLa.CIITA cells were transiently transfected with a vector encoding *DOB*0101*–AcGFP (the most common *DOB* allele) together with a control empty vector (EV-mRuby) or vectors encoding *DOA*0101*, *DOA*0102*, *DOA*0103*, or *DOA*0104*. Seventy-two hours later, the transiently transfected cells were stained as in Fig. 1 prior to analysis by flow cytometry. Histogram overlays on left show representative data for MHCII and

DM and on right for MHCII–CLIP and DO after gating as indicated for MHCII+ and DM+, respectively, in cells expressing both the *DOA* and *DOB* expression constructs (mRuby+ AcGFP+). Shaded histograms are levels obtained for unstained cells as a negative control. Colors used in histogram overlays for each *DOA* common allele and empty vector control (EV-mRuby) are shown on right. gMFI values for MHCII, DM, MHCII–CLIP, and DO are shown on each histogram for each corresponding combination, color-coded as on right. Data are representative of one of four to five independent experiments. **(C)** Quantification of independent experiments shown in **(B)**. Background gMFI for MHCII–CLIP and DO was eliminated by subtracting the gMFI value of the EV-mRuby/*DOB*0101*–AcGFP control from each sample. gMFI values measured for MHCII, DM, MHCII–CLIP, and DO were normalized to the value obtained after transfection of *DOA*0101* (with *DOB*0101*) to allow for analysis across independent experiments (black bars). **(D)** The relative function of each *DOA* allele was determined by calculating the ratio of MHCII–CLIP to DO from the values obtained in **(C)** to correct for different DO protein levels relative to the value obtained for *DOA*0101* (with *DOB*0101*). Blue bars indicate alleles that have an increased function relative to DOA*0101 (with *DOB*0101*; black bar). Data were combined from four to five individual experiments. Symbols and error bars represent the mean ± SD. Significance was calculated using an unpaired, two-tailed Student t test. **p* = 0.0147, *****p* < 0.0001.

Functional analysis of common DOA-DOB combinations

The HLA genetic locus has strong linkage disequilibrium, and as such, specific *DOA* and *DOB* alleles are associated as pairs within individual haplotypes. This led us to ask if naturally occurring DO allotypes may have altered function because our studies above demonstrated functional differences in the *DOA* common alleles. Using rsSNPs[62] present in the individual *DOA* and the five *DOB* common alleles[60, 61] (Fig. 2.3A), the 1000GP[63] publicly available sequence data were parsed to determine the naturally occurring DO haplotypes. We have previously used a similar approach to define the naturally occurring DM haplotypes[64]. *DOA*0103* and *DOA*0104* were present in <1% of the population, and thus, there were not sufficient data to determine their contributions to the naturally occurring haplotypes. *DOA*0101* was found in combination with all five

common *DOB* alleles, whereas *DOA*0102* was found with all but *DOB*0103* (Fig. 2.3B). Frequencies for each combination were compiled from the 1000GP database for ALL and for individuals in each of the following subpopulations: African (AFR), American, East Asian, European, and South Asian (Fig. 2.3B). In line with the commonly accepted idea that DO is nonpolymorphic, 65.6% of ALL were either homozygous or heterozygous for *DOA*0101*/*DOB*0101*, and 32.8% of individuals had *DOA*0101* paired with one of the other *DOB* common alleles. Thus, *DOA*0101* paired with any of the common *DOB* alleles accounted for 98.4% of all DO haplotypes. *DOA*0102* was found in combination with all *DOB* common alleles except for *DOB*0103*, with *DOA*0102*/*DOB*0101* found in 1.08% of the 1.72% of ALL that have *DOA*0102* in combination with one of the *DOB* alleles. Whereas *DOA*0101* was found in all subpopulations, *DOA*0102* was found in all but the AFR population.

We next determined if the naturally occurring *DOA*0102*/*DOB* common allele natural haplotypic combinations resulted in DO proteins with altered function by transfecting vectors expressing *DOA*0102* and the four individual *DOB* common alleles into HeLa.CIITA cells. Seventy-two hours later, MHCII protein levels were determined by flow cytometry. As a control, we also coexpressed *DOA*0101* with the five common *DOB* alleles because we previously reported that the five *DOB* common alleles all functioned similarly[53]. Fig. 2.3C shows a summary of the expression levels obtained for MHCII, MHCII–CLIP, DO, and DM combined from at least four independent experiments after transfection of the various combinations of *DOA* and DOB alleles into

HeLa.CIITA cells. To facilitate comparison across independent experiments, results were normalized to the *DOA*0101* and *DOB*0101* control for each experiment. As we previously reported, all five *DOB* common alleles expressed similar levels of MHCII pathway proteins when cotransfected with *DOA*0101*[53]. When *DOA*0102* was paired with the four *DOB* common alleles to generate the naturally occurring haplotypic pairs, MHCII, MHCII–CLIP and DM levels were also similar to the levels obtained for the *DOA*0101*/*DOB*0101* pair; however, for all naturally occurring DOA*0102 haplotypic pairs, DO protein levels were about half that observed for the *DOA*0101*/*DOB*0101* pair. Calculation of the relative functional activity of DO by determination of the MHCII–CLIP/DO ratio showed that, when compared with *DOA*0101* paired with any of the *DOB* common alleles, all four naturally occurring *DOA*0102*/*DOB* haplotypic pairs produced DO proteins with increased function (Fig. 2.3D). Interestingly, specific subpopulations of individuals had unique expression patterns for *DOA*0102* paired with the different *DOB* alleles (Fig. 2.3B). *DOA*0102*/*DOB*0101* and *DOA*0102*/*DOB*0102* heterozygotes were found in all the subpopulations except AFR; however, *DOA*0102*/*DOB*0101* homozygotes were found only in South Asians. Similarly, *DOA*0102*/*DOB*0104* and *DOA*0102*/*DOB*0105* heterozygotes were found only in Europeans and Americans, respectively.

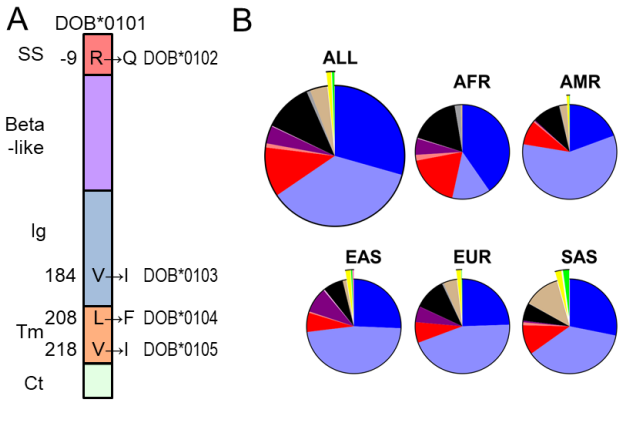

Natural Haplotypes	Frequency					
	ALL	AFR	AMR	EAS	EUR	SAS
DOA*0101/DOB*0101	29.4	40.3	25.6	19.4	24.5	28.2
DOA*0101/DOB*0101-homo	36.2	13.1	47.4	58.2	44.9	37.1
DOA*0101/DOB*0102	11.4	18.7	6.62	8.36	7.09	10.2
DOA*0101/DOB*0102-homo	0.94	1.95	0.43	0.47		0.99
DOA*0101/DOB*0103	4.05	5.60	8.76	0.32	5.35	0.57
DOA*0101/DOB*0103-homo	0.17	0.27	0.43		0.14	
DOA*0101/DOB*0104	11.3	17.5	6.84	9.62	11.0	6.08
DOA*0101/DOB*0104-homo	0.85	2.13		0.32	0.58	0.14
DOA*0101/DOB*0105	4.05	0.53	1.28	2.37	4.63	12.5
DOA*0102/DOB*0101	1.08		1.71	0.79	1.59	2.12
DOA*0102/DOB*0101-homo	0.03					0.14
DOA*0102/DOB*0102	0.52		0.43	0.16	0.14	2.12
DOA*0102/DOB*0104	0.03				0.14	
DOA*0102/DOB*0105	0.06		0.43			

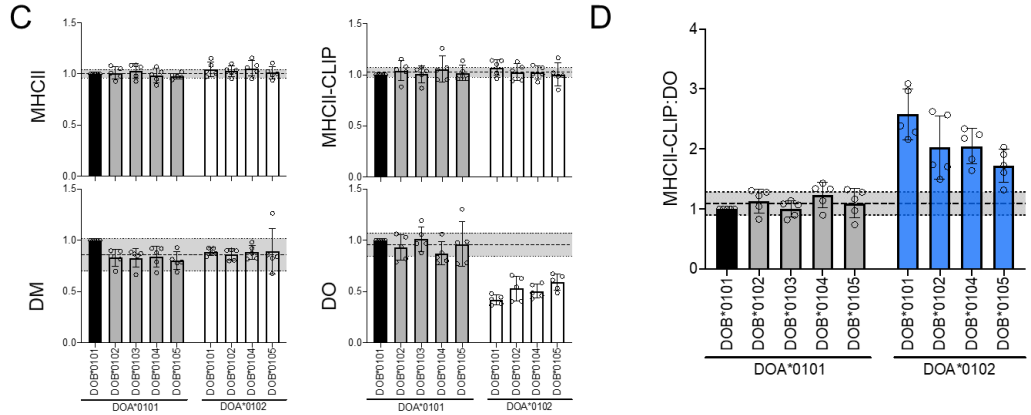

Figure 2.3 Analysis of *DOA* and *DOB* allelic variations and their natural haplotype combinations. **(A)** Schematic showing amino acid differences in the DOβ proteins produced by the *DOB* common alleles relative to the DOβ protein encoded by the conical *DOB*0101* gene. DOβ contains the following domains as indicated: a signal sequence (SS), an MHCII β-like (β-like), an Ig-like (Ig), a transmembrane (TM), and a cytoplasmic tail (Ct). The four other common alleles have single missense mutations that result in single amino acid changes, which are shown. Numbering indicates amino acid number starting before (negative) or after SS cleavage and the amino acid encoded by the *DOB*0101* gene is shown in the rectangle domains followed by an arrow showing amino acid changes for *DOB*0102*, *DOB*0103*, *DOB*0104*, and *DOB*0105* alleles. **(B)** Association of *DOA* and *DOB* allelic variants into haplotypes and their corresponding frequencies shown as a pie charts for ALL covered by the 1000GP and the corresponding subpopulations. Enlarged pie pieces show frequencies of *DOA*0102*. The table on the right side depicts the color code used for each haplotype in the pie charts and the frequency of homozygous (homo) and heterozygous allotypes containing *DOA* allelic variants different from the canonical *DOA*0101* is given for ALL and each subpopulation. Combinations that were not found in the 1000GP database are left blank. The following SNPs were used to search 1000GP: *DOA*0102* (rs11575906), *DOA*0103* (rs41542323), *DOA*0104* (rs41541116), *DOB*0102* (rs2071554), *DOB*0103* (rs2621330), *DOB*0104* (rs2070121), and *DOB*0105* (rs11575907). The two

SNPs resulting in substitutions for the *DOA*0103* and *DOA*0104* allelic variants in the IMGT-HLA are not found in the 1000GP dataset and are not shown. **(C)** To determine if natural DOA–DOB haplotype combinations described in **(B)** resulted in DO proteins with altered function, HeLa.CIITA cells were transiently transfected with vectors encoding *DOA*0101* and *DOB*0101*, *DOB*0102*, *DOB*0103*, *DOB*0104*, *DOB*0105*, or *DOA*0102* and *DOB*0101*, *DOB*0102*, *DOB*0104*, or *DOB*0105*, and the gMFI values for MHCII, DM, MHCII–CLIP, and DO levels in mRuby+ AcGFP+ cells were determined as in Fig. 1. Background gMFI for MHCII–CLIP and DO was eliminated by subtracting the gMFI value of the EV-mRuby/EV-AcGFP control from each sample. Data from five independent experiments were normalized to the values obtained for *DOA*0101*/*DOB*0101* combination (black bars). The gray zones correspond to the average of DOA*0101 with each of the five common *DOB* alleles 62 SD (MHCII [1.00 $\pm$ 0.04], DM [0.86 $\pm$ 0.16], MHCII–CLIP [1.02 $\pm$ 0.05], and DO [0.96 $\pm$ 0.11]). Blue bars indicate haplotype combinations with reduced DO levels. **(D)** DO proteins resulting from *DOA*0102* paired with four *DOB* allotypes have altered function. MHCII–CLIP/DO ratios for each of the natural DOA–DOB combinations were calculated and normalized to that of the *DOA*0101*/*DOB*0101* combination (black bar). The gray zone corresponds to the average of DOA*0101 with each of the five common *DOB* alleles $\pm$2 SD (1.09 $\pm$ 0.19). Blue bars indicate haplotype combinations with function. EAS, East Asians; EUR, Europeans; SAS, South Asians.

Functional analysis of naturally occurring DOA variants

In our previous work, we examined over 60,000 exomes from the Exome Aggregation Consortium database[54] for *DOA* allelic variants. These analyses identified 107 different allelic variants, including the *DOA*0102*, **0103*, and **0104* common alleles. The variants had frequencies ranging from 8.24×10^{-6} to 0.012[53]. Of the 107 *DOA* variants, 12 were predicted to be null because of frameshift mutations, mutations that generated premature stop codons or mutations that disrupted the start codon. The other 95 variants had single missense mutations. Twenty of the more abundant 95 DOA variants with single missense mutations and one allele encoding a nonsense mutation were chosen for functional analyses. The missense variants chosen for analyses had single

amino acid substitutions that were distributed throughout the protein (Fig. 2.4). As above, function was determined by cotransfection of the individual *DOA* gene variants with *DOB*0101* (most common *DOB* allele) into HeLa.CIITA cells, and 3 days later, MHCII, MHCII–CLIP, DM, and DO levels were determined by flow cytometry. The results of these analyses are presented as a compilation of the levels obtained for these proteins from four or more independent experiments normalized to the levels obtained after coexpression of *DOA*0101*/*DOB*0101* in HeLa.CIITA (Fig. 2.5). Because expression of *DOA*0101* with each of the five *DOB* common alleles did not significantly alter MHCII, MHCII–CLIP, DO, or DM expression levels in transfected cells[53] (Fig. 2.3C), we considered any *DOA* variant with MHCII pathway protein levels $\pm$2 SD above or below the average obtained for *DOA*0101* coexpressed with the five common *DOB* alleles as an allele with altered protein levels. Many of the 21 *DOA* variants when expressed individually with *DOB*0101* in HeLa.CIITA cells produced DO proteins that had altered MHCII–CLIP and DO levels (Fig. 2.5B), whereas DM and MHCII levels remained unchanged (Fig. 2.5A). As predicted, HeLa.CIITA cells expressing the Q58stop nonsense DOα variant had no detectable DO protein, and as a result, no increase in MHCII–CLIP was observed (Fig. 2.5B). Surprisingly, HeLa.CIITA cells expressing the DOα F114L missense mutation also did not produce any detectable DO protein and consequently also did not show increased MHCII–CLIP (Fig. 2.5B). HeLa.CIITA cells expressing seven of the 21 DOα alleles (V92M, R97W, P103T, R124H, G126R, R147C, and H150R) had reduced DO protein levels, but all but one (R147C) had normal MHCII–CLIP levels (Fig.

2.5B). The R147C variant had a slight but significant reduction in MHCII–CLIP. The phenotype for these seven variants was similar to what was observed for HeLa.CIITA expressing *DOA*0102* when paired with four *DOB* common alleles (Fig. 2.3) and previously for the DOβ R70G and G77V variants when paired with *DOB*0101*[53]. Finally, HeLa.CIITA cells expressing the DOα I67M allele exhibited significantly higher DO expression but also had normal MHCII–CLIP.

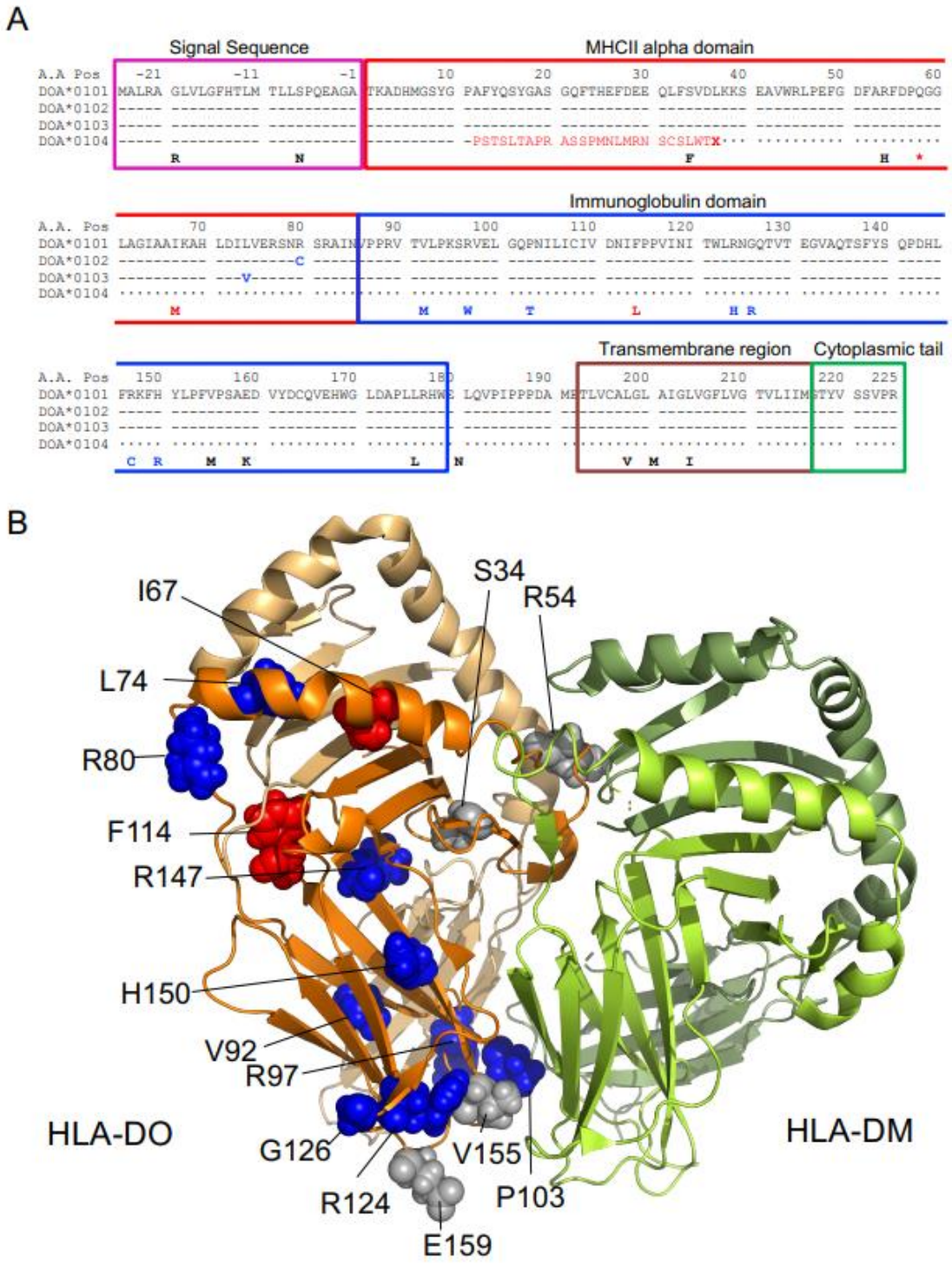

Figure 2.4 Amino acid alignment of DOα common alleles and variants analyzed. **(A)** Alignment of the four common DOα alleles to *DOA*0101*. Dashes indicate similarity, and the dots indicate a truncated protein (for *DOA*0104*). Missense and the stop mutation for the 21 *DOA* variants selected for the screen are indicated below the amino acid sequences for the common variants. DOα alleles

that form DO proteins with decreased function relative to *DOA*0101*/*DOB*0101* are colored red, those with increased function are in blue, and those in black have normal function (see Fig. 2.5). DOα protein domains are marked by colored frames as indicated. **(B)** The structure of the DM–DO complex[22] with the side chains of amino acids mutated in the DOα variants investigated in this study are shown as spheres. The backbone cartoon of DMα is shown in light green, and the backbone cartoon of DMβ is in dark green. DOα, carrying the mutated residues, is depicted in dark orange, and DOβ is in light orange. As in **(A)**, residues with enhanced function are colored blue, those leading to reduced function are in red, and mutations without an effect on functionality are shown in gray. Mutations occurring in the transmembrane region are shown as the crystal structure did not contain this domain. The figure was created by PyMol[65] using the Protein Data Bank file 4I0P.

The function of the DO proteins produced after transfection of the individual DOα variants with *DOB*0101* into HeLa.CIITA cells was quantified by calculating the ratio of the protein levels for MHCII–CLIP to DO levels (Fig. 2.5C). Fifty-two percent of the 21 DOα variants had MHCII–CLIP/DO ratios that fell within 2 SD of ratios obtained after expression of the of *DOA*0101* with five common *DOB* alleles and thus were considered variants with normal function. Of the remaining alleles, two DOα alleles (Q58Stop and F114L) were null alleles as they produced no detectable DO protein after expression in HeLa CIITA cells, and thus, an MHCII–CLIP/DO ratio could not be calculated. After expression in HeLa.CIITA cells, the DOα I67M allele resulted in significantly higher DO protein levels that resulted in an MHCII–CLIP/DO ratio that was about half of that obtained for the controls. Finally, the remaining seven DOα variants (V92M, R97W, P103T, R124H, G126R, R147C, and H150R) had MHCII–CLIP/DO ratios that were 1.5–2-fold higher than controls, showing that these variants produced DO proteins with increased activity.

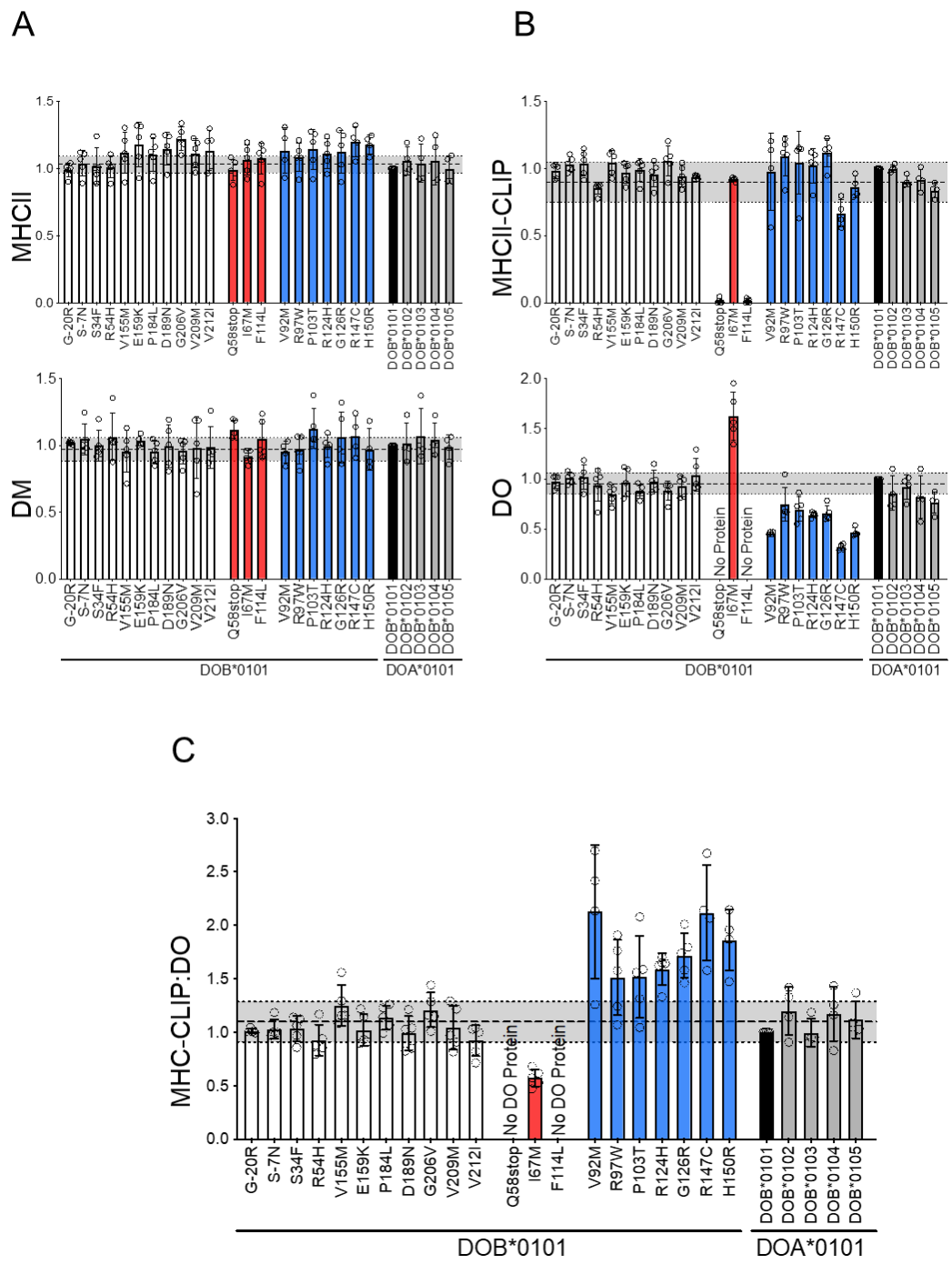

Figure 2.5 Functional analysis of naturally occurring DOα variants. **(A and B)** HeLa.CIITA cells were transiently transfected with a vector encoding *DOB*0101* and vectors encoding each of the individual 21 *DOA* variants. Cells were analyzed by flow cytometry 72 h later, and the gMFI values for MHCII and MHCII–CLIP **(A)** and DM and DO **(B)** levels in mRuby+ AcGFP+ cells were determined as in Fig. 1. Background gMFI for MHCII–CLIP and DO was eliminated by subtracting the gMFI value of the EV-mRuby/*DOB*0101*-AcGFP

control from each sample. Data from four to five independent experiments were normalized to the values obtained for *DOA*0101*/*DOB*0101* combination (black bars). The gray zones correspond to the average of *DOA*0101* with each of the five common *DOB* alleles ±2 SD: MHCII (1.03 ± 0.06), DM (0.97 ± 0.09), MHCII–CLIP (0.90 ± 0.15), and DO (0.95 ± 0.11). **(C)** MHCII–CLIP/DO ratio for each of the *DOA* variants combined with *DOB*0101*. The ratios were normalized to that of the *DOA*0101*/*DOB*0101* combination (black bar) from four to five independent experiments. Constructs transfected are indicated below the bar graphs. The gray zone corresponds to the average ±2 SD of the values obtained from *DOA*0101* combined with each of the five common *DOB* alleles (1.10 ± 0.19). DOα variants with altered function (increased: blue bars, decreased: red bars) were defined as possessing an MHCII–CLIP/DO ratio that fell outside this range.

Biochemical analysis of alleles with altered function

Our studies identified 10 DOα variants that produced DO proteins with either a reduced or enhanced ability to modify the peptide loading of MHCII molecules by DM. DO is an MHCII substrate mimic and binds to DM, preventing DM from interacting with MHCII and mediating peptide loading. Thus, we hypothesized that the DO proteins with altered function might interact either more (increased function) or less (decreased function) efficiently with DM. To test this idea, the DO heterodimer and any coassociated DM molecules were captured from HeLa.CIITA cell lysates expressing the individual 10 DOα variants with altered activity followed by Western blotting for any coassociated DM (Fig. 2.6A). As a positive control, HeLa.CIITA cells expressing *DOA*0101*/ *DOB*0101* were used, and mock-transfected cells were used as a negative control. Western blotting of total cell lysates for DOβ and DMβ confirmed the successful expression of DO for each variant as well as similar DM expression levels. Assembled DO αβ heterodimers were immunoprecipitated from all cells that expressed the individual DOα variants except for the *DOA*0104* and DOα F114L

variants (Fig. 2.5B), confirming the flow cytometric results showing that these two null alleles did not produce a functional heterodimer (Fig. 2.2B, 2.2C). All the remaining DOα variants that resulted in an assembled DO $\alpha\beta$ heterodimer were found complexed with DM (Fig. 2.6A).

To determine the relative amount of DM coprecipitated with the DO heterodimer from cells expressing the individual DOα variants, the amount of DO (DOβ) and DM (DMβ) in the immunoprecipitations was quantitated across five independent experiments and compared with the amount of protein immunoprecipitated after expression of *DOA*0101*/*DOB*0101*. The resulting values were also normalized to correct for differences in transfection efficiencies using the expression of the reporter molecules, mRuby and AcGFP (see Materials and Methods for details). Relative to the amount of DO immunoprecipitated for the control, reduced levels of DO were recovered for *DOA*0102* and **0103* and DOα V92M, R97W, P103T, R124H, G126R, R147C, and H150R, whereas DOα I67M had increased DO levels (Fig. 2.6B). These results correlated well with the DO levels measured by flow cytometry (Figs. 2.2B, 2.2C, 2.5B). Unexpectedly, the amount of DM associated with DO was reduced for all DOα variants with altered function, including those with enhanced function and DOα I67M that had increased DO levels (Fig. 2.6C).

We had expected to find more DM associated with DO in the DOα variants with enhanced function. Therefore, we next estimated how much DM was recovered bound to DO in each immunoprecipitation relative to the amount of

recovered DO. With the exception of the DOα I67M and R147C variants, the remaining DOα variants had DO/DM ratios that were similar to the control (*DOA*0101*/*DOB*0101*) (Fig. 2.6D). This indicated that, although the missense mutations in the DOα variants resulted in less overall assembled DO, the resulting DO heterodimer interacted normally with DM, at least as measured using coimmunoprecipitation. Counterintuitively, this also indicates that there should be more free DM (DM not bound to DO) in HeLa.CIITA cells expressing these DOα variants, resulting in lower MHCII–CLIP levels. However, these DOα variants had MHCII–CLIP levels that were similar to controls (Fig. 2.5B). The DOα R147C variant had a reduced DO/DM ratio, which indicates that more DM coprecipitated with this variant relative to the amount of DO in the complex. Surprisingly, the DOα I67M variant that had increased DO levels had reduced DM levels. DO must assemble and associate with DM to exit the ER[41]; thus, reduced DM associated with the DOα I67M variant suggests that it may traffic from the ER somewhat independent of DM as has been reported for the previously described DOα P11V DO variant[43].

Finding less DO associated with DM after the expression of the DOα variants with altered function in HeLa.CIITA cells suggested that these variants should have increased free DM. If so, these variants should show lower MHCII–CLIP, yet we observed MHCII–CLIP levels that were similar to the control cells. Studies in EBV-transformed human B cell lines and primary human B cells showed that ~50% of DM is DO associated[37, 66]. Thus, a possible explanation for our observed result is that expression of DO in HeLa.CIITA cells by transient

transfection resulted in overexpression of DO that quantitatively bound up all DM in the cells, resulting in high MHCII–CLIP levels. To test this idea, we expressed a selection of DOα variants (*DOA*0101*, *DOA*0102*, *DOA*0103*, *DOA*0104*, and H150R) in HeLa.CIITA cells and sort purified mRuby and AcGFP double expressing, DO positive cells. As a control, we also purified mRuby and AcGFP double expressing HeLa.CIITA cells that had been transfected with the EV-mRuby (no *DOA*0101*) with *DOB*0101* (i.e., AcGFP+) and also included (unsorted) cells that had been mock transfected without any vectors. Equal numbers of cells were lysed and divided into two equal aliquots. One aliquot was depleted of DO by three sequential immunoprecipitations with a DO heterodimer-specific mAb and the other aliquot mock depleted using a nonspecific Ab. We then determined if any DM remained in the DO-depleted lysates by Western blotting for DM. Western blotting of the lysates prior to depletion verified DO and DM expression (Fig. 2.6E), and Western blotting of the three sequential anti-DO immunoprecipitated for DO demonstrated successful depletion of DO from the lysates (Fig. 2.6F). Finally, Western blotting of the DO- and control-depleted lysates showed DM remaining in the lysates, even in the DO-depleted samples (Fig. 2.6G). Indeed, DO depletion only removed a small proportion of the DM from the lysates (compare the amount of DM in the control compared with the DO immunoprecipitation), indicating that only a small proportion of the total DM is complexed with DO. These studies indicate that a large pool of free DM (i.e., not bound to DO) is present after transient transfection of DO into HeLa.CIITA cells. It is unclear how DOα variants with altered function inhibit DM, resulting in high

levels of MHCII–CLIP; however, the explanation is not due to a lack of free DM in the cells.

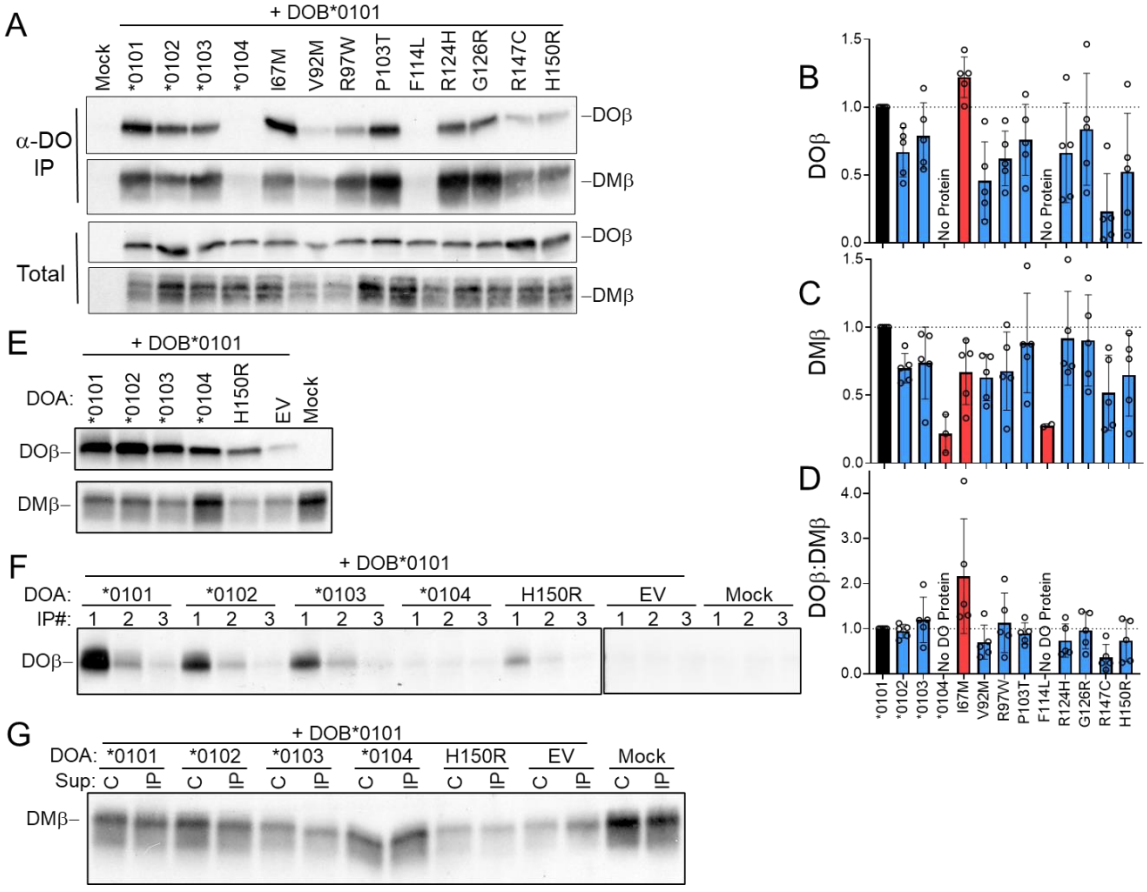

Figure 2.6 Biochemical analysis of DO proteins produced by the DOα variant alleles. **(A)** HeLa.CIITA cells were transiently transfected with vectors encoding *DOB*0101* and *DOA*0101* or one of the DOα variants with altered function (*DOA*0102*, *DOA*0103*, *DOA*0104*, I67M, V92M, R97W, P103T, F114L, R124H, G126R, R147C, and H150R; labeled across the top of the blots). Mock-transfected HeLa.CIITA cells (Mock) were used as a negative control. Cells were harvested 72 h later and lysed, and DO was immunoprecipitated with the DO heterodimer-specific Ab Mags.DO5[39]. The resulting precipitated proteins (α-DO-IP) were separated by SDS-PAGE, transferred to membranes, and Western blotted to determine DOβ [R.DOB/c[25]] or DMα protein (clone EPR7981) levels. Western blot analyses of the lysates (Total) used for the immunoprecipitations are included to confirm protein expression (bottom). **(B and C)** Quantification of the amount of DOβ **(B)** and coassociated DMβ **(C)** protein detected in each α-DO immunoprecipitation. Values were either normalized to correct for transfection efficiency based on the number of mRuby+ AcGFP+ cells in each sample. Values were then normalized to the amount of DOβ or DMβ protein obtained

after transfection of *DOA*0101*/*DOB*0101* (black bar) to allow for comparison across four independent experiments. **(D)** Ratio of the amount of DOβ to DMβ obtained for each α-DO immunoprecipitation combined for the four independent experiments. Values from **(B)** and **(C)** were normalized to the ratio obtained after transfection of *DOA*0101*/*DOB*0101* (black bar) to allow for comparison across the four independent experiments. **(E–G)** HeLa.CIITA cells were transiently transfected with vectors encoding *DOB*0101* and *DOA*0101*, one of a few select DOα variants with altered function (*DOA*0102*, *DOA*0103*, *DOA*0104*, and H150R) or as negative controls EV-mRuby only or no vectors (Mock). Cells were harvested 72 h later, and mRuby+ AcGFP+ cells were purified by cell sorting, except for the mock transfection. **(E)** Western blotting of lysates verified DO and DM expression in the cells. **(F)** Equal numbers of cells were lysed, and the resulting lysates were split into two equal aliquots. DO was depleted by three sequential anti-DO immunoprecipitations with Mags.DO5[39], and from one aliquot and as a negative control, three sequential immunoprecipitations were performed using mouse IgG. The resulting precipitated proteins were separated by SDS-PAGE, transferred to membranes, and blotted to confirm DO depletion by blotting for DOβ [R.DOB/c[25]]. **(G)** Control **(C)** and DO-depleted (IP) supernatants from the third immunoprecipitation were probed for DM (DMβ; clone EPR7981) to determine if any DM remained after DO removal.

DM-DO complexes assemble in the endoplasmic reticulum (ER) and remain associated during and after transport through the Golgi and into endosomal compartments [41]. One possible explanation for the DOα variants with lower DO protein levels, yet normal MHCII-CLIP levels could be that these variant DOα proteins assemble and traffic from the ER more efficiently than the *DOA*0101*/*DOB*0101* DO protein resulting in a larger pool of functional DO bound to DM specifically in endosomal compartments. To test this idea and also to determine if the DOα I67M protein was also trafficking more efficiently from the ER, the DO proteins were again immunoprecipitated from HeLa.CIITA cell lysates that had been previously transfected with the selected DOα variants together with *DOB*0101*. The glycans on the captured DO proteins were digested or mock digested with endoglycosidases H (EndoH) prior to western

blotting for DOβ (Fig. 2.7A). Glycoproteins that have left the ER are resistant to digestion by EndoH whereas those that are ER-resident remain sensitive thus, allowing for the measurement of how efficiently molecules are trafficking from the ER. To ensure the correct identification the DOβ EndoH sensitive and resistant bands on the western blots, total lysate from HeLa.CIITA cells transfected with *DOA*0101*/*DOB*0101* were mock treated, treated with EndoH, or treated with Peptide N-glycosidase F (PNGaseF) to remove all glycans (Fig 2.7A). To determine the relative amount of DOβ that was ER resident for each DOα variant relative to *DOA*0101*/*DOB*0101*, the bands corresponding to EndoH sensitive (ER resident) and resistant DOβ (trafficked from the ER) were quantified across multiple experiments and as above, the data was normalized for transfection efficiency (Fig. 2.7A and 2.7B). These data showed that the observed increased DO protein levels were, indeed, due to increased trafficking of DOα 167M from the ER, perhaps independently of DM like DOα P11V [67]. In contrast, the DOα variants (*DOA*0102*, *DOA*0103*, V92M, R97W, P103T, R124H, G126R, R147C, and H150R) that resulted in lower levels of DO were preferentially ER retained. These DOα variants resulted in normal levels of cell surface MHCII-CLIP suggesting that at least in this transient transfection assay, that the variant DO proteins may somehow function to inhibit DM from leaving the ER and moving to the endosomes to interact with MHCII-CLIP. If this is the case, then DM from cells transfected with a more functional variant of *DOA* should also be more EndoH sensitive than DM from cells transfected with *DOA*0101*. This was tested by performing DO immunoprecipitations as described previously, digesting the

precipitated protein with EndoH, and blotting for DMβ instead of DOβ (Fig. 2.7C). This blot shows that the majority of DMβ is EndoH resistant and thus ER exited, which indicates that the ER retained DO is not holding DM in the ER as hypothesized.

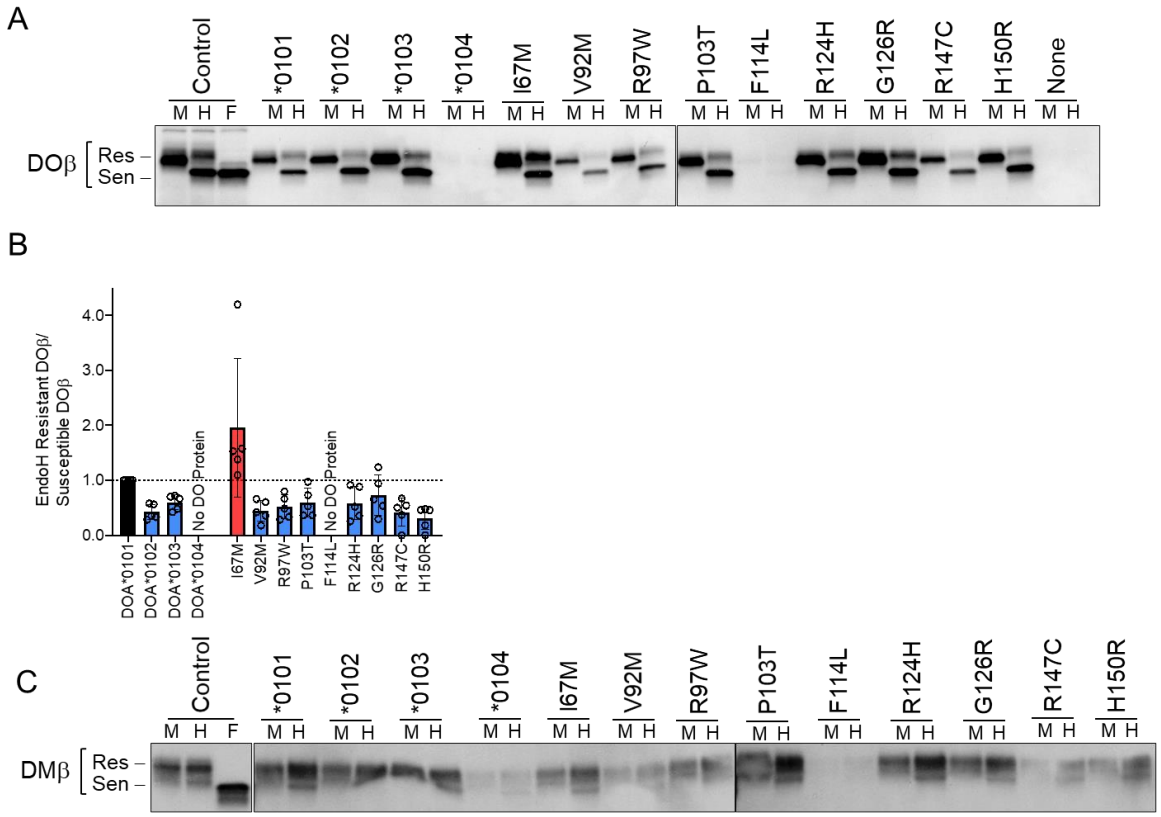

Figure 2.7 EndoH digestion of immunoprecipitated DO and DM protein. **(A)** DO proteins that had been immunoprecipitated as in Fig. 2.6 were eluted from the beads and mock (M) treated or treated with EndoH (H) prior to analysis by western blotting. As a control to demonstrate the location of deglycosylated DOβ, total lysate from *DOA*0101*/*DOB*0101* transfected cells HeLa.CIITA cells was mock treated (M), EndoH treated, or PNGaseF (F), which cleaves immature and mature glycans. The identification of ER-resident EndoH susceptible DOβ and EndoH resistant DOβ are indicated on the left side of the blots. **(B)** Quantification of the ratio of EndoH resistant to EndoH susceptible DOβ across 4 independent experiments. Ratios were normalized to that of *DOA*0101*/*DOB*0101*. **(C)** DM associated DO protein was immunoprecipitated, eluted, and either mock treated or digested as described in **(A)**. The

identification of ER-resident EndoH susceptible DMβ and EndoH resistant DMβ are indicated on the left side of the blots.

The experiments performed thus far have not provided a satisfying answer as to how the DOα gain-of-function mutants are able to inhibit DM activity to the same extent as *DOA*0101*. The reduced expression of these variants suggests that they have reduced stability, and their increased ER retention suggests that they do not interact with DM stably enough to leave the ER bound to DM. We hypothesize that perhaps binding to DO permanently alters DM activity, even if DO is no longer bound due to instability.

To test this idea, we performed an *in vitro* DM peptide loading assay. A peptide loading assay is an assay in which DM is combined with MHCII-CLIP and a peptide at pH 5, and the mixture is incubated at 37°C for 2 hours[68]. Functional DM will interact with MHCII and facilitate the release of CLIP, which will be replaced by the peptide in solution. HLA-DR3:CLIP was purified from T2.DR3 cells and used for this assay, and the peptide used that replaces CLIP was biotinylated mitochondrial outer membrane protein (MOMP) peptide (MOMP-bio). MOMP-bio cannot be edited out of DR3 by additional DM interaction, so the DR3:MOMP-bio complex is irreversible in this assay. The DR3:MOMP-bio can be measured on a Western blot with streptavidin-HRP. We sorted positively transfected HeLa.CIITA expressing either *DOA*0101* or DOα V92M, lysed the sorted cells (1.5 million each), and depleted DO and associated DM from the lysates as described in Figure 6. Mock DO depletion was also performed on

untransfected HeLa.CIITA lysate (Fig. 2.8A). Remaining free DM was then immunoprecipitated from the DO depleted supernatant, and the lack of any remaining associated DO was verified (Fig. 2.8B). The precipitated DM was then tested for its capability to facilitate the release of CLIP from MHCII and load MOMP-bio. We compared the functionality of the precipitated free DM from the sorted *DOA*0101* and DOα V92M expressing cells by performing a peptide loading assay with this DM (Fig. 2.8C). Precipitated DM from 2 million T2.DM cells was used as a positive control for peptide loading[68]. DM-negative HeLa cells were mock immunoprecipitated for DM, which served as a negative control for this assay. In addition, the DR3:MOMP-bio complex falls apart when heated to 95°C, so a fraction of the T2.DM loaded DR3 was incubated at 95°C to verify that the band observed on the blot is correct. The DR3:MOMP-bio bands were quantified and normalized to the intensity of *DOA*0101* (Fig. 2.8D). This was done because the amount of loading that takes place in this assay is directly proportional to the amount of DM in the assay[68]. This blot was also probed for the presence of DM, which revealed that more DM from HeLa.CIITA cells was loaded than the other two samples (Fig. 2.8C, 2.8E). The quantification of DR3:MOMP-bio was then normalized to the amount of DM in each lane (Fig. 2.8F). This analysis revealed that DM from HeLa.CIITA was 82% as effective as DM from DOA*0101 expressing cells, and DM from DOα V92M expressing cells was only 63% as effective when compared to *DOA*0101*. This result is very interesting, as it suggests that DO effects DM activity even when the two are not bound.

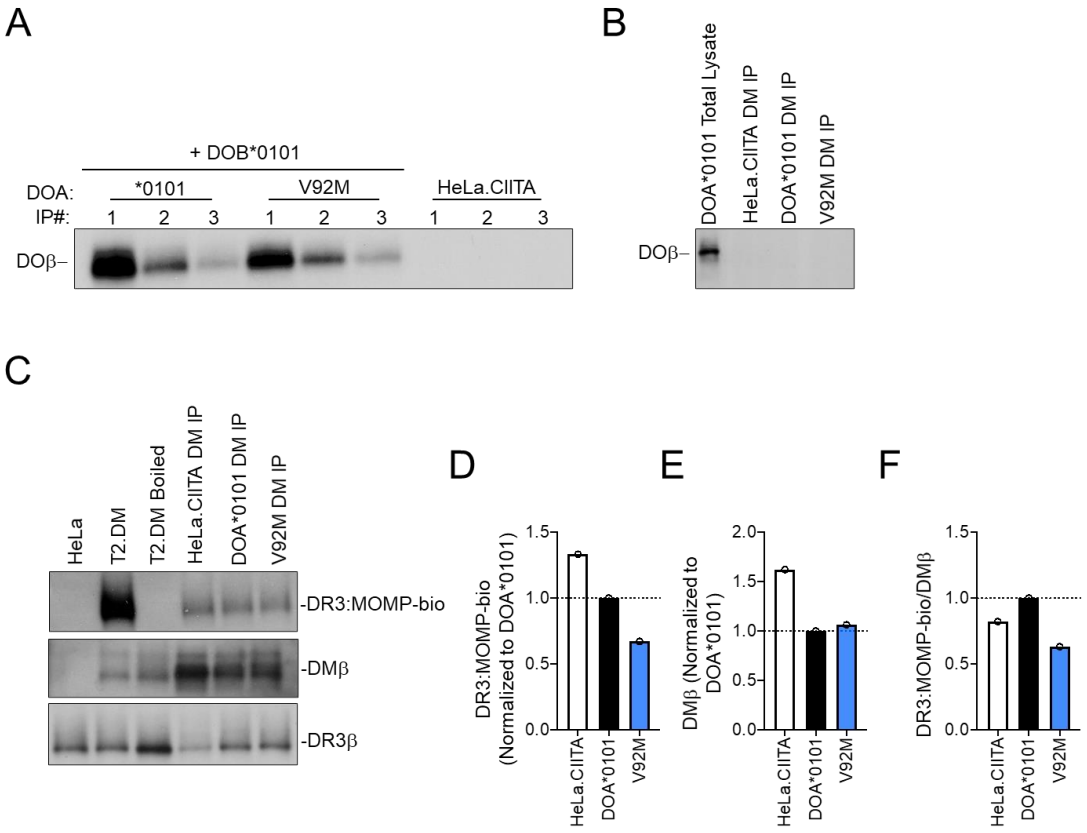

Figure 2.8 Peptide loading assay of free DM from DO expressing cells. **(A)** 1.5 million sorted HeLa.CIITA cells expressing *DOA*0101*/*DOB*0101* or DOα V92M/*DOB*0101*. Untransfected HeLa.CIITA cells were mock depleted as a negative control. **(B)** Free DM from DO depleted supernatant from **(A)** was immunoprecipitated and checked for associated DO. Total lysate from *DOA*0101*/*DOB*0101* expressing cells was used as a positive control for DOβ blotting. **(C)** Free DM from DO depleted supernatant from **(A)** was tested for its ability to load DR3 with MOMP-bio peptide via a peptide loading assay. DM from T2.DM cells was used for loading as a positive control, and DM negative HeLa cells were used as a negative control. This blot was probed for the presence of DR3:MOMP-bio and re-probed for DMβ and free DR3β. **(D)** Quantification of DR3:MOMP-bio from **(C)**, normalized to DOA*0101. **(E)** Quantification of DMβ from **(C)**, normalized to DOA*0101. **(F)** Ratio of DR3:MOMP-bio to DMβ.

Structural Implications of DOA Alleles

The crystal structure of DO bound to DM has been determined [22]. Using this structure, the location of the DOα missense variants analyzed in this study

were mapped onto the DOα crystal structure. The more functional alleles (*DOA*0102*, *DOA*0103*, V92M, R97W, P103T, R124H, G126R, R147C, and H150R) are shown in blue, the less functional missense alleles (I67M and F114L) are shown in red, and alleles that did not affect DO function (S34F, R54H, V115M, and E159K) are shown in white (Fig. 2.9A). Mutations in the signal sequence, transmembrane domain, and cytoplasmic tail of DOA are not shown as these domains were not part of the crystal structure. *DOA*0102*, *DOA*0103*, and DOα I67M are located in the MHCII alpha domain which preferentially interacts with the MHCII beta domain of DOβ (Fig 2.4 and 2.9A). DOα V92M, R97W, P103T, F114L, R124H, G126R, R147C, and H150R are found in the Ig domain of DOα (Figure 2.4 & 2.9A). The Ig domains of DOα and DMα are closely aligned (Fig. 2.9B), an interaction that has been demonstrated to be critical for DO/DM binding via mutagenesis studies [55]. In addition, DM binds to DO similar to how DM binds to MHCII, and mutagenesis of DM showed that residues in the Ig domain of DMα important for DM/MHCII binding make contacts with the Ig domain of DOα [22]. Guce and colleagues defined the contact between the DOα and DMα Ig domains as Interface II, which makes up about one third of the buried surface area of the DM-DO complex [22]. Our screen identified numerous mutations in this region of DOα that resulted in reduced DO expression, which suggests that these mutations interfered with DO-DM binding. Reduced DO expression would then be due to degradation of DO that is not stably bound to DM. It could also be possible that the reduced DO expression of these mutants is due to issues with DO heterodimer stability. However, the DO

crystal structure shows that the Ig domains of DOα and DOβ are not aligned in the same fashion as DOα and DMα (Fig. 2.9C). This observation suggests that mutations in the Ig domain of DOα have more implications for DO:DM interactions and less so for DO heterodimer stability.

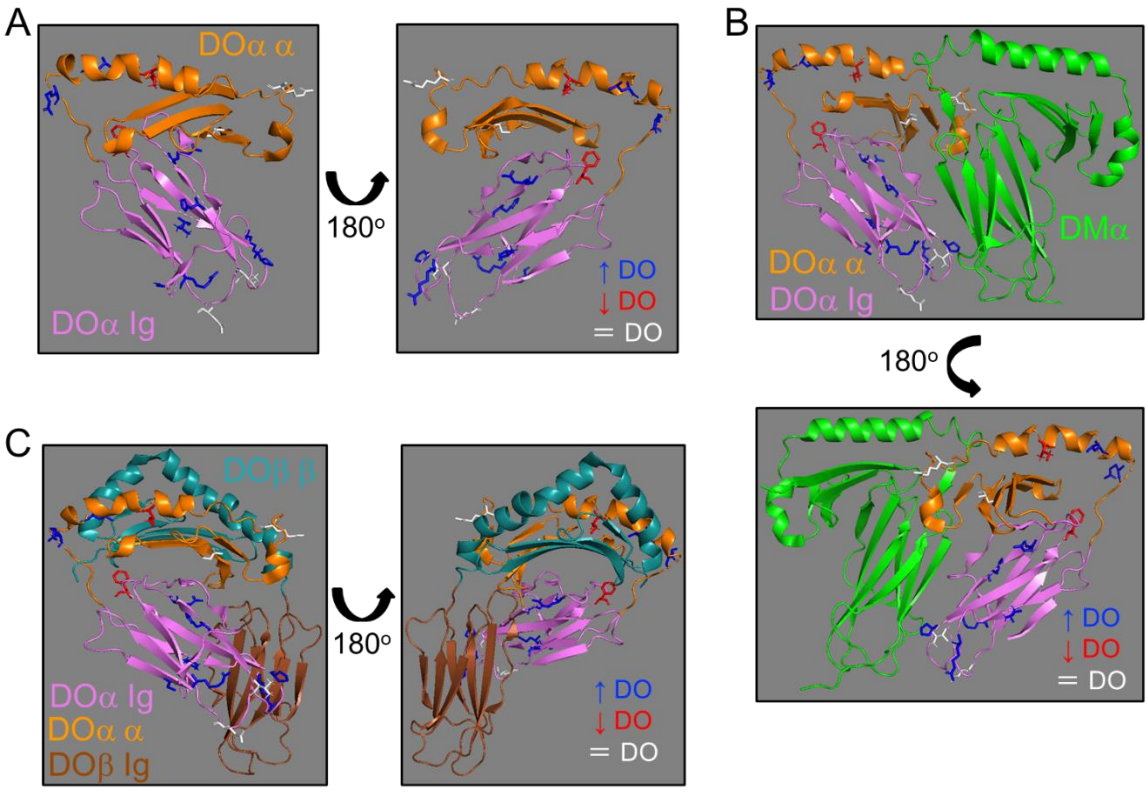

Figure 2.9 Most of the DOα variants with altered function fall within the DOα Ig domain that preferentially interacts with DMα. **(A)** Model of DOα based upon the published DM-DO crystal structure showing the location of DOα variants with higher function (blue), variants with reduced function (red) and variants that did not affect DO function (white). The MHCII alpha-like domain is shown in orange and the Ig domain is shown in pink. The arrow shows the same image but rotated 180° to allow for an additional display of residues. Images were generated using PyMOL. **(B)** As in panel **(A)** with the addition of DMα (green). **(C)** As in panel **(A)** with the addition of DOβ. The MHCII beta-like domain and Ig domain are shown in turquoise and brown, respectively.

DOA variants linked to human hepatitis B viral infection

Evidence is accumulating that DO function has implications for the immune responses against viruses[53, 69]. In mice, a neutralizing Ab response to mouse retroviruses is generated in a strain of mice with a loss of function allele of H2-O and also in H2-O–deficient mice[53]. Conversely, a gain-of-function allele of DOβ (G77V) in humans was genetically linked to individuals with persistent HCV infection[53]. Seven of the DOα variants discovered in the screen described above exhibited a similar enhanced function phenotype to DOβ G77V. Therefore, we searched for possible linkages of these DOA alleles to the outcomes of viral infections in humans.

HLA-DP is one of the polymorphic classical MHCII molecules that have been previously associated with the positive and negative outcomes of viral infections[25]. In individuals from some Asian populations, the 'C' and 'T' SNP rs3077 in *DPA1*, the gene that encodes for the α-chain of HLA-DP, had been previously associated with HBV persistence and Ab-mediated HBV clearance, respectively[70]. Therefore, we asked if any of the DOA alleles that resulted in DO proteins with altered function were in linkage disequilibrium with the specific alleles of *DPA1*. Of the *DOA* alleles identified with altered function, *DOA*0102*, **0103*, and **0104*, DOα F114L, and H150R were associated with known coding region SNPs. Using the LDpair platform tool[71], we found that the rs11575906 SNP in the *DOA*0102* allele was in linkage disequilibrium with the 'C' allele of the rs3077 SNP in *DPA1* (Fig. 2.10). Conversely, the rs34987694 SNP in DOα F114L was in linkage disequilibrium with the 'T' allele of *DPA1* (Fig. 2.10). The

finding that the *DOA* and *DPA1* rsSNPs were in linkage disequilibrium indicates that the specific alleles of *DOA* are as likely as the specific alleles of *DPA1* to impact the immune response to HBV. Importantly, our data therefore support that in the case of HBV, the more functional *DOA*0102* allele may be detrimental to viral immunity, perhaps by impeding the generation of a neutralizing Ab response that contributes to the development of viral persistence. Conversely, the nonfunctional allele DOα F114L may be beneficial by promoting a neutralizing Ab response and viral clearance. However, in the case of the null allele, individuals may need to be homozygous for a beneficial response. Collectively, these data support that naturally occurring variation in *DOA* contributes to the control of human viral immune responses.

Table 2.1 DOA variants linked to certain MHCII genes associated with specific outcomes of HBV infection.

Variant Phenotype (SNP)	**Linked to: Gene (SNP)**	**Linkage Disequilibrium D'**	**Associated Viral Phenotype**
DOA*0102 Gain of Function	HLA-DPA1 (rs3077 – 'C' allele)	1 p<0.0001	HBV Persistence
DOα F114L Loss of Function	HLA-DPA1 (rs3077 – 'T' allele)	1 p<0.0001	Ab-mediated HBV Clearance

Discussion

Peptide loading of MHCII molecules is mediated by DM and modulated by DO. We asked if naturally occurring variation in the DOα subunit of DO impacts function and found several *DOA* missense gene variants with altered function. In comparison with DO formed by the pairing of *DOA*0101* and *DOB*0101*, the two most common alleles of each subunit, two of the other *DOA* common alleles, *DOA*0102* (R80C) and *DOA*0103* (L74V), were found to be more functional. The only other common allele, *DOA*0104* (P11 del FS), was shown to be a functionally null allele as no protein was produced. Naturally occurring haplotypic combinations of the *DOA* and *DOB* common alleles were identified from the 1000GP database and analyzed for functional differences. This analysis showed that *DOA*0102* paired with any of the *DOB* common alleles resulted in DO proteins with increased function. An analysis of 21 rare *DOA* gene variants with single missense mutations located throughout the DOα coding region showed that 10 variants (48%) produced DO proteins that had altered function. Seven variants had enhanced function, one had reduced function, and two did not produce detectable protein. Counterintuitively, all *DOA* variants with altered function that produced an assembled DO protein interacted normally with DM and robustly inhibited MHCII peptide loading despite low DO protein levels for most of the variants. Finally, SNPs in two of the *DOA* gene variants were found to be in linkage disequilibrium with *DPA1*, a classical MHCII allele that was previously associated with the immune response to HBV. These data support

the notion that natural variation in the *DOA* gene may influence the outcomes of chronic viral infections.

Of the four known *DOA* common alleles, 98% of ALL have at least one *DOA*0101* allele[63]. The other three *DOA* common alleles are actually quite uncommon, and only *DOA*0102* was found in >1% of any population[63]. *DOA*0103* and *DOA*0104* should perhaps be considered rare variants and not common alleles. Indeed, the DOα F114L null variant is found at a higher frequency (0.45%) in the 1000GP database than either *DOA*0103* or *DOA*0104*[63]. In contrast, although *DOB*0101* is the predominant allele and is found in ~74% of individuals, the other four common alleles accounted for the remaining 25% of total *DOB* allelic variation. Thus, the *DOA* gene is less polymorphic than DOB, which may indicate that amino acid substitutions in DOβ are better tolerated than changes in DOα. This idea is supported by our previous study showing that all five *DOB* common alleles produced DO proteins that functioned similarly when paired with *DOA*0101*[53]. However, when the *DOB* common alleles were paired with *DOA*0102* in combinations found as naturally occurring haplotypes, all *DOB-DOA*0102* combinations had enhanced function. Thus, changes in DOα altered function, whereas changes in the common DOβ alleles did not. It is not obvious why changes in DOα might be less well tolerated, but it is possible that structural elements in DOα are more prone to local perturbations that lead to altered ab heterodimer formation or disruption of DM–DO interactions.

In addition to examining the functional consequences of polymorphisms in the common *DOA* alleles, we also analyzed DO proteins resulting from the pairing of 21 other naturally occurring *DOA* variants (when paired with *DOB*0101*). The DOα variants chosen for analyses were alleles that were present at higher frequencies from the list of 107 *DOA* variants we had previously identified[53]. The 21 variants had single amino acid changes that were located throughout the DOα coding region and in each of the individual domains of DOα, except for the cytoplasmic tail (Fig. 2.4). Variants that had missense mutations in DOα signal sequence and transmembrane domain were well tolerated and did not impact DO activity. Mutations that impacted DO function were located throughout the MHCII α-like and Ig domains, indicating that these domains both contributed to DO activity. The MHCII α-like domain preferentially associates with the MHCII β-like domain of DOβ, indicating that mutations in this region are likely important for DO heterodimer. Indeed, substitution of a methionine for isoleucine at DOα 67 (DOα I67M) located in the helix (Fig. 2.4B) resulted in increased DO protein. This suggests that a mutation in the MHCII a-like domain produced a DO heterodimer that was more stable and may traffic from the ER partially independent of DM, similar to the previously described DOα P11V variant[43]. The Ig domain of DOα associates closely with the Ig domain of DOβ as well as that of DMα[22] (Fig. 2.4B, 2.9). Seven of the ten variants analyzed with amino acid substitutions in the Ig domain had altered function, and one produced a null protein (DOα F114L). The mutations were located throughout the Ig domain and did not cluster in one particular region of the domain (Fig. 2.4B, 2.9).

Many of the contacts made with DMα are located in this contact region, defined as Interface II, which makes up about one third of the buried surface area of the DM–DO complex[22], suggesting that changes in the DOα domain may disrupt DM–DO interactions. However, the DO proteins produced by these variants maintained interaction with DM and thus many of the mutations identified in this region resulted in reduced DO expression, suggesting they destabilized the DO heterodimer.

DO is an MHCII substrate mimic that binds to DM, thereby preventing DM from interacting with MHCII, facilitating CLIP dissociation, and catalyzing peptide loading[22, 25]. As a consequence, CLIP remains bound to MHCII, resulting in higher levels of MHCII–CLIP in DO-expressing cells[25]. Moreover, DO protein levels directly correlate with MHCII–CLIP levels[25, 37, 39, 53]. The DM–DO crystal structure shows a 1:1 stoichiometry for the DM–DO complex. Therefore, it was unexpected that the DOα variants identified in this screen as having altered function expressed approximately half the amount of DO protein as compared with the control (*DOA*0101*/*DOB*0101*) yet had the similar levels of MHCII–CLIP. Approximately 50% of DM is free (not bound to DO) in primary APCs[37, 66]. Thus, it was possible that expression of DOα and DOβ in HeLa.CIITA by transient transfection resulted in overexpression of DO such that no free DM remained in the cells. However, several lines of evidence support that this was not the case. First, if all DO was complexed with DM (i.e., DM–DO), then the same amount of DM should have been recovered for all DOα variants. However, biochemical analysis showed that less DM was found bound to DO for the DOα

variants that had produced less DO protein (Fig. 2.6C). Second, we previously showed that MHCII–CLIP levels increased in HeLa.CIITA cells that expressed the canonical DOα and DOβ alleles as DO protein levels increased[53], as would be predicted from published literature[25, 37, 39]. Our previous study also identified multiple *DOB* allelic variants that behaved as would be predicted. Several of these *DOB* variants expressed in HeLa.CIITA made reduced DO protein, which resulted in correspondingly lower MHCII–CLIP levels[53]. Finally, the depletion of DO from DO-expressing HeLa.CIITA cell lysates showed that most of the DM remained free of DO in these cells (Fig. 2.6G). What remains unclear, however, is how the DOα gain-of-function variants are able to inhibit DM to the same extent as *DOA*0101*, despite reduced DO protein expression. Nonetheless, it is clear that reduced DO expression results in less DM binding (Fig. 2.6C) and that free DM remains in these cells, but the free DM did not result in efficient CLIP removal from MHCII. While much of the DO expressed in the DOα gain-of-function variants is retained in the ER, this did not result in increased retention of DM in the ER. The results of the peptide loading assay suggests that these gain-of-function variants negatively affect the functionality of the free DM in those cells. While quite unexpected, this result could explain why the gain-of-function mutants are able to inhibit DM similarly to *DOA*0101* despite reduced expression. If these variants are somehow rendering DM less effective, then less DO may be necessary for the same measure of inhibition. This result requires further confirmation and investigation, but overall, this study suggests that DO function may be more complex than previously appreciated.

Uncovering the precise mechanisms by which the DO proteins with altered activity function will require the development of an experimental system that allows for the analysis of *DOA* variants in which all the components of the MHCII Ag processing pathway are present at endogenous levels. Such a system could be achieved by using Crispr-cas9–mediated gene editing to create EBV B cell lines expressing individual *DOA* that have altered activity. Furthermore, the *DOA* variants with altered function identified in this paper are rare variants, and homozygous individuals would be uncommon. Using this system, it would also be possible to create cells in which one chromosome was expressing the canonical *DOA*0101* allele and the other chromosome expressing one of the rare *DOA* gene variants identified in this screen as having altered function. This system could also be used to evaluate previously described alleles of *DOB*, *DMA*, and *DMB* with altered function[53, 64, 72, 73].

The role of the classical MHCII genes in antiviral immunity are well defined and are usually attributed to the efficient presentation of viral-derived peptides on specific MHCII alleles that results in a robust CD4 T cell immune response targeted against the virus. It is well appreciated that other genetic modifiers are encoded in the MHC locus. However, the discovery of these modifiers has been hampered by the density of MHC genes (>140), the strong linkage disequilibrium across the MHC, and the effects of multiple HLA loci. Our previous studies in which we characterized rare, naturally occurring *DOB* gene variants identified a gain-of-function allele (DOβ G77V)[53], with a phenotype similar to the gain-of-function DOα alleles identified in this study. In this study, we showed that DOβ

G77V was associated with an SNP that was in linkage disequilibrium with an SNP located in the *DQA2-DQB2* locus, which had been previously associated with HBV and HCV persistence[53, 74]. The link of viral persistence to the *DQA2-DQB2* locus was assumed to be due to the restriction of peptides presented by this classical MHCII allele, leading to viral persistence. However, our studies showed that viral persistence phenotype could instead be due to altered DO function mediated by the linked DOβ G77V allele. Or in other words, the MHC-encoded DOβ G77V allele was as likely to be the genetic modifier that leads to the viral persistent phenotype as the specific DQ allele. In this study, we similarly identified variant *DOA* alleles with altered function and linked them to the outcome hepatitis B viral infection. A more functional *DOA*0102* allele was associated with an SNP that was in linkage disequilibrium with the C allele of the *DPA1* allele, which had previously been associated with HBV persistence[70]. Conversely, the T allele of the same *DPA1* allele was associated with hepatitis B clearance and the generation of an early neutralizing Ab response[70, 75, 76]. Remarkably, our studies showed that this *DPA1* 'T' allele was linked to the DOα F114L loss-of-function variant. Consequently, as for DOβ G77V, our studies in this article also showed that two *DOA* alleles with altered function were as likely to be the genetic modifiers that leads to the viral clearance or persistent phenotypes as the specific *DPA1* allele that encodes for a classical MHCII presentation molecule.

Most strains of mice are susceptible to the retrovirus MMTV. Our recent studies showed that loss of H2-O function allowed mice to become resistant to

MMTV. The mechanism for resistance was shown to be via the production of a neutralizing Ab response[53]. Although the mouse-based studies allowed us to directly link the neutralizing Ab response to a nonfunctional H2-Oβ protein (mouse DOβ), our studies thus far in humans are based on genetics and thus are correlative. Nevertheless, collectively, our discovery of *DOA* and *DOB* functional gene variants together with our mouse-based studies showing control of the neutralizing Ab response to retroviruses by H2-O supports that the naturally occurring variation in the DO/H2-O genes contributes to the outcome of chronic viral infection in mice and humans.

A

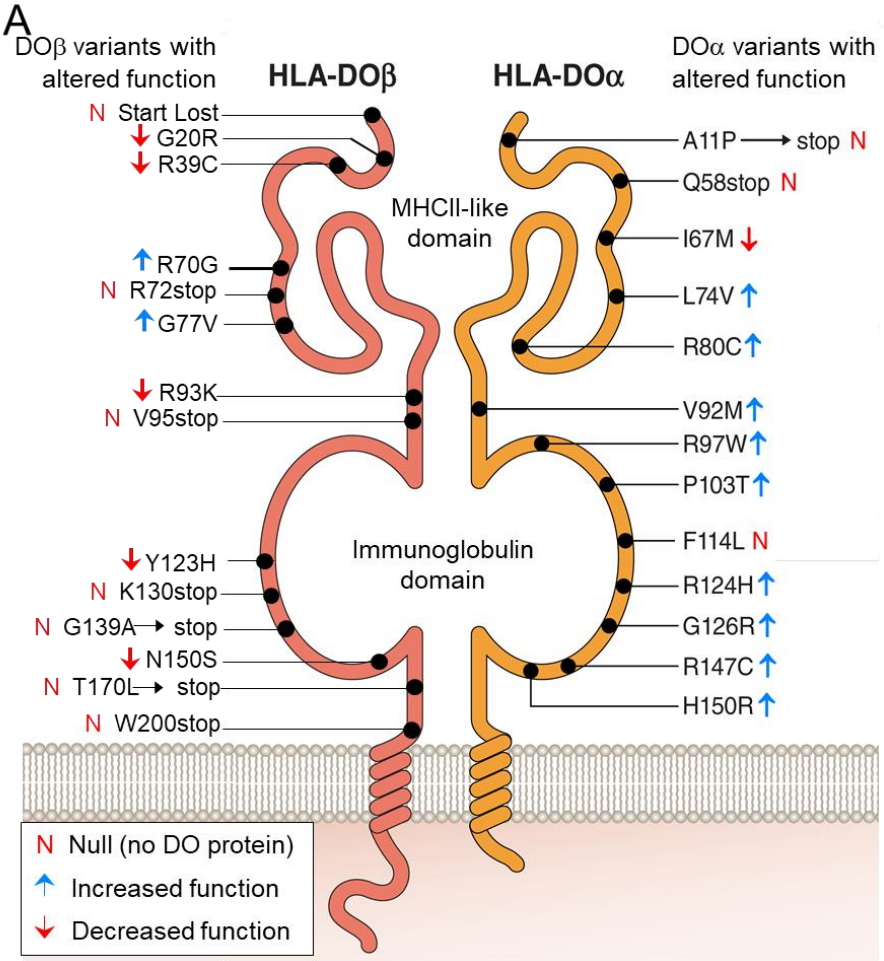

B

Infection phenotype	Linkage to MHCII allele (SNP ID)	Linkage to *DOA* or *DOB* Function (SNP ID)
HBV persistence	HLA-DPA1 rs3077 (G)	DOA*0102 Gain of function rs11575906 (A)
HBV persistence	HLA-DPA1 rs3077 (A)	DOα F114L Loss of function rs34987694 (G)
HCV persistence	HLA-DQB1 Rs4273729 (C)	DOβ G77V Gain of function rs144814623 (G)

Figure 2.10 Summary of *DOA* and *DOB* variant studies. **(A)** Model of DO labeled with each characterized variant found to produce protein with altered function. **(B)** Alleles of *DOA* and *DOB* with altered function were linked to human viral immune responses.

CHAPTER 3: CHARACTERIZING H2-O DOWNREGULATION AS A RESULT OF TLR7 STIMULATION

Introduction

One of the innate immune mechanisms that immune cells can use to detect pathogens are a class of receptors known as toll-like receptors (TLRs)[77]. TLRs are found both intracellularly and extracellularly and recognize different PAMPs. For example, TLR4 expressed on the cell surface and is stimulated by lipopolysaccharide (LPS), which is commonly found on the surface of many bacteria. An example of an intracellular receptor of this type is TLR7, which resides in endosomes and detects single-stranded RNA from viruses. Stimulation of these TLRs contributes to the activation of innate immune cells like macrophages and dendritic cells, which recruit and alert other immune cells to the presence of a pathogen by secreting cytokines and presenting antigens. Activation of these innate immune receptors is an important step for stimulating antigen presentation and generating an adaptive immune response. It is therefore important to understand how molecules involved in antigen presentation are regulated following TLR stimulation.

MHCII presentation on the surface of dendritic cells is known to be upregulated in response to TLR stimulation[78, 79]. A study published by Porter and colleagues characterized the regulation of H2-O in response to various TLR stimulations in CD8α- and CD8α+ dendritic cells as well as B cells. These two populations of dendritic cells display different expression patterns of H2-O and

H2-M. CD8α- dendritic cells express higher H2-M and lower H2-O, while CD8α+ dendritic cells express lower H2-M and higher H2-O[36, 38]. This is consistent with studies that have shown that MHCII presentation is more efficient in CD8α- than CD8α+ dendritic cells[80]. One of the key findings of this study was that when these dendritic cells are stimulated through their toll-like receptors, H2-Oβ, and to a lesser extent H2-M, is downregulated 16h after injection[40]. In contrast to the response in dendritic cells, B cells did not show a reduction in H2-Oβ expression upon TLR7 stimulation. However, H2-Oβ downregulation does occur in B cells upon activation and differentiation into germinal center B cells. This downregulation of H2-Oβ observed in antigen presenting cells upon activation most likely occurs to allow for more efficient loading of MHCII with via H2-M interaction during activation of these cells[40, 79].

Several experiments were performed to further characterize the downregulation of H2-Oβ in response to TLR7 stimulation. TLR7 timecourse stimulation revealed that the downregulation of H2-Oβ begins 8 h after injection. We also attempted to elicit H2-Oβ downregulation in B cells via a series of TLR7 stimulations but were unsuccessful. Finally, we hypothesized that perhaps MMTV interferes with the downregulation of H2-Oβ and tested this by looking for H2-Oβ downregulation in MMTV infected mice following TLR7 stimulation. It would be advantageous for MMTV to have this activity, as TLR7 is the innate immune receptor that senses MMTV viral RNA[81]. If MMTV does have the capability to interfere with H2-O regulation, this could explain why H2-O deficient

mice would be resistant to this activity and thus respond better to MMTV infection. We found that MMTV infection did not interfere with H2-Oβ downregulation in dendritic cells following TLR7 stimulation.

Results

TLR7 stimulation timecourse

When does the downregulation of H2-Oβ in response to TLR7 stimulation begin, and how long does it last? To answer this question, B6 mice were intraperitoneal (IP) injected with 50 μg of the TLR7 agonist, R848, and splenic B cells and dendritic cells were analyzed for H2-Oβ expression at various times after injection (Fig. 3.1.). Splenic B cells were identified in these experiments as B220+ CD11c-, and total splenic dendritic cells (DCs) were B220- CD11c+. Total DCs were divided into CD8α- and CD8α+ DCs (Fig. 3.1A). B cells and dendritic cell populations were checked for extracellular MHCII expression and intracellular H2-Oβ and H2-M expression. H2-O and H2-M expression in B cells did not change 2-16 hours after injections (Fig. 3.1B). B cells began expressing the activation marker CD69 2 h after R848 injection, indicating that TLR7 stimulation was successful (Fig. 3.1B). CD69 expression was not observed 3 days or later after injection (Fig. 3.1E). H2-Oβ downregulation in CD8α+ and CD8α- DCs began 8 h after injection, but slight H2-M downregulation was not observed until 16 h after injection (Fig. 3.1C and 3.1D). H2-Oβ and H2-M expression returned to normal by 3 days after injection (Fig. 3.1F and 3.1G).

These experiments revealed that H2-Oβ downregulation in dendritic cells begins at about 8 h post injection and does not last more than a day.

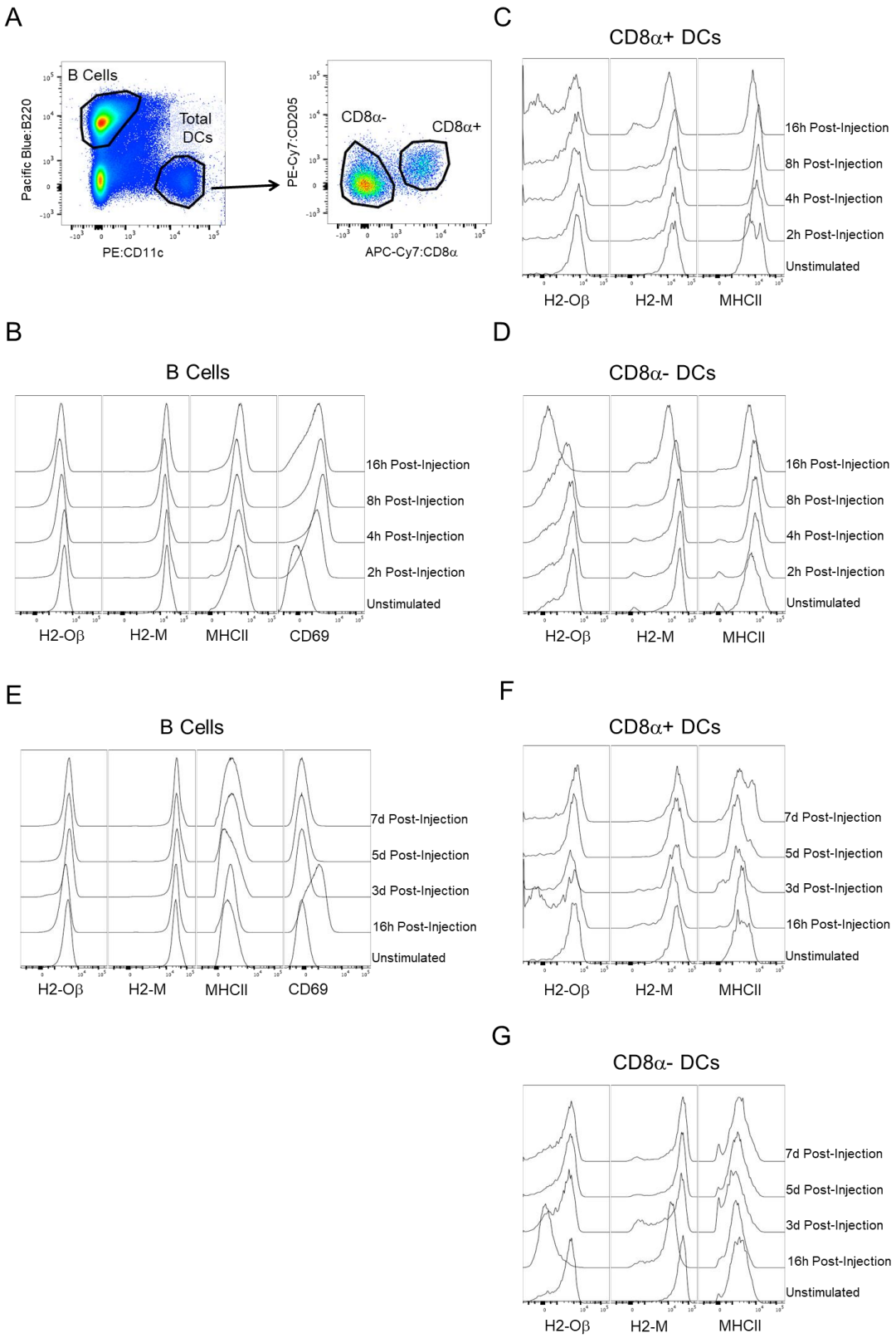
A
B Cells
Total DCs
Pacific Blue:B220
PE:CD11c
CD8α-
CD8α+
PE-Cy7:CD205
APC-Cy7:CD8α
C
CD8α+ DCs
16h Post-Injection
8h Post-Injection
4h Post-Injection
2h Post-Injection
Unstimulated
H2-Oβ
H2-M
MHCII
B
B Cells
16h Post-Injection
8h Post-Injection
4h Post-Injection
2h Post-Injection
Unstimulated
H2-Oβ
H2-M
MHCII
CD69
D
CD8α- DCs
16h Post-Injection
8h Post-Injection
4h Post-Injection
2h Post-Injection
Unstimulated
H2-Oβ
H2-M
MHCII
E
B Cells
7d Post-Injection
5d Post-Injection
3d Post-Injection
16h Post-Injection
Unstimulated
H2-Oβ
H2-M
MHCII
CD69
F
CD8α+ DCs
7d Post-Injection
5d Post-Injection
3d Post-Injection
16h Post-Injection
Unstimulated
H2-Oβ
H2-M
MHCII
G
CD8α- DCs
7d Post-Injection
5d Post-Injection
3d Post-Injection
16h Post-Injection
Unstimulated
H2-Oβ
H2-M
MHCII

Figure 3.1 Mouse TLR7 stimulation timecourse. B6 mice were IP injected with 50 μg of the TLR7 agonist R848, and splenic lymphocytes were analyzed at various times after R848 injection. Unstimulated mice were analyzed as a negative control. Spleen cells were extracellular stained for B220, CD11c, CD8α, CD205, CD69, and MHCII. Samples were then fixed and permeabilized and stained for H2-Oβ and H2-M. **(A)** Representative gating for splenic B cells and Total DCs. Total DCs were further separated into CD8α- and CD8α+ populations. **(B)** H2-Oβ, H2-M, MHCII, and CD69 expression of B cells 2-16 hours after R848 injection. **(C-D)** H2-Oβ, H2-M and MHCII expression of CD8α+ and CD8α- DCs 2-16 hours after R848 injection. **(E)** H2-Oβ, H2-M, MHCII, and CD69 expression of B cells 16 h to 7 days after R848 injection. **(F-G)** H2-Oβ, H2-M and MHCII expression of CD8α+ and CD8α- DCs 16 h to 7 days after R848 injection.

Repeated TLR7 stimulation of B6 mice

As shown in figure 3.1, B cells do not downregulate H2-Oβ in response to TLR7 stimulation. Is it possible to elicit H2-Oβ downregulation in B cells with repeated TLR7 stimulation? Adult B6 mice were repeatedly IP injected with 50 μg of R848 over the course of 7 days, resulting in individual mice which received either 1, 2, 3, 4, and 6 injections (Fig. 3.2A). H2-Oβ staining of splenic B cells from these mice revealed that H2-Oβ downregulation did not occur despite repeated R848 injection (Fig. 3.2B). Interestingly, CD69 expression was only found increased B cells that received a single dose of R848 1 day before analysis. B cells from mice that had received as many as 6 consecutive injections did not express CD69, indicating that they had potentially become desensitized to R848. Regardless, we were not able to successfully reduce H2-O expression in B cells with TLR7 stimulation alone.

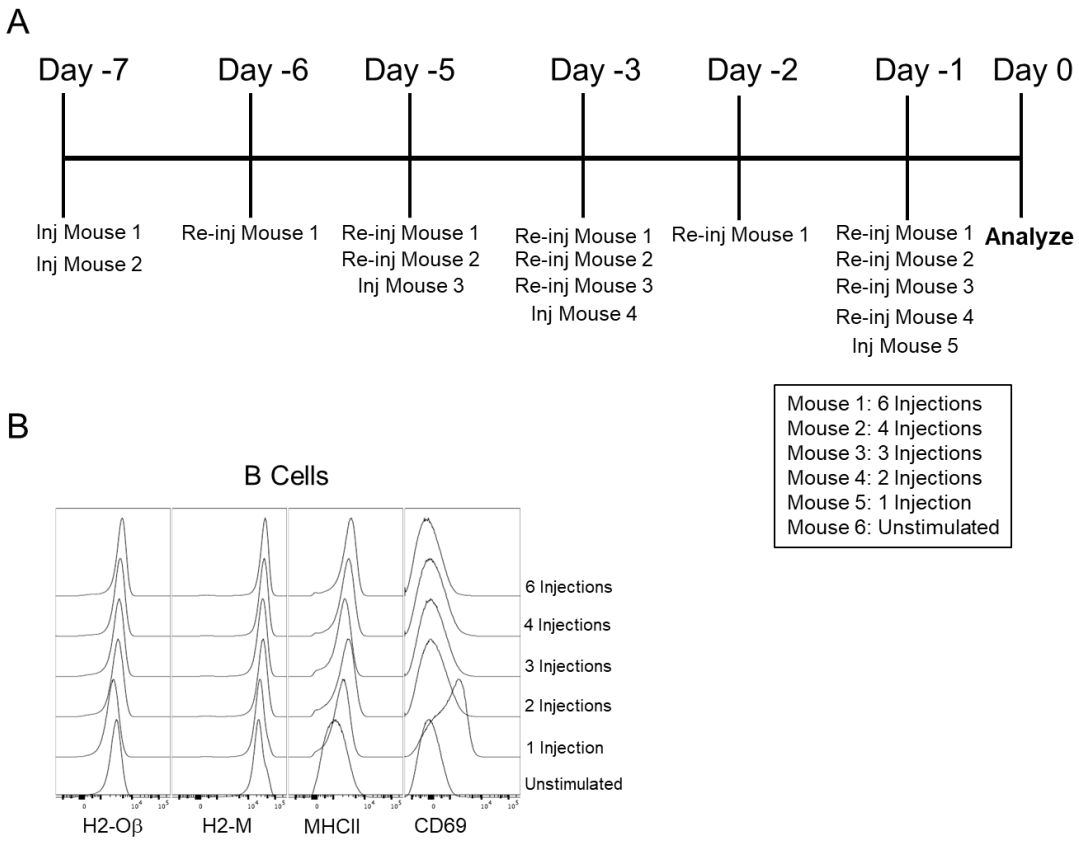

Figure 3.2 The effect of repeated TLR7 stimulation on splenic B cells. **(A)** Six B6 mice were given consecutive injections of 50 μg of R848 according to this schedule. **(B)** Splenic B cells from each mouse from **(A)** were checked for H2-Oβ, H2-M, MHCII, and CD69 expression.

TLR7 stimulation of MMTV infected mice

H2-O downregulation in response to TLR7 stimulation is particularly interesting in the context of MMTV infection because TLR7 is the innate immune receptor that recognizes MMTV viral RNA. We know that H2-O is somehow involved in blocking the neutralizing antibody response to MMTV, therefore we hypothesized that perhaps MMTV interferes with H2-Oβ downregulation the occurs after TLR7 stimulation in dendritic cells. This would be interesting, as it

would indicate that MMTV requires H2-O's modulation of antigen presentation to successfully evade a neutralizing antibody response. We tested this by investigating the capability of DCs in MMTV infected mice to downregulate H2-Oβ after TLR7 stimulation. A chronically MMTV infected B6 mouse was IP injected with 50 μg of R848 and splenic B cells and dendritic cells were analyzed 16 h later. An unstimulated, uninfected mouse was used as a negative control. As was observed in previous experiments with naïve mice, H2-Oβ was downregulated in CD8α- and CD8α+ dendritic cells from chronically MMTV infected (Fig. 3.3B and 3.3C), but not B cells (Fig 3.3A). CD69 expression on B cells indicated that these cells were successfully stimulated by R848 injection. H2-M expression was slightly reduced in dendritic cells as well (Fig. 3.3B and 3.3C). Overall, the responses of B cells and dendritic cells in MMTV infected mice to R848 injection did not differ from those responses in uninfected mice.

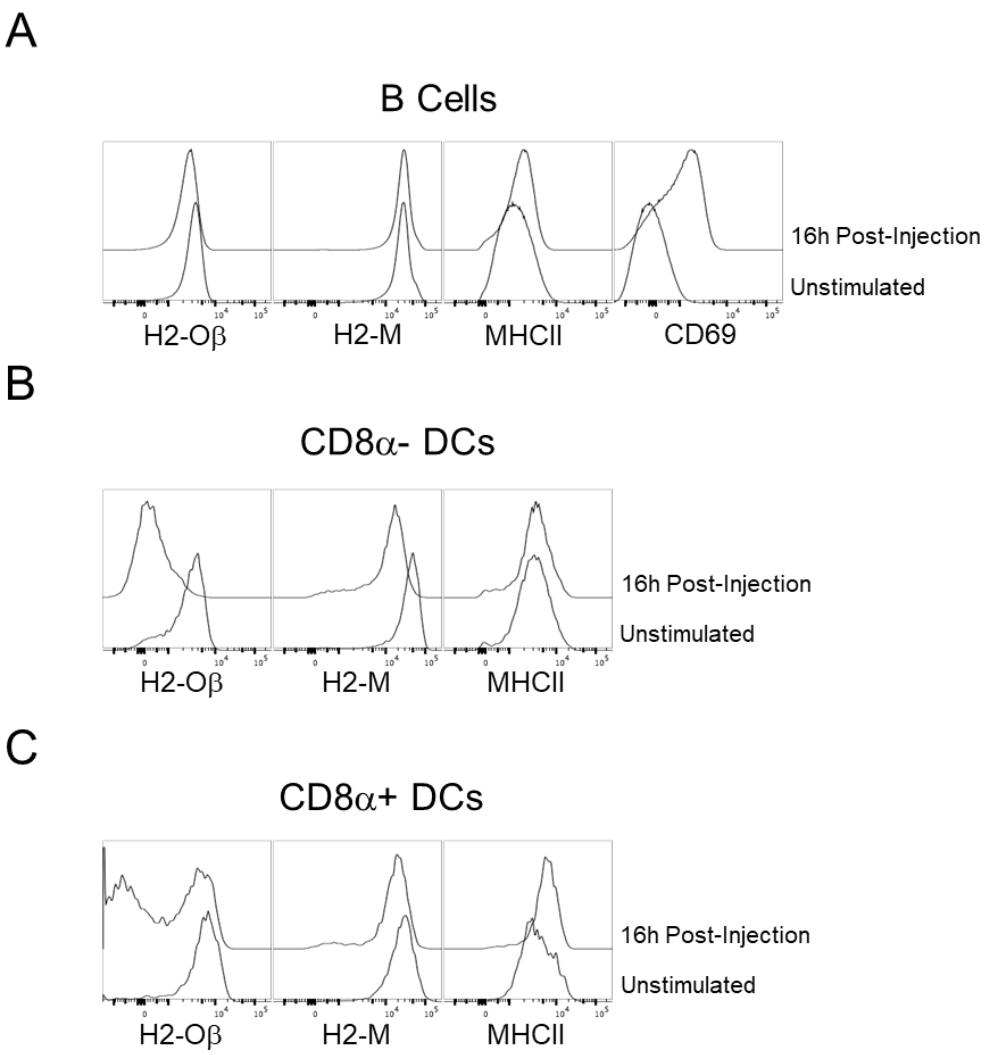

Figure 3.3 TLR7 Stimulation of MMTV infected mice. A chronically infected B6 mouse was IP injected with 50 μg of R848 and splenic B cell and dendritic cells were analyzed 16 h later as described in Fig. 3.1. **(A)** Stimulated B cells compared to unstimulated, uninfected control. B cells were checked for H2-Oβ, H2-M, MHCII, and CD69 expression. **(B-C)** Stimulated CD8α- and CD8α+ dendritic cells compared to unstimulated, uninfected control. Dendritic cells were checked for H2-Oβ, H2-M, and MHCII expression.

Discussion

The above experiments helped to further characterize the timing of H2-Oβ downregulation in dendritic cells after stimulation through TLR7. We found that

H2-Ob downregulation in these cells begins 8 hours after R848 injection, but these effects are short lived and are not detected 3 days later. We also attempted to force downregulation of H2-Oβ in B cells with repetitive TLR7 stimulation, which was unsuccessful. B cells are known to downregulate H2-O expression upon differentiation into germinal center B cells[39], which is a process that requires stimulation through the B cell receptor and stimulation from a helper T cell. It is likely that only stimulating B cells through TLR7 with no second stimulus does not reach the threshold necessary to elicit H2-O downregulation.

We also found that H2-O downregulation in dendritic cells was unaffected by MMTV infection. One important caveat to this result is that we do not currently have a method for identifying cells undergoing active MMTV infection by flow cytometry. It is possible that in dendritic cells during active MMTV infection do not downregulate H2-O as well as uninfected dendritic cells. It is also possible that MMTV interferes with H2-O downregulation as B cells differentiate into GC B cells, but again, we would need to stain for H2-O in cells actively infected with MMTV. Experiments like this will have to wait until we have better reagents.

CHAPTER 4: COMPARING THE INNATE IMMUE RESPONSES OF H2-O DEFICIENT AND SUFFICIENT B CELLS IN COMPETITION

Introduction

Much our recent research has focused on determining what effects differences H2-O deficiency has on antigen presenting cells. In the context of MMTV infection, we know that H2-O deficient mice respond with an effective

neutralizing antibody response. Neutralizing antibodies are, of course, secreted by B cells, and our collaborators have found that transferring H2-O deficient B cells into WT mice and infecting said mice with MMTV successfully generates a neutralizing antibody response. It is for these reasons, that we hypothesized that perhaps there are intrinsic differences between H2-O deficient and sufficient B cells. Preliminary studies investigated B cell receptor signaling in H2-O deficient and sufficient B cells. We cross-linked B cell receptors *in vitro* and analyzed phosphorylation of the signaling protein spleen tyrosine kinase (Syk), which is directly downstream of the B cell receptor in the B cell receptor signaling pathway[82]. Our *in vitro* experiments suggested that p-Syk was reduced in H2-O deficient B cells, so we moved to *in vivo* experiments to verify these results. However, in vivo stimulation of B cells showed the opposite result, with enhanced p-Syk in H2-O deficient B cells. These conflicting results led us to use a different experimental approach to answer these questions.

A key issue with our preliminary experiments is that there could have been variability in the stimuli that the H2-O deficient and sufficient mice were receiving. To cut down on this kind of uncertainty, a better experiment would be to stimulate H2-O deficient and sufficient B cells together in the same mouse. Our previous studies have already demonstrated that the optimal environment for determining differences between WT and H2-O deficient B cells is where the two can compete[83]. In a study published by Draghi et al, antigen specific H2-O deficient and WT B cells were placed in a competitive environment and examined during an adaptive immune response. These studies were performed using B cells from

H2-O deficient and sufficient B1-8^{hi} knock-in mice[84]. B1-8^{hi} knock-ins possess a B1-8 immunoglobulin heavy chain which, when combined with a λ light chain, forms a B cell receptor (BCR) that is specific for the small aromatic hapten, NP[84]. B cells with the NP specific BCR constitute 5-10% of the total B cell population in the spleen. WT and H2-O deficient NP-specific B cells were mixed and transferred into B6 mice. These chimeras were immunized with NP-CCG, which activates NP-specific B cells in a T-dependent manner. When the resulting germinal centers were analyzed, H2-O deficient B cells were found to preferentially inhabit the germinal center. T cell proliferation assays found that NP-specific H2-O deficient B cells present antigen to CD4+ T cells better that H2-O sufficient cells. This finding explains how NP-specific H2-O deficient cells are preferentially inhabiting the germinal center, as entry into and cycling through the germinal center is dictated by the capability of B cells to present antigen[85, 86, 87]. Furthermore, the discrepancy between H2-O deficient and sufficient B cells in the germinal center was alleviated when the authors transferred excess T cells into these mice as well, which revealed that H2-O deficient B cells were outcompeting WT B cells for T cell help to enter the germinal center[83].

These findings led us to investigate potential differences between H2-O deficient and WT B cells when activated in an innate, T-independent manner. As discussed in the previous chapter, LPS is found on the surface of many bacteria, and it is recognized by the innate immune receptor TLR4. B cells require two activations signals to become fully activated, the first signal being BCR stimulation by antigen binding, and the second signal being either binding by an

activated T cell or stimulation through an innate immune receptor. NP-CGG induces a T-dependent activation of B cells because the second signal comes from binding of activated T cells (specific to NP-CGG) to antigen specific B cells. NP-LPS however induces a T-independent response because the second signal comes from TLR4 activation. T-dependent B cell activation induces the eventual development of plasma cells which secrete high affinity, class switched antibodies, a process which can take up to 7 days. T-independent B cell activation instead induces differentiation into plasmablasts, which develop much quicker than plasma cell but secrete lower affinity antibodies for a shorter amount of time.

Another motivator for comparing the responses of WT and H2-O deficient B cells to LPS is due to the fact that MMTV comes coated in LPS from the intestinal microbiota[88]. The effect of this is that it induces IL-6 secretion which induces expression of the inhibitory cytokine, IL-10[88]. Based on this finding, it would be very interesting if H2-O deficient B cells responded differently to stimulation by NP-LPS than WT B cells, and may draw us closer to understanding the differential responses these cells have to MMTV infection.

Results

Splenocytes from B1-8 WT (CD45.1/.2) and B1-8 H2-Oa$^{-/-}$ (CD45.1) were isolated and stained to determine the frequency of NP-specific B cells (CD19+ NP+). Based on the frequency of NP-specific B cells in the WT and H2-Oa$^{-/-}$ (Oa$^{-/-}$) samples, a 50/50 mix of NP-specific B cells was transferred into B6 (CD45.2) mice via intravenous (IV) injection. Twenty-four hours later, chimeric mice were

stimulated with 100 μg of NP-LPS via IP injection, and splenocytes of these mice were analyzed 3, 4, and 5 days after injection (Fig. 4.1).

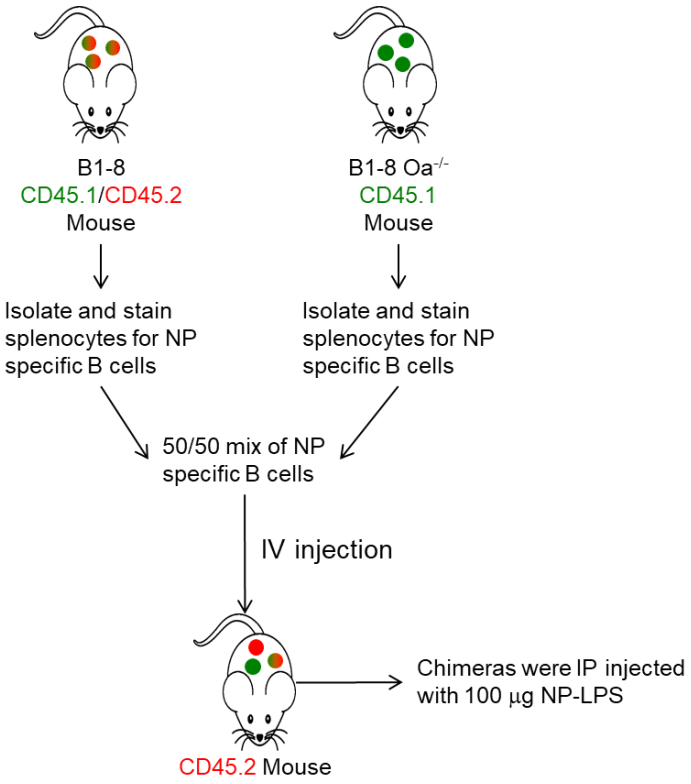

Figure 4.1 Diagram of splenocyte chimera set up. Splenocytes from B1-8 WT CD45.1/.2 and B1-8 $Oa^{-/-}$ CD45.1 mice were isolated and stained for NP-specific B cells. Splenocytes from these mice were mixed to form a 50/50 mix of NP-specific B cells, up to a maximum of 20 million total cells. Mixes of cells were IV injected into WT CD45.2 mice.

In each of the experiments performed, one chimera was not injected with NP-LPS. These unstimulated mice were used as an assumed baseline for the mix of NP-specific WT and $Oa^{-/-}$ B cells transferred into the other members of each cohort pre-injection (Fig. 4.2A). In this particular cohort, 30.1% of the NP+ $CD19^{high}$ cells were CD45.1/.2, indicating that these were B1-8 WT cells. 67.1% of these cells were CD45.1, which were B1-8 $Oa^{-/-}$ cells. We also examined the

frequency of B1-8 $Oa^{-/-}$ and B1-8 WT cells that were CD19-, which remain unchanged as these cells should be unaffected by NP-LPS injection. We then investigated how the frequencies of B cells changed after NP-LPS injection (Fig. 4.2B). We observed an expansion of NP-specific B cells in immunized mice, indicating that the stimulation was successful. B1-8 $Oa^{-/-}$ cells made up 69.1% of the NP+ $CD19^{high}$ population, a slight increase from the uninjected control. In the immunized mice, a new population of NP+ $CD19^{low}$ cells appeared. These are most likely plasmablasts, as these cells are known to expresses an intermediate amount of CD19 when compared to naïve B cells[89]. B1-8 $Oa^{-/-}$ cells made up 78.4% of this NP+ $CD19^{low}$ population, an increase of over 10% compared to the uninjected control. This result could indicate that H2-O deficient B cells were outpacing WT B cells in plasmablast formation. In order to quantify and compare these results over several experiments, the ratio of $Oa^{-/-}$ to WT cells in each population was calculated and normalized to the ratio of the corresponding population in the unstimulated mouse (Fig. 4.2C). Plasmablast frequencies had to be normalized to the NP+ CD19+ frequencies of unstimulated mice since these mice did not have plasmablasts. As we expected, the ratio of $Oa^{-/-}$ to WT CD19- cells did not significantly change after injection. We also did not observe a significant change in the ratio of $Oa^{-/-}$ to WT cells in the NP+ $CD19^{high}$ population. However, a significant increase in the frequency of $Oa^{-/-}$ cells in the NP+ $CD19^{low}$ population 3 and 5 days after NP-LPS injection was observed.

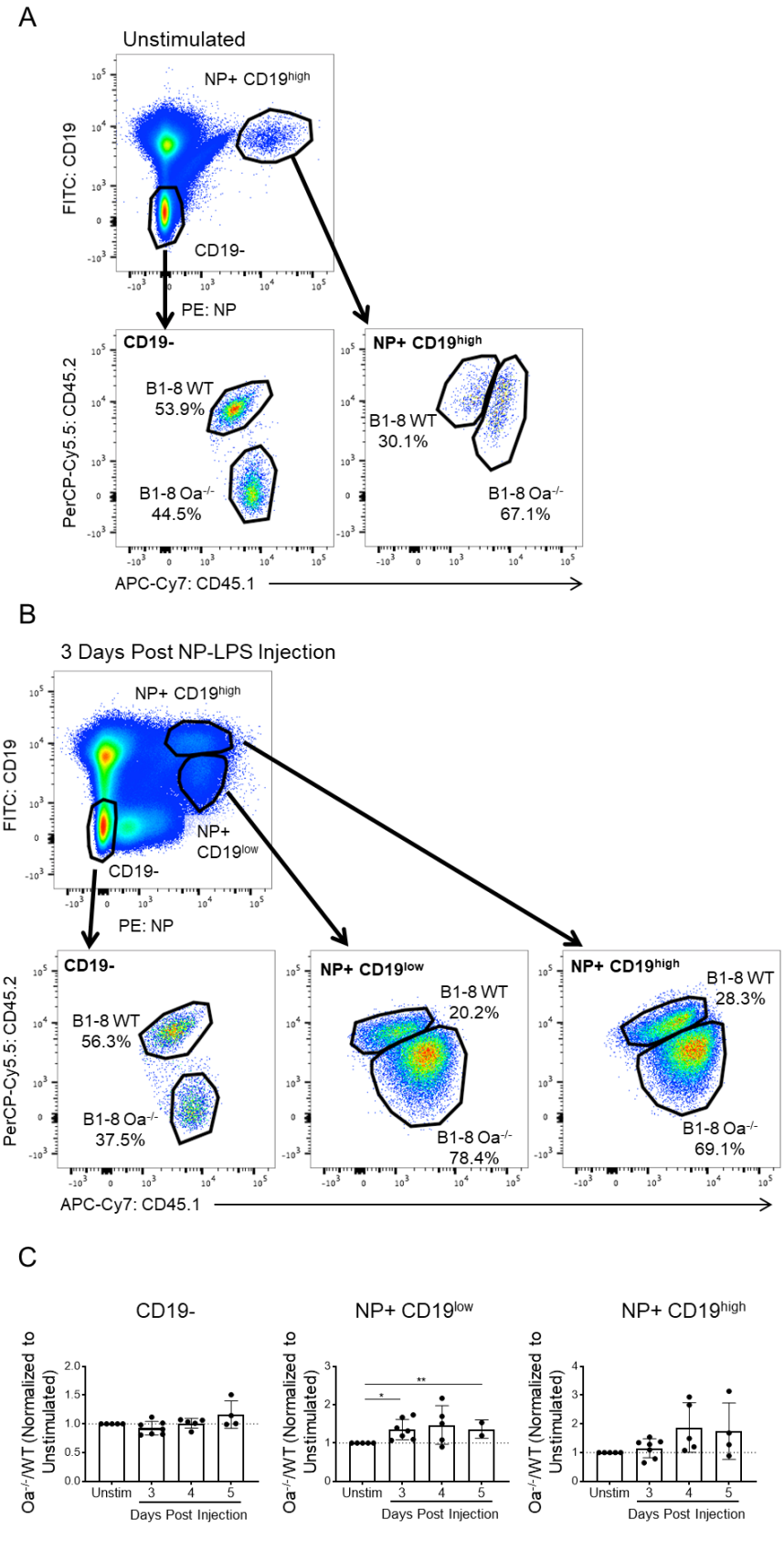
A
Unstimulated
NP+ CD19high
FITC: CD19
CD19-
PE: NP
CD19-
B1-8 WT
53.9%
B1-8 Oa-/-
44.5%
NP+ CD19high
B1-8 WT
30.1%
B1-8 Oa-/-
67.1%
PerCP-Cy5.5: CD45.2
APC-Cy7: CD45.1
B
3 Days Post NP-LPS Injection
NP+ CD19high
NP+
CD19low
FITC: CD19
CD19-
PE: NP
CD19-
B1-8 WT
56.3%
B1-8 Oa-/-
37.5%
NP+ CD19low
B1-8 WT
20.2%
B1-8 Oa-/-
78.4%
NP+ CD19high
B1-8 WT
28.3%
B1-8 Oa-/-
69.1%
PerCP-Cy5.5: CD45.2
APC-Cy7: CD45.1
C
CD19-
NP+ CD19low
NP+ CD19high
Oa-/-/WT (Normalized to Unstimulated)
Unstim
3
4
5
Days Post Injection
*
**

Figure 4.2 Analysis of splenocyte chimeras after NP-LPS injection. **(A)** Baseline chimerism for each cohort is established by an unstimulated chimera which shows a mix of B1-8 WT (CD45.1/.2) and B1-8 $Oa^{-/-}$ (CD45.1) in the CD19- and NP+ $CD19^{high}$ populations. **(B)** NP-specific B cells in splenocyte chimeras expand after 100 μg NP-LPS injection. CD19-, NP+ $CD19^{high}$, and NP+ $CD19^{low}$ populations contained a mix of B1-8 WT (CD45.1/.2) and B1-8 $Oa^{-/-}$ (CD45.1) cells. **(C)** Normalized ratios of $Oa^{-/-}$ derived cells to WT derived cells in each population 3, 4, or 5 days after NP-LPS injection. Significance was calculated with an unpaired, two-tailed, Student t test. Data is from 6 independent experiments.

Discussion

We hypothesized that $Oa^{-/-}$ B cells would be more responsive to NP-LPS injection than WT B cells and found that this is most likely not the case. The activation of B cells through NP-LPS works independently of any T cell interaction, meaning that the MHCII presentation is not involved in this process. Therefore, H2-O should not have had any effect on this process. That being said, future studies investigating the difference in pathogenesis of MMTV in WT and H2-O deficient mice may need to examine plasmablasts in these mice. Research has shown that plasmablasts formed during MMTV infection make up the majority of infected B cells in WT mice[90]. Future experiments should investigate the presence of plasmablasts in H2-O deficient mice during MMTV infection. Perhaps these plasmablasts do not form as easily in H2-O deficient mice during MMTV infection.

CHAPTER 5: COMPARING THE INTESTINAL IMMUNE SYSTEMS OF H2-O DEFICIENT AND SUFFICIENT MICE

Introduction

A question central to our study of H2-O is how and why does it block the neutralizing antibody response to MMTV? The challenge in answering this question comes from the finding that wild type (WT) and H2-O deficient mice do not display obvious differences in their peripheral immune system when infected with MMTV. It is understood that only H2-O deficient mice are able to produce an effective antibody response, but this is not accompanied by an expected increase in germinal center (GC) B cells or T follicular helper cells in the spleen.

Peyer's patches are lymphoid follicles found along the small intestine, especially the distal ileum. These follicles are composed of germinal centers containing GC B cells and T follicular helper cells, which are surrounded by the subepithelial dome containing a mix of B cells, T cells, and myeloid cells. The whole follicle is surrounded by follicle-associated epithelium (FAE), where specialized microfold (M) cells transport luminal antigen to the follicle which leads to either tolerance or an immune response to organisms in the gut[91, 92]. Due to their close interaction with the gut flora, Peyer's patches have been studied in the pathogenesis of diseases like Crohn's disease, graft versus host disease, *Salmonella* infection, and ulcerative colitis[91, 92, 93, 94, 95]. The Peyer's patches are also an important site of MMTV infection[90, 96]. As was discussed previously, MMTV infection spreads from infected mothers to their newborn pup through viral particles in her milk. Infection in newborn pups begins when the virus infects the

Peyer's patches of the small intestine. It is here where the virus first establishes itself before eventually spreading to the mesenteric lymph nodes, and eventually all lymphoid organs[96]. As MMTV makes its way throughout the secondary lymphoid organs, the infection in the Peyer's patches is maintained into adulthood[97]. We currently do not have a way to stain for intracellular MMTV by flow, we cannot inspect cells that are undergoing active infection. Since MMTV infection begins in the gut, analyzing Peyer's patches allows us to access an environment where the immune system is much more active and MMTV infection may be more concentrated. It is for these reasons that we decided to investigate the Peyer's patches to explore potential differences between WT and H2-O deficient mice, both naïve and MMTV infected.

The following studies revealed that the composition of H2-O deficient Peyer's patches differ significantly from Peyer's patches of WT mice. These differences included total cell number and GC B cell, T follicular helper cell, T regulatory cell (Treg), T follicular regulatory cell, and activated T cell frequencies. However, these differences appeared to be dependent on age. Additionally, MMTV infected WT Peyer's patches were significantly different from naïve WT Peyer's patches, but not OKO Peyer's patches. We also compared Peyer's patches from OKO and WT mice after cross-fostering on MMTV infected mothers, which interestingly did not reveal significant differences.

Results

Analysis of Peyer's patches in young mice

We began by analyzing spleen and Peyer's patch lymphocytes from C57BL/6J (WT), C57BL/6J *H2-Ob* deficient ($Ob^{-/-}$), and MMTV infected WT (WT.MMTV) mice. The experiments in this section were performed with 6 week old mice, which were a mix of male and female. Spleen and Peyer's patch samples were stained with fluorescent antibodies and analyzed by flow cytometry. Samples were divided in half and one half was stained with a panel of antibodies recognizing B cell subsets and the other half a panel specific for T cell subsets. The B cell panel consisted of CD45, CD19, CD38, Fas, GL7, MHCII, and CLIP, and the T cell panel consisted of CD45, CD4, CD19, CD44, CD62L, CXCR5, PD-1, and FoxP3. The cells stained with the B cell mix were analyzed alive, while the cells stained with the T cell mix underwent fixation and nuclear permeabilization in order to stain for the transcription factor, FoxP3. When dissecting the Peyer's patches from these mice, it was apparent that the Peyer's patches from the $Ob^{-/-}$ and WT.MMTV mice were larger than those found in the WT mice. This finding is reflected in the total number of live cells that were analyzed from Peyer's patches from each group (Fig. 5.1A). Significantly more live cells were recovered from $Ob^{-/-}$ and WT.MMTV infected Peyer's patches as compared to WT Peyer's patches. This was a very encouraging result, as it could indicate that the intestinal immune system is more active in $Ob^{-/-}$ mice which may prime these mice to respond to MMTV infection in the Peyer's patches.

As was discussed earlier, no difference in GC B cell frequency is observed in the spleens of WT.MMTV mice when compared to uninfected mice (Fig. 5.1C). However, when we looked to the Peyer's patches, there were significantly more GC B cells in WT.MMTV Peyer's patches compared to WT uninfected Peyer's patches. This was the case both in terms of frequency and total cell number (Fig. 5.1D). Surprisingly, $Ob^{-/-}$ Peyer's patches had significantly more GC B cells than WT both in frequency and total cell number (Fig. 5.1D). This is a very exciting result, as it suggests that there may be differences in the development of the intestinal immune system in $Ob^{-/-}$ mice. This may prime these mice to better respond to MMTV infection and thus mount a neutralizing antibody response.

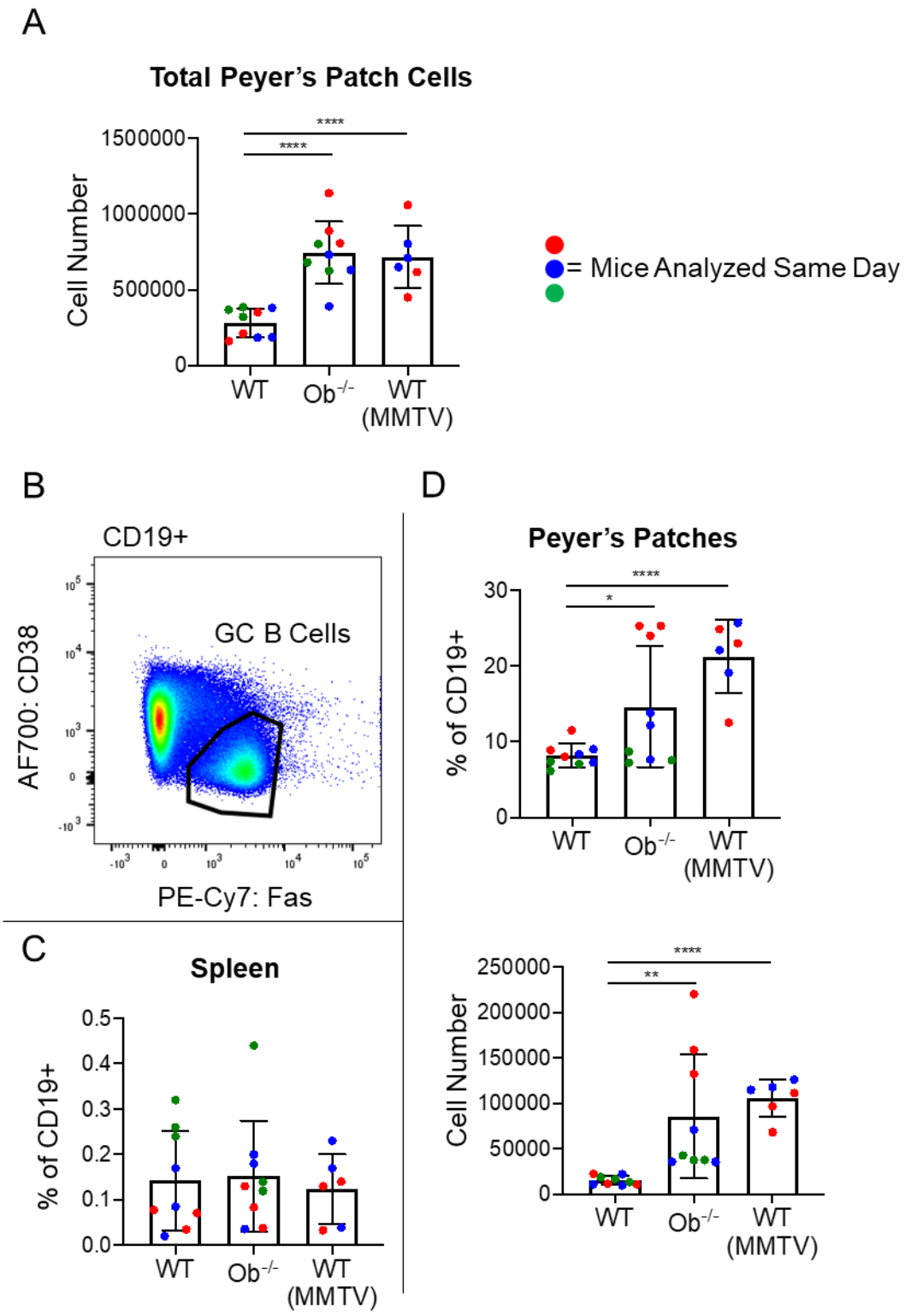

Figure 5.1 Live staining data from 6 week old spleen and Peyer's patches. **(A)** Total number of live lymphocytes collected from Peyer's patch samples. **(B)** Representative gating of germinal center B cells. Germinal center B cells were

defined as CD19+ cells that were Fas+ and CD38-. **(C)** Quantification of splenic germinal center B cells as a percentage of all CD19+ cells. **(D)** Quantification of Peyer's patch germinal center B cells as a percentage of all CD19+ cells (upper panel) and as total cell number (lower panel). Circles of like colors indicates mice that were analyzed on the same day. Significance was calculated with an unpaired, two-tailed, Student t test.

If the observed difference in GC B cells between WT and $Ob^{-/-}$ mice is legitimate, then we would expect to see a similar difference in T follicular helper cells as well. As discussed previously, T follicular helper cells assist GC B cells by secreting cytokines that help maintain germinal centers and by supporting the survival of the highest affinity B cells that will go on to secrete antibodies. T follicular helper cells are defined as CD4+ T cells that express PD-1 and CXCR5 (Fig. 5.2A). As was observed with GC B cells in the spleen, there was no differences between the three groups in the frequency of T follicular helper cells in the spleen (Fig. 5.2B). We did however see significant differences in the frequency and total cell number of T follicular helper cells in the Peyer's patches. $Ob^{-/-}$ mice had significantly more T follicular helper cells than WT mice, and WT.MMTV mice had significantly more T follicular helper cells than both WT and $Ob^{-/-}$ (Fig. 5.2C).

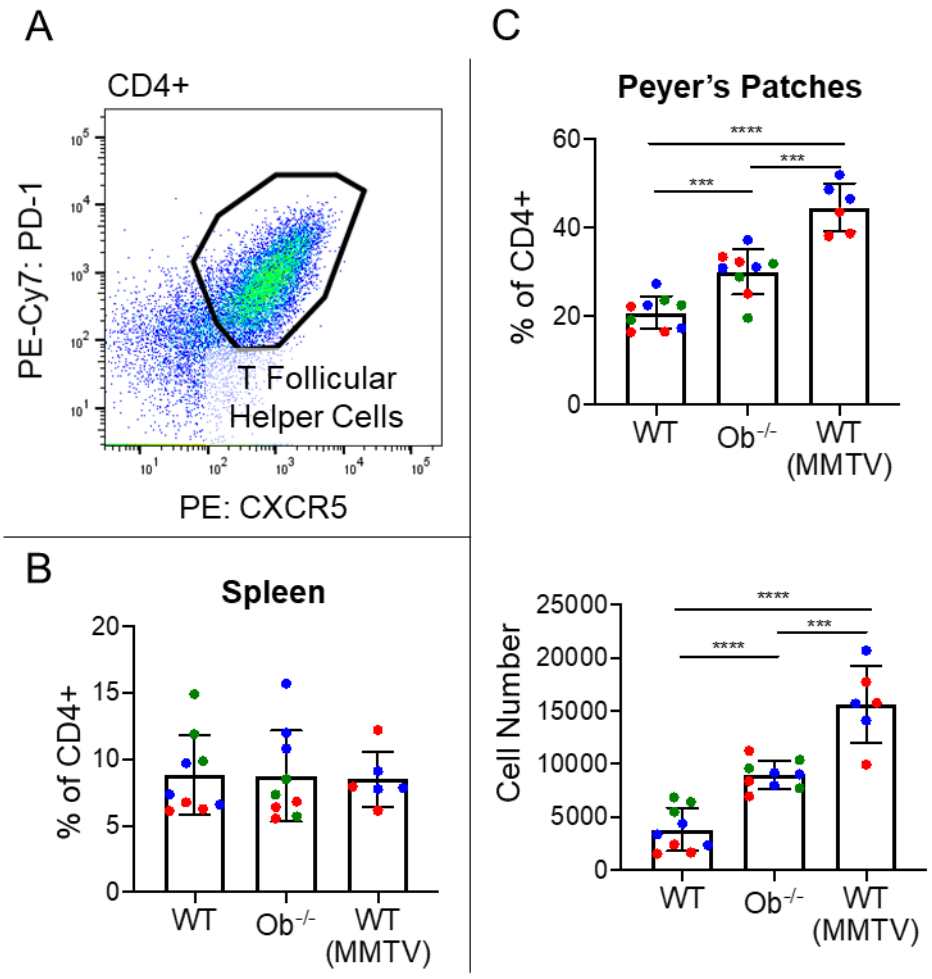

Figure 5.2 T follicular helper cell staining data from the spleen and Peyer's patches of 6 week old mice. **(A)** Representative gating of T follicular helper cells. T follicular helper cells were defined as CD4+ T cell which express PD-1+ and CXCR5+. **(B)** Quantification of splenic T follicular helper cells as a percentage of all CD4+ cells. **(C)** Quantification of Peyer's patch T follicular helper cells as a percentage of all CD4+ cells (upper panel) and as total cell number (lower panel). Circles of like colors indicates mice that were analyzed on the same day. Significance was calculated with an unpaired, two-tailed, Student t test.

We further investigated the T cell landscape in the Peyer's patches of these mice by staining for the T cell activation markers CD62L and CD44. Activated T cells can be identified as CD62L- and either CD44+ or CD44-. For the purposes of examining all activated T cells, we classified all CD62L- CD4+ T

cells as activated (Fig. 5.3A). No differences in activated T cell populations were found between WT, Ob$^{-/-}$, and WT.MMTV spleens (Fig. 5.3B). Consistent with our previous results, Ob$^{-/-}$ and WT.MMTV Peyer's patches showed significantly more activated T cells than WT both in percentage of CD4+ T cells and total cell number (Fig. 5.3C).

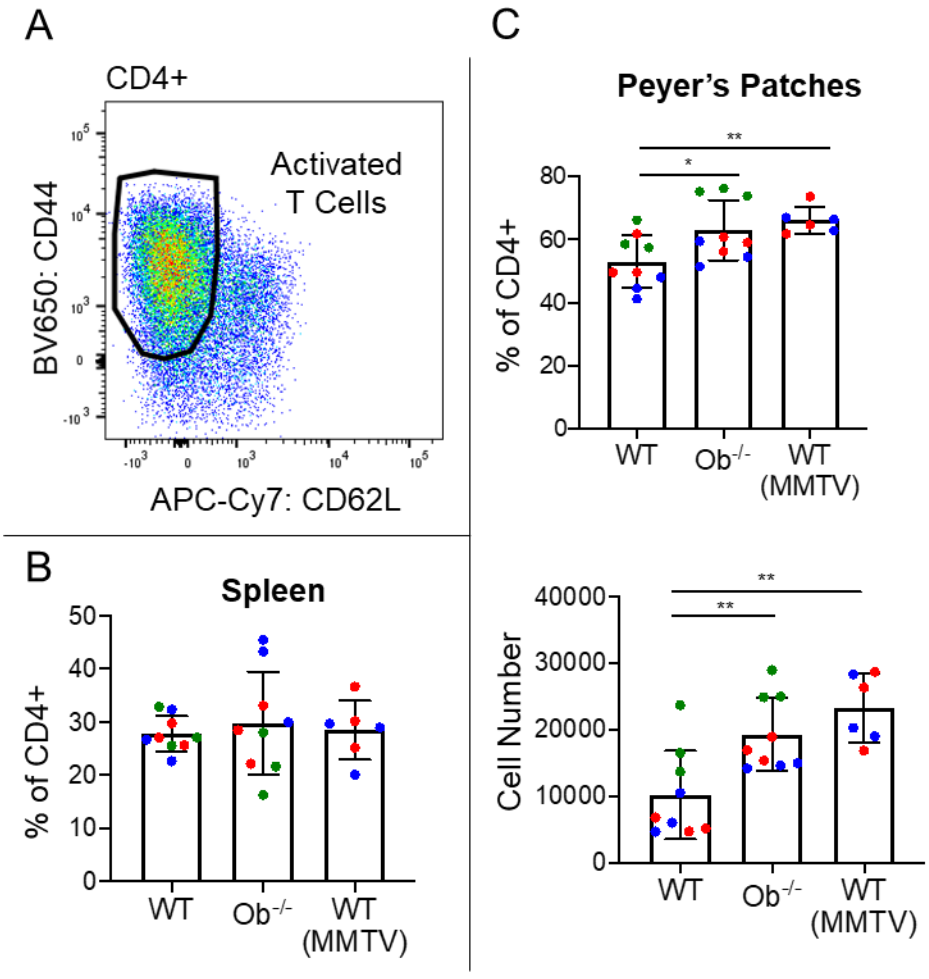

Figure 5.3 Activated T cell staining data from the spleen and Peyer's patches of 6 week old mice. **(A)** Representative gating of activated T cells. Activated T cells were defined as CD4+ T cells which were CD62L-. **(B)** Quantification of splenic activated T cells as a percentage of all CD4+ cells. **(C)** Quantification of Peyer's patch activated T cells as a percentage of all CD4+ cells (upper panel) and as total cell number (lower panel). Circles of like colors indicates mice that

were analyzed on the same day. Significance was calculated with an unpaired, two-tailed, Student t test.

We next asked if there were differences in Tregs between WT, $Ob^{-/-}$, and WT.MMTV mice. So far we have found more overall immune activation in the Peyer's patches of $Ob^{-/-}$ and WT.MMTV mice, evidenced by the increase in activated T cells and GC B cells. We would then expect there to be a reduction in Tregs in these mice compared to WT Peyer's patches, as Tregs negatively regulate immune activity through secretion of the inhibitory cytokine IL-10 and through cell-cell interaction. We identified Tregs by staining CD4+ T cells for the transcription factor FoxP3, which is required Treg differentiation (Fig. 5.4A). Once again, no difference was observed in the spleens of these mice, but analysis of the Peyer's patches showed a significant reduction in the frequency of Tregs in WT.MMTV Peyer's patches compared to WT and $Ob^{-/-}$ (Fig. 5.4B and 5.4C).

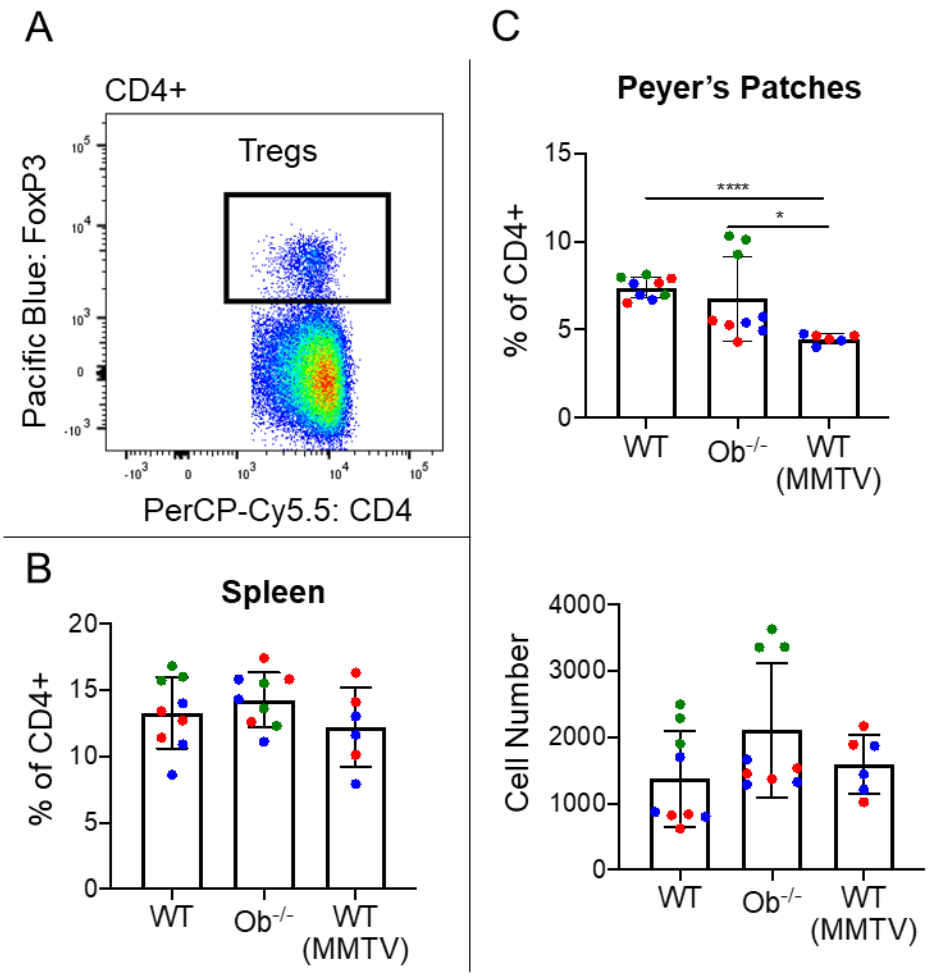

Figure 5.4 Treg staining data from the spleen and Peyer's patches of 6 week old mice. **(A)** Representative Treg gating. Tregs were defined as CD4+ T cells which expressed FoxP3. **(B)** Quantification of splenic Tregs as a percentage of all CD4+ cells. **(C)** Quantification of Peyer's patch Tregs as a percentage of all CD4+ cells (upper panel) and as total cell number (lower panel). Circles of like colors indicates mice that were analyzed on the same day. Significance was calculated with an unpaired, two-tailed, Student t test.

The final population of cells we analyzed in these experiments were T follicular regulatory cells. These are either Tregs that enter the follicle, or T follicular helper cells that differentiate into Tregs and suppress the germinal center response[98, 99]. It has also been reported that T follicular regs accumulate in germinal centers over time and are important for germinal center contraction[98].

T follicular regs were identified by staining T follicular helper cells for the transcription factor FoxP3 (Fig. 5.5A). We observed no differences in T follicular regs between WT, $Ob^{-/-}$, and WT.MMTV spleens (Fig. 5.5B). The frequency of these cells in the spleen was found to be ~30% of T follicular helper cells, which is consistent with the low frequency of GC B cells in the spleen (Fig. 5.5B and 5.1C). In the Peyer's patches, which demonstrated a much higher frequency of GC B cells (Fig. 5.1D), the frequency of T follicular regulatory cells was reduced. WT Peyer's patches, in which we observed the lowest frequency of GC B cells, had significantly more T follicular regs than $Ob^{-/-}$ and WT.MMTV Peyer's patches (Fig. 5.5C). It is not surprising to see a reduction in these cells in WT.MMTV Peyer's patches because these follicles are undergoing an active MMTV infection. However, it is surprising that $Ob^{-/-}$ Peyer's patches had significantly reduced T follicular regs. These results, combined with the increase in total Peyer's patch cells, GC B cells, activated T cells, and T follicular helper cells strongly suggests that the intestinal immune system in $Ob^{-/-}$ mice is more active than in WT mice.

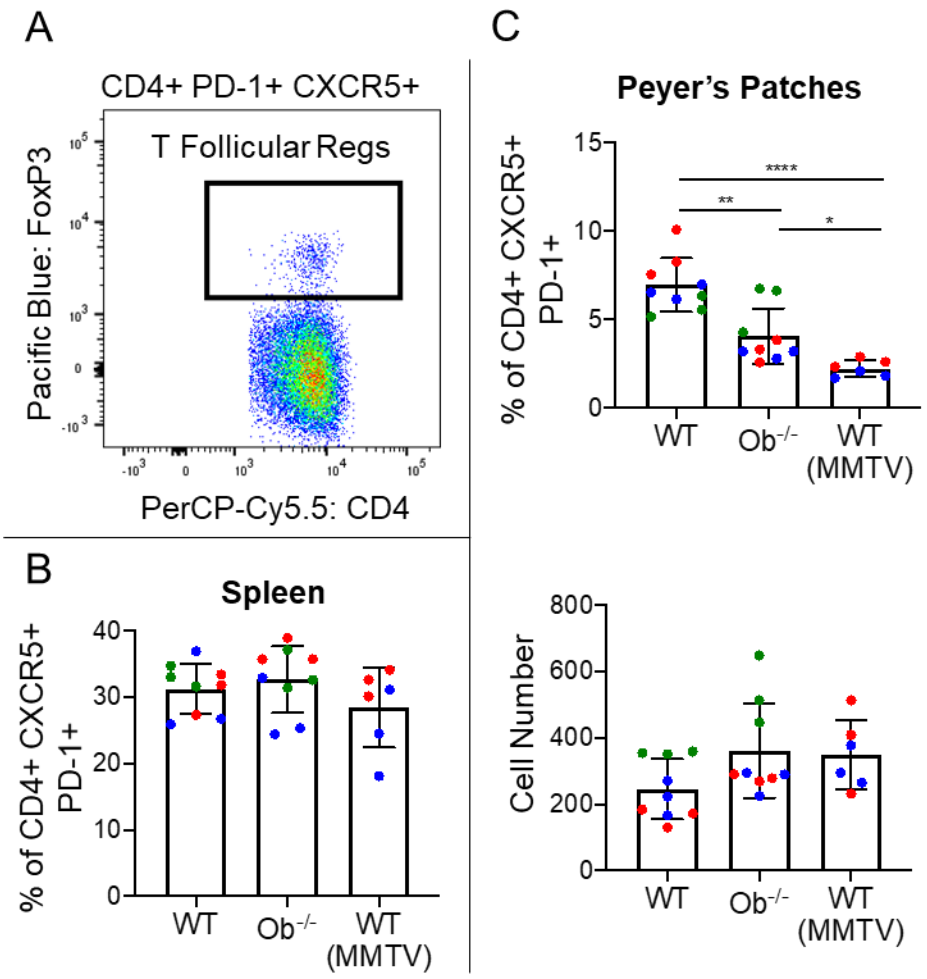

Figure 5.5 T follicular regulatory cell staining data from the spleens and Peyer's patches of 6 week old mice. **(A)** Representative gating of T follicular regs. T follicular regs were defined as CD4+ PD-1+ CXCR5+ which expressed FoxP3. **(B)** Quantification of splenic T follicular regs as a percentage of all T follicular helper cells. **(C)** Quantification of Peyer's patch T follicular regs as a percentage of all T follicular helper cells (upper panel) and as total cell number (lower panel). Circles of like colors indicates mice that were analyzed on the same day. Significance was calculated with an unpaired, two-tailed, Student t test.

Analysis of Peyer's patches of 11-24 week old mice

We also investigated spleens and Peyer's patches of older WT, OKO, and WT.MMTV mice. Due to limited mouse availability during the pandemic, we performed one experiment with $Oa^{-/-}$ mice and another was performed with $Ob^{-/-}$

mice. The mice analyzed in this section varied in age, ranging from 11 weeks old to 24 weeks old and were a mix of male and female. Interestingly, many of the striking differences we observed between WT and $Ob^{-/-}$ 6 week old mice were not observed in these older mice. Unlike in 6 week old mice, there were no differences in the total number of live lymphocytes in the Peyer's patches of WT, $Oa^{-/-}$, $Ob^{-/-}$, and WT.MMTV mice (Fig. 5.6A). WT.MMTV mice had a significantly higher frequency of GC B cells in the spleen when compared to WT uninfected mice, and $Ob^{-/-}$ mice had a significantly higher frequency of GC B cells than WT or $Oa^{-/-}$ mice (Fig. 5.6B). Analysis of the Peyer's patches of these mice showed a reduction of GC B cells in OKO mice compared to WT, a reversal of the trend seen in the 6 week old mice. WT.MMTV maintained a higher frequency of GC B cells. No differences were observed between samples in terms of total GC B cell number in the Peyer's patches (Fig. 5.6B).

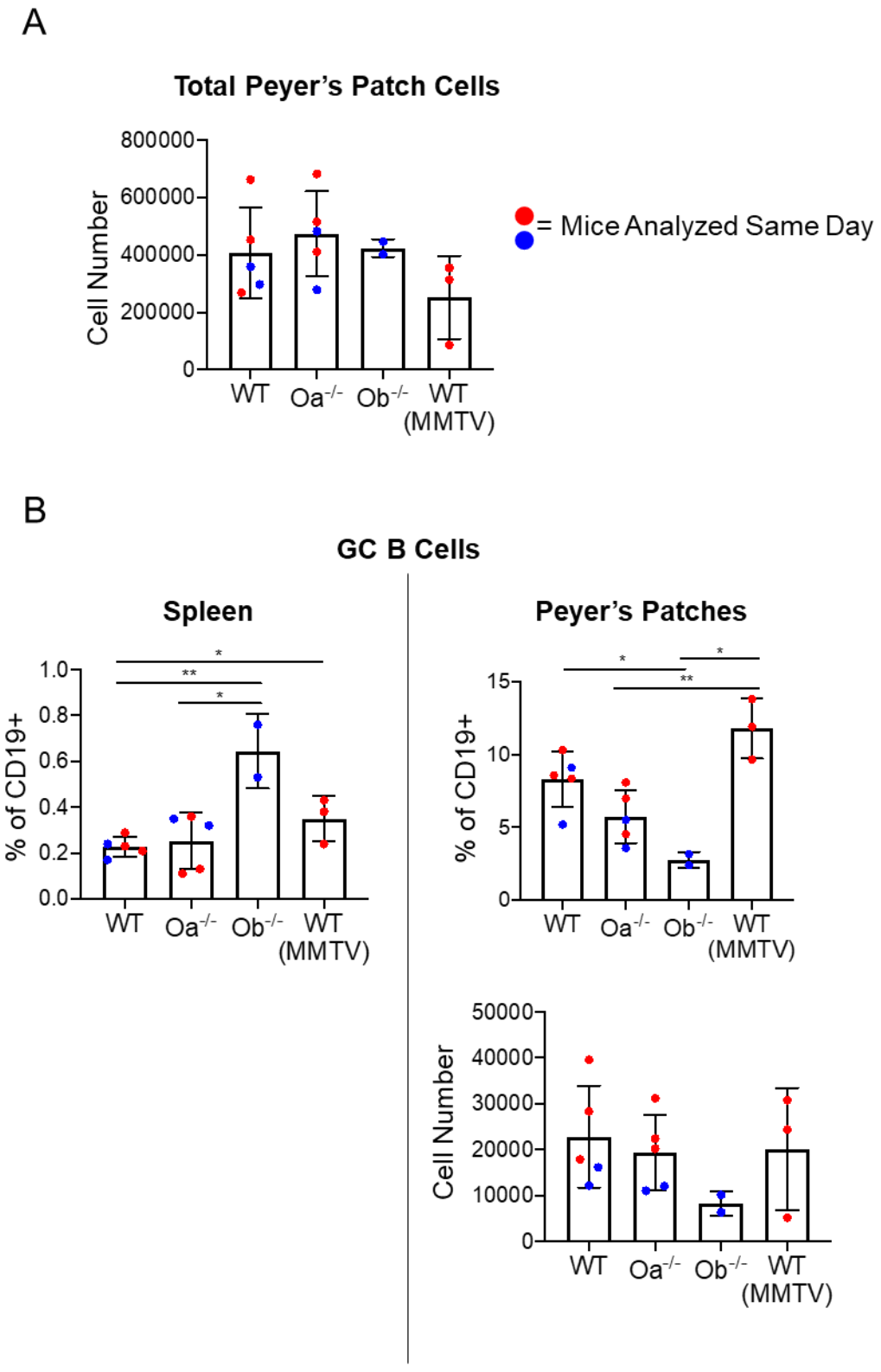

Figure 5.6 Live cell staining data from 11-24 week old spleen and Peyer's patches. **(A)** Total number of live lymphocytes collected from Peyer's patch

samples. **(B)** Quantification of splenic and Peyer's patch germinal center B cells as a percentage of all CD19+ cells and total cell number. Circles of like colors indicates mice that were analyzed on the same day. Significance was calculated with an unpaired, two-tailed, Student t test.

We then analyzed the T follicular helper cells in the spleen and Peyer's patches of 11-24 week old mice. While we did see a reduction of T follicular helper cells in the spleens of WT.MMTV mice, we saw no difference in the frequency of T follicular helper cells in the Peyer's patches of these mice (Fig. 5.7).

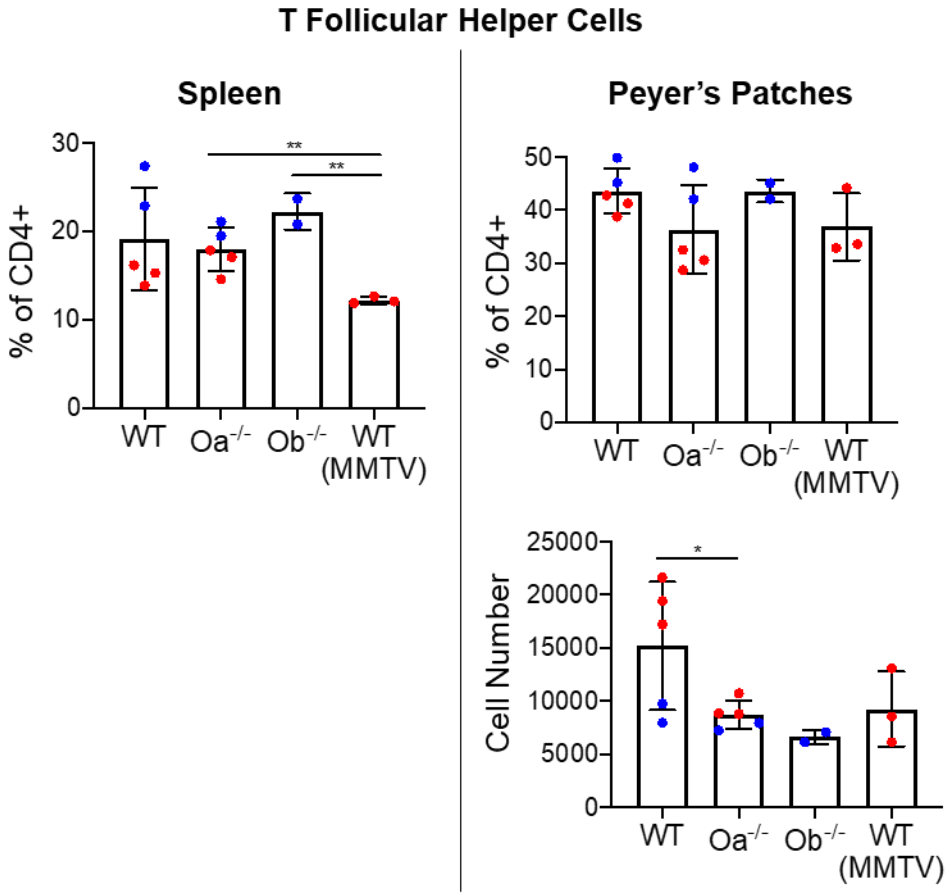

Figure 5.7 T follicular helper cell staining data from 11-24 week old spleen and Peyer's patches. Quantification of splenic and Peyer's T follicular helper cells as a percentage of all CD4+ cells and total cell number. Circles of like colors

indicates mice that were analyzed on the same day. Significance was calculated with an unpaired, two-tailed, Student t test.

Staining for activated T cells in 11-24 week old spleens and Peyer's patches contrasted with the results obtained from 6 week old mice. H2-O deficient and MMTV infected mice no longer displayed significantly more activated T cells in their Peyer's patches when compared to WT mice (Fig. 5.8).

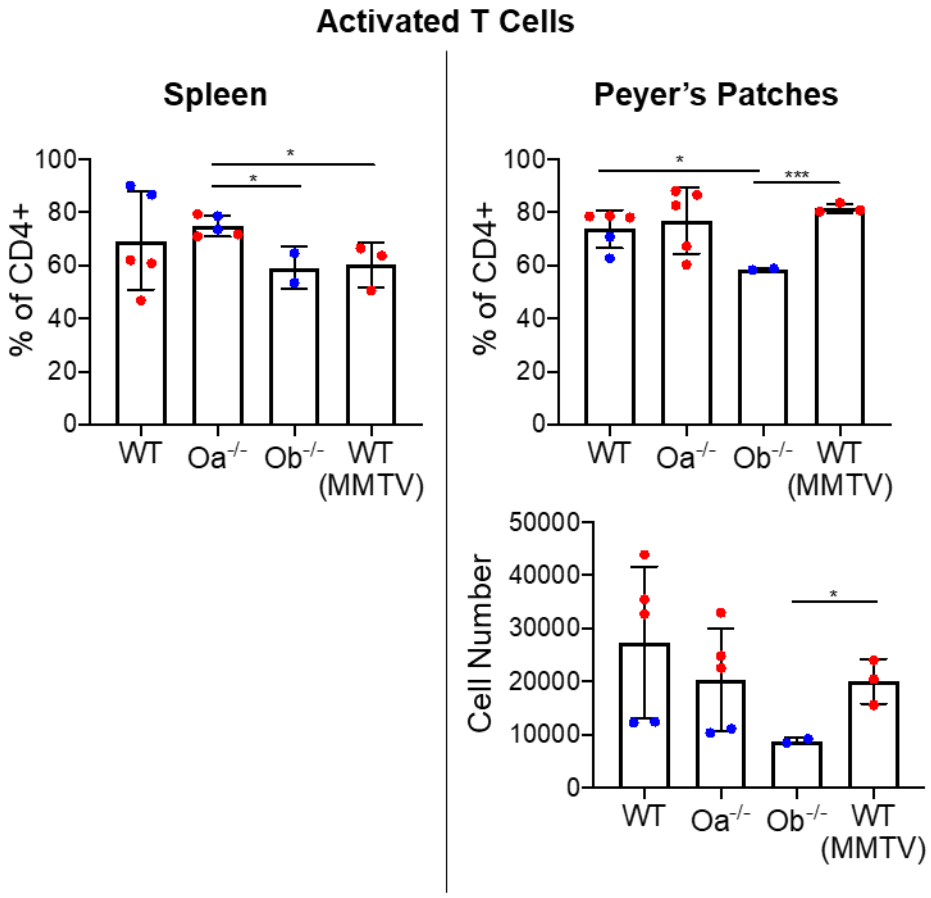

Figure 5.8 Activated T cell staining data from 11-24 week old spleen and Peyer's patches. Quantification of splenic and Peyer's Activated T cells as a percentage of all CD4+ cells and total cell number. Circles of like colors indicates mice that were analyzed on the same day. Significance was calculated with an unpaired, two-tailed, Student t test.

We observed no significant differences in the frequency of Tregs between WT and H2-O deficient mice. The WT mice in this experiment did show significantly more Tregs in terms of total cell number in the Peyer's patches. It is also worth noting that the MMTV infected mice analyzed in this experiment had the lowest frequency and total number of Tregs (Fig. 5.9).

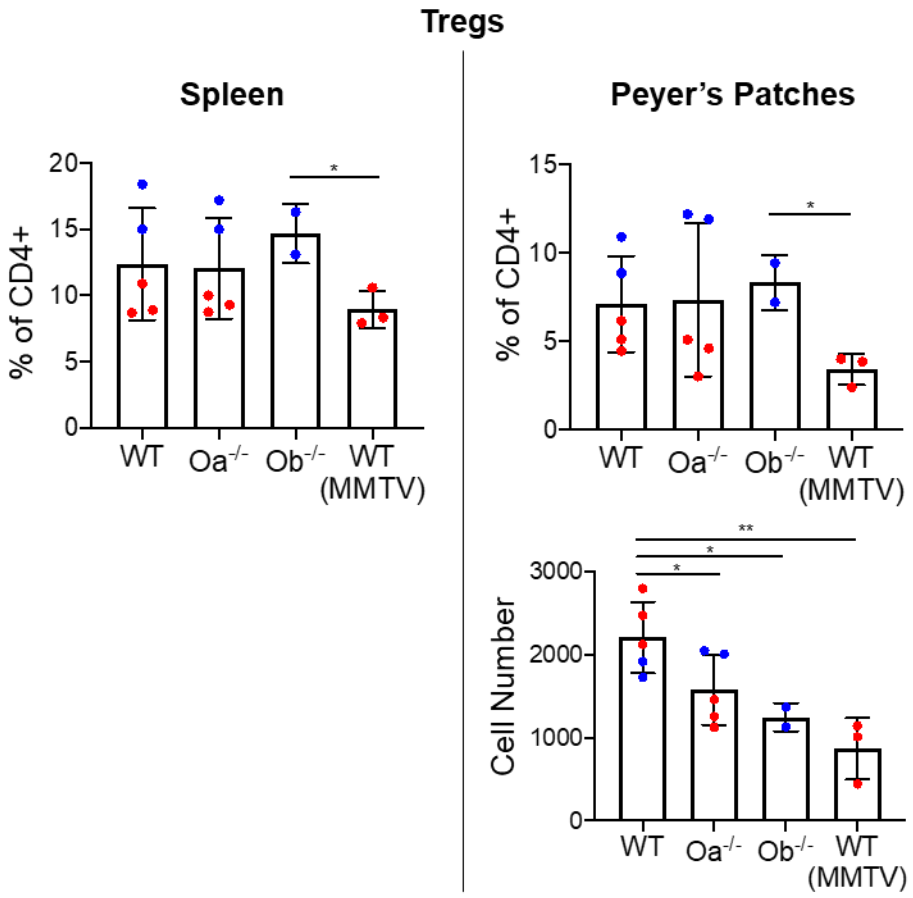

Figure 5.9 Regulatory T cell staining data from 11-24 week old spleen and Peyer's patches. Quantification of splenic and Peyer's Tregs as a percentage of all CD4+ cells and total cell number. Circles of like colors indicates mice that were analyzed on the same day. Significance was calculated with an unpaired, two-tailed, Student t test.

Finally, we checked the spleens and Peyer's patch of the 11-24 week old mice for T follicular regulatory cells and found that WT.MMTV continued to show reduced frequency of T follicular regs in the Peyer's patches. Also, neither $Oa^{-/-}$ mice nor $Ob^{-/-}$ mice showed a significant reduction in the frequency of T follicular regs compared to WT. They did however show a significant reduction in terms of total cell number (Fig. 5.10). Overall, many of the interesting differences observed between WT and $Ob^{-/-}$ mice were not conserved as these mice aged, although these experiments were performed with fewer mice and with a much larger age range.

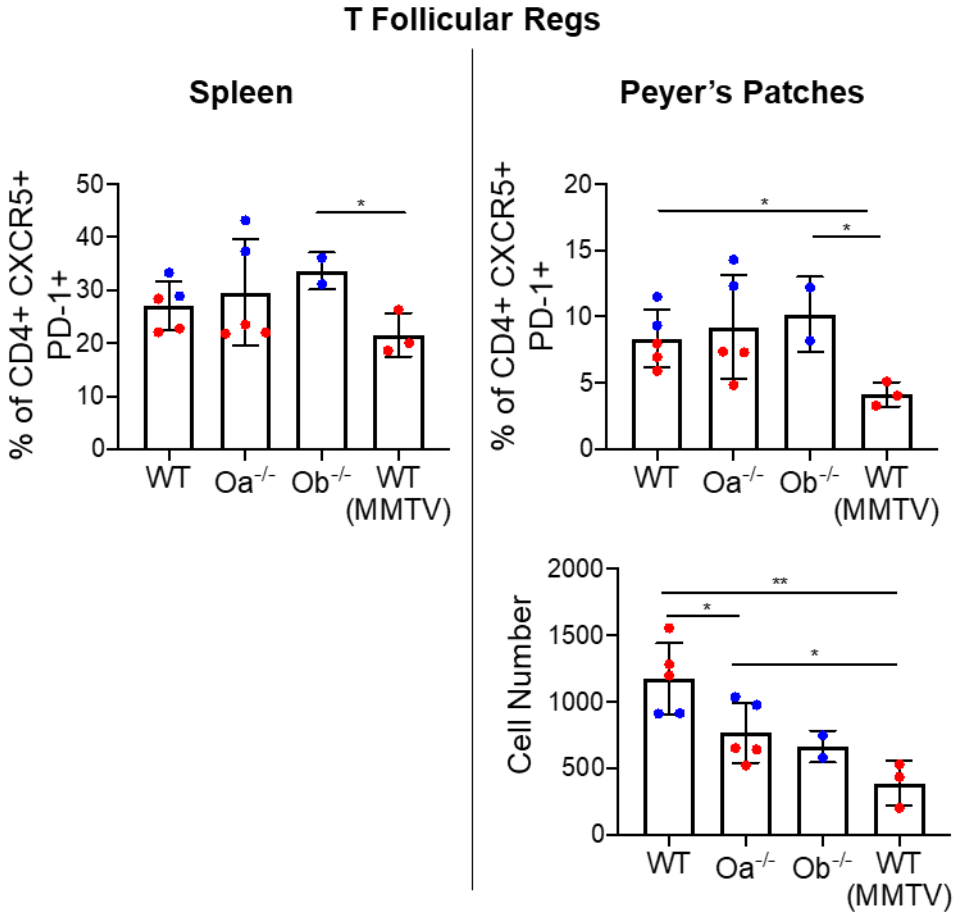

Figure 5.10 T follicular regulatory cell staining data from 11-24 week old spleen and Peyer's patches. Quantification of splenic and Peyer's T follicular regs as a percentage of all CD4+ CXCR5+ PD-1+ cells and total cell number. Circles of like colors indicates mice that were analyzed on the same day. Significance was calculated with an unpaired, two-tailed, Student t test.

Analysis of cross-fostered MMTV infected mice

We have previously established that Peyer's patches of 6 week old $Ob^{-/-}$ mice displayed significant differences from WT mice. We also saw similarities between $Ob^{-/-}$ and WT.MMTV Peyer's patches in terms of total cell number and GC B cell frequency (Fig. 5.1A and 5.1D). It is for this reason that we were very interested in analyzing $Ob^{-/-}$ Peyer's patches during MMTV infection. Based on what was observed in $Ob^{-/-}$ Peyer's patches, we would expect for $Ob^{-/-}$ Peyer's patches during MMTV infection to show significant differences from WT.MMTV Peyer's patches. In order to properly investigate this, we need to infect $Ob^{-/-}$ mice through the natural path which occurs by nursing on an MMTV infected mother. Unfortunately, because $Ob^{-/-}$ mice make neutralizing antibodies to MMTV, infected mothers do not successfully pass on the infection to their pups. $Ob^{-/-}$ pups would instead need to be cross-fostered to an MMTV infected, WT mom. To do this, we transferred newborn WT and $Ob^{-/-}$ pups to an MMTV infected, WT mother. It is worth noting that WT and $Ob^{-/-}$ pups were cross-fostered on the same MMTV infected mother which ensures that the pups received a similar viral load. We analyzed the spleen and Peyer's patches of two separate cohorts of cross-fostered mice at 5-6 weeks of age. Spleen and Peyer's patch cells were analyzed in the same manner as described in previous

sections. Surprisingly, we observed no significant differences in the spleens or Peyer's patches of cross-fostered WT and Ob$^{-/-}$ mice. This was the case both in terms of Peyer's patch total cell number, as well as the frequency of GC B cells in the spleen and Peyer's patches (Fig. 5.11).

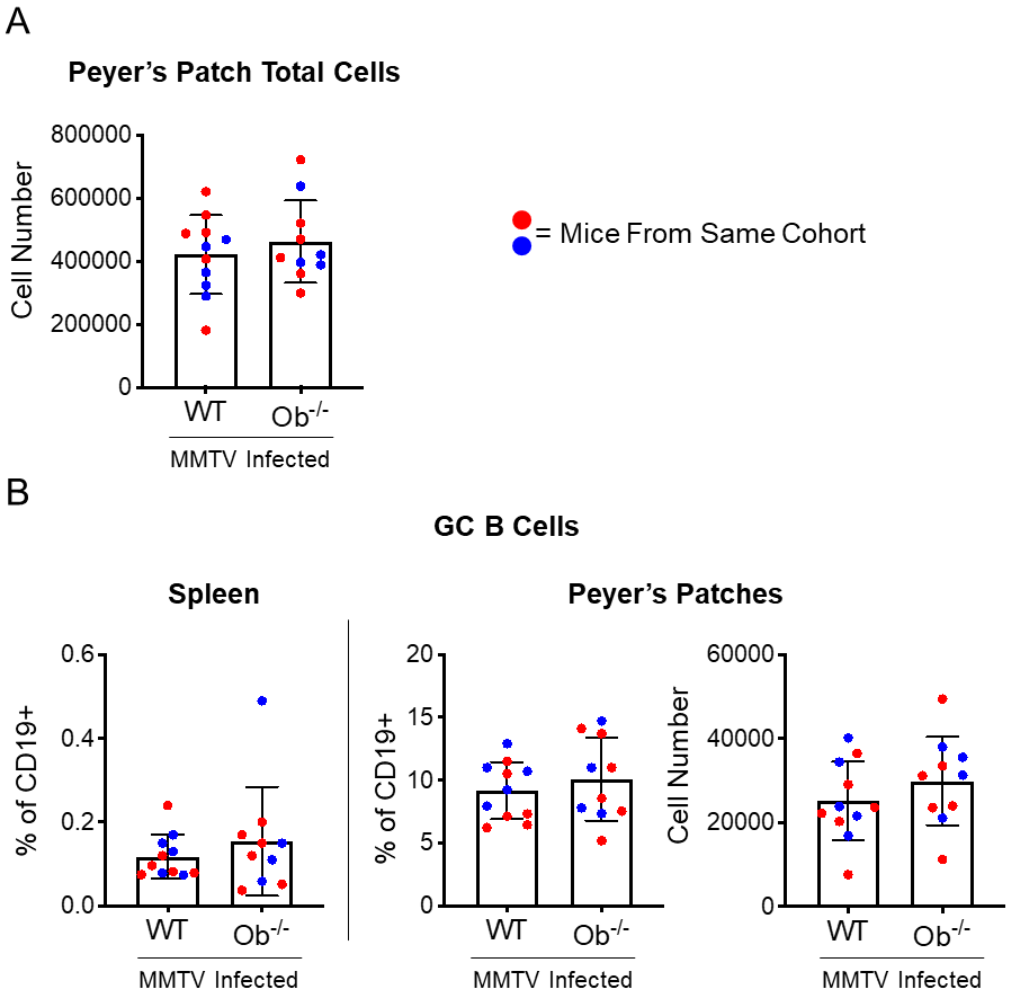

Figure 5.11 Live cell staining data of 5-6 week old cross-fostered WT and Ob$^{-/-}$ spleen and Peyer's patches. **(A)** Total number of live lymphocytes collected from Peyer's patch samples. **(B)** Quantification of splenic and Peyer's patch germinal center B cells as a percentage of all CD19+ cells and as total cell number. Circles of like colors indicates mice from the same cross-foster cohort.

T follicular helper cell and activated T cell data from WT and cross-fostered mice is shown in figure 5.12. As in figure 5.11, there were no observed differences in either T follicular helper cells or activated T cells in the spleen and Peyer's patches between WT and $Ob^{-/-}$ cross-fostered mice (Fig. 5.12).

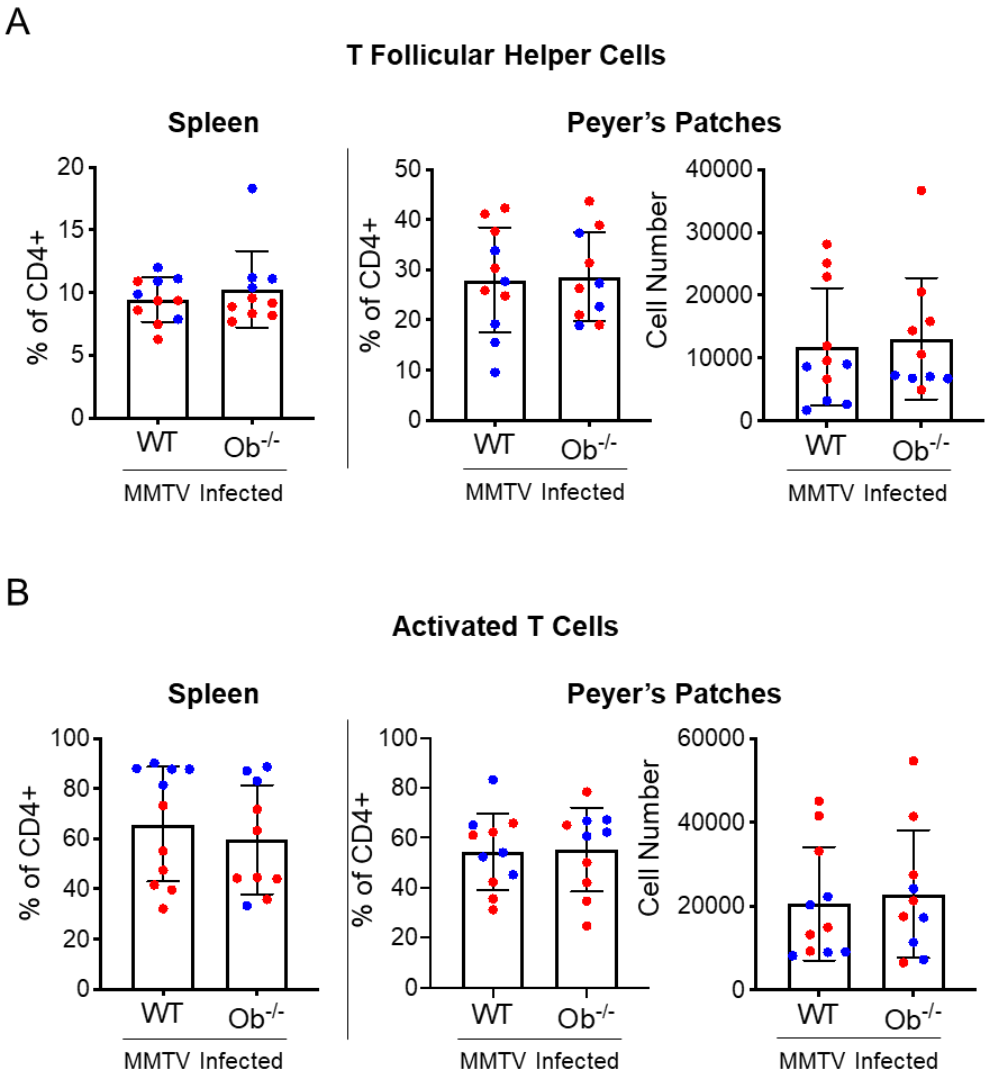

Figure 5.12 T follicular helper cell and activated T cell staining data of 5-6 week old cross-fostered WT and $Ob^{-/-}$ spleen and Peyer's patches. **(A)** Quantification of splenic and Peyer's patch T follicular helper cells. **(B)** Quantification of splenic and Peyer's patch activated T cells. Circles of like colors indicates mice from the same cross-foster cohort.

Finally, we analyzed Tregs and T follicular regulatory cells in cross-fostered WT and Ob$^{-/-}$ mice. This analysis again did not find any differences in these populations between WT and cross-fostered mice.

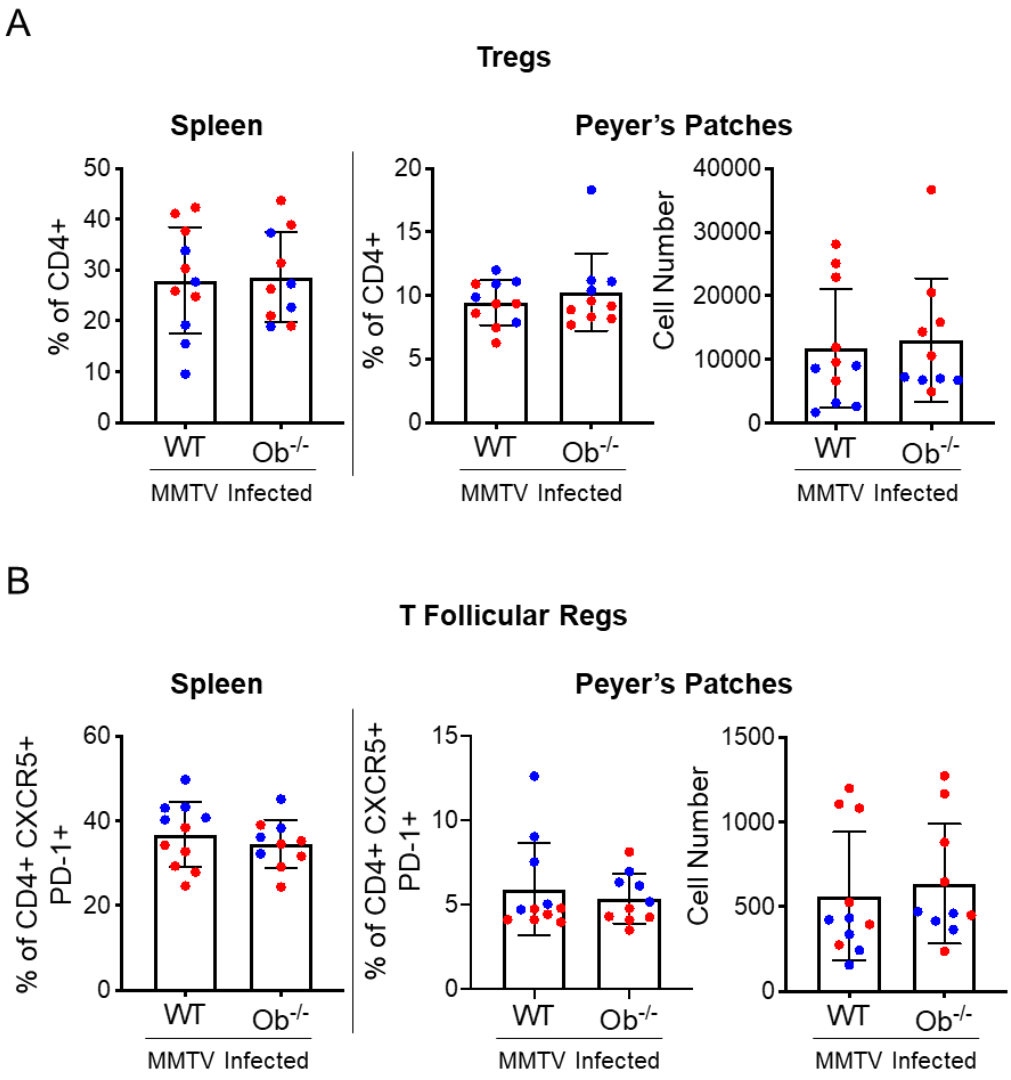

Figure 5.13 Treg and activated T follicular regulatory cell data of 5-6 week old cross-fostered WT and Ob$^{-/-}$ spleen and Peyer's patches. **(A)** Quantification of splenic and Peyer's patch Tregs. **(B)** Quantification of splenic and Peyer's patch T follicular regs. Circles of like colors indicates mice from the same cross-foster cohort.

Discussion

The experiments presented above showed that WT and $Ob^{-/-}$ mice differed significantly in the composition of their Peyer's patches, however this difference may be dependent on age. More experiments with mice of various ages will be needed to verify this result. While the result of the 6 week old study were very exciting, it is all the more puzzling when we see that there were no observed differences between WT and $Ob^{-/-}$ mice after cross-fostered MMTV infection. It is worth mentioning that these cross-foster experiments were not adequately controlled. It is known that cross-fostering can have long term effects on the pups into adulthood, including increased weight gain and behavioral differences. It is possible that the stress induced by cross-fostering could be masking a real difference between these mice during MMTV infection. To control for this, WT and $Ob^{-/-}$ pups should be cross-fostered to an uninfected WT mother at the same time as WT and $Ob^{-/-}$ pups are fostered on an infected mother. This experiment better controls for the effect that fostering may have on the immune system. Another more likely possibility is that perhaps the differences observed in the naïve WT and $Ob^{-/-}$ mice (Fig. 5.1-5.5) was due to a difference in the intestinal microbiota of the two strains of mice. This hypothesis is bolstered by evidence that WT and $Ob^{-/-}$ mice are populated by differing species of bacteria which was discovered by our collaborators in the Golovkina lab. It is known that the mouse microbiota is seeded by the mother, and that cross-fostered pups receive the microbiota of their foster mother[100]. This most likely means that our cross-fostered WT and $Ob^{-/-}$ pups were colonized by the same microbiota. The lack of

difference between them may therefore indicate that the differences observed in 6 week old mice was due to this factor. To control for this, we would need to establish germ free strains WT and $Ob^{-/-}$ mice and then colonize them with the same microbiota before Peyer's patch analysis.

CHAPTER 6: DISCUSSION

We unfortunately did not observe any differences between WT and $Ob^{-/-}$ mice spleens or Peyer's patches during MMTV infection. While at first this result was puzzling, recent research out of the Golovkina lab has revealed why we may have observed this result. While it is true that $Ob^{-/-}$ mice make neutralizing antibodies to MMTV, this response has thus far only been observed when $Ob^{-/-}$ mice were infected with MMTV via viral injection during adulthood. A recent study by Cullum et al found that when $Ob^{-/-}$ mice are fostered on MMTV infected mothers, these mice do not produce neutralizing antibodies, and are tolerant to the virus[101]. However, it is possible to break tolerance in these mice by providing a booster shot of Triton x-100 treated MMTV that is adjuvanted with CFA. In contrast to this, I/LnJ mice produce a neutralizing antibody response to MMTV regardless of whether the infection begins in adulthood or as neonates. This result indicates that there is a second gene governing neonatal tolerance that must be altered in I/LnJ mice. This locus is currently referred to as virus infectivity controller 2 (*vic2*), and its identity is still under investigation[101]. The results of my cross-fostered experiments serve to reinforce the findings of this study since we did not see enhanced immune activity in the Peyer's patches of cross-fostered $Ob^{-/-}$ mice. An interesting future experiment would be to cross-

foster $Ob^{-/-}$ pups on MMTV infected moms, followed by a booster shot of adjuvanted MMTV later in life. We know that this immunization breaks tolerance, and we would expect this broken tolerance to manifest as an increase in activated immune cells. Where exactly we would see this activation is not known, and these experiments would need to look in multiple tissues such as the spleen, Peyer's patches, and mesenteric lymph nodes. We would also recommend that the Peyer's patches of I/LnJ mice be examined during natural MMTV infection. This experiment would very likely reveal enhanced immune activity in the Peyer's patches during infection.

HLA-DO is known to alter the repertoire of peptides presented on the surface of antigen presenting cells[27]. The actual immunological consequences of these changes are still the subject of much study. Our previous work study of DO in NOD mice illustrated the consequences of DO expression on the immune response quite well[46]. To summarize, we expressed human DO in NOD dendritic cells and demonstrated that our NOD.DO mice were protected from developing type 1 diabetes. Furthermore, we proved that this protection was due to a change in the presentation of the immunogenic antigen. In fact, CD4+ T cells from NOD.DO mice were shown to maintain their autoreactivity outside of NOD.DO mice, which means that their lack of reactivity was due to an absence of the immunogenic peptide on the surface of NOD.DO dendritic cells. Interestingly, the autoreactive CD4+ T cells are made up of two different populations of T cells that recognize insulin derived peptide differently depending on if the peptide was loaded on to MHCII in the presence of H2-M or not[45, 102].

Peptide loaded in the presence of H2-M are more stable and are recognized by what are referred to as type A T cells. MHCII complexes loaded in the absence of H2-M are much less stable and are recognized by type B T cells[45]. In NOD mice, the type A T cells recognize processed insulin derived peptide that is expressed in thymic medullary epithelial cells, indicating these cells escaped thymic deletion. Type B cells instead are specific for a variant of insulin derived (B chain) peptide only found in the pancreas, meaning deletion of these cells in the thymus is not possible. Based on our NOD.DO study, we can infer that the overexpression of DO in NOD dendritic cells reduced H2-M activity, and therefore reduced the presentation of the insulin derived peptide that is recognized by type A T cells. The type B T cells, however, should be unaffected by DO expression in dendritic cells because the B chain peptide is susceptible to H2-M editing which is dampened by the presence of DO. The autoreactive type B response should be conserved in NOD.DO mice, but we know that these mice are protected from developing diabetes. This raises questions about what happens to the type B cells in NOD.DO mice. Is this subset alone insufficient to generate autoimmunity, or does DO expression in these mice somehow limit the presentation of the B chain peptide as well? Analysis of type A and B T cells in NOD.DO mice found that the frequency of these cells was unaffected (Emil Unanue, Personal Communication). This finding suggests that while the type A T cells are still there, they are not generating an autoimmune response because the antigen they recognize must be presented at a reduced level on NOD.DO dendritic cells. What remains unclear is why the type B cells are also unreactive

in these mice. As discussed above, the antigen that type B T cells respond to in NOD mice cannot bind to MHCII in the presence of H2-M because it does not form a stable enough complex with MHCII to outcompete H2-M interaction. DO activity should therefore either have no effect on the presentation of this less stable antigen, or even enhance its presentation due to reduced H2-M activity. Why then, do the type B T cells not generate an autoimmune response to this antigen? Either DO is able to limit the presentation of the B chain peptide through some unforeseen mechanism, or the type B response alone is not enough to generate autoimmunity. This could be tested by isolating the type B T cells alone from NOD.DO mice and transferring them into NOD.RAG1 mice and checking for development of type 1 diabetes.

Our previous study revealed that the mutations in *H2-Ob* of I/LnJ mice render H2-O protein non-functional and give these mice the ability to generate a neutralizing antibody response to MMTV. What remains unclear is how these mutations render I/LnJ H2-O non-functional. I/LnJ H2-O is expressed at levels similar to WT, and associates with DM similar to WT H2-O[53]. The Mellins lab has shown that as DM:DO complexes are exposed to increasingly acidic pH conditions found in the late endo/lysosomes, DO becomes destabilized and eventually degraded[44]. Perhaps these mutations reduce I/LnJ H2-O stability under low pH and result in an earlier destabilization of the H2-O:H2-M complex as the two traffic to vesicles with increasingly acidic pH. To test this hypothesis, lysate from C57BL/6J (B6) and I/LnJ B cells could be incubated at increasingly acidic pH at 37°C. These samples would then be neutralized and H2-M

immunoprecipitated. If it is true that I/LnJ H2-O is less stable at low pH than B6 H2-O, then western blotting will show a reduction in associated I/LnJ H2-O with H2-M at low pH. This finding could explain how I/LnJ H2-O loses its function despite appearing to associate normally with H2-M. If I/LnJ H2-O is unable to withstand the same conditions as B6 H2-O, this would mean that the late endo/lysosomes have a reduced H2-O presence similar to in H2-O deficient cells.

The result of the final experiment in our *HLA-DOA* variant screen potentially revealed something very interesting about DO function. To recap, free DM from cells that were transfected with a more functional variant of DOA showed reduced capability to release CLIP from MHCII and load peptide when compared to free DM from cells transfected with *DOA*0101*. How would it be possible for DM unbound by DO to have reduced functionality, and what would this have to do with what variant of DO is expressed in those cells? We propose that DO has a previously undescribed function in which binding to DM permanently alters DM's ability to bind to MHCII. The reason why this function has not been observed up until this point is that under normal conditions, DM:DO do not readily dissociate[44], and this new function would be masked as normal DM:DO binding. Because of the reduced stability of the more functional variants we analyzed, these forms of DO may be able to bind and dissociate multiple DM molecules. This would result in free DM that had previously been bound by this unstable DO, and we have shown that this free DM has reduced functionality.

This new function of DO could explain previously unexplained phenomena we have observed studying H2-O in mice. For example, during the process of generating the *H2-Ob*$^{-/-}$ mouse strain, our collaborators created a strain of mice in which only 6 bp was removed from the sequence of *H2-Ob*, resulting in an in-frame, 2 amino acid deletion in the immunoglobulin domain. Rather than discard this strain, it was decided they should be infected with MMTV, and the expression of H2-O characterized. These mice were found to express H2-O at a very reduced level compared to WT, and this mutant H2-O was found to, almost entirely, inhabit the endoplasmic reticulum. Based on the expression of H2-O in these mice, we expected them to be functionally similar to an H2-O deficient mouse. However, these mice did not produce a neutralizing antibody response to MMTV. This result was very unexpected and has yet to be explained. This observation could be explained if DO/H2-O binding to DM/H2-M permanently alters DM/H2-M functionality. Perhaps this mutant H2-O functions similar to the more functional variants of *DOA* we identified in our screen. As discussed previously, we currently do not understand why H2-O in I/LnJ is functionally null. Another possible mechanism could be that the mutations in the immunoglobulin domain of I/LnJ H2-Oβ render it unable to permanently alter H2-M function. This finding would be particularly surprising, as it could de-couple H2-O's ability to bind to H2-M from its ability to functionally alter H2-M. Regardless of if this mechanism we propose turns out to be correct or not, what has become clear through our recent research is that DO/H2-O does not function as simply as is currently accepted.

CHAPTER 7: MATERIALS AND METHODS

Cell line

HeLa cells transfected with the CIITA[58] were grown in DMEM with 5% FBS at 37°C and 5% CO_2. CIITA expression allowed for the expression of the Ii, MHCII, and DM but no detectable DO protein[53].

Functional analysis of DOA variants

DOA variants were synthesized and cloned into pCDH-EF1-MCS-IRESmRuby (System Biosciences) by GenScript. Common *DOB* alleles were synthesized and cloned into pEF1a-MCS-IRES-AcGFP1 (Clontech Laboratories) also by GenScript as previously described[53]. HeLa.CIITA cells were seeded in six-well plates and 12–24 h later were transfected with 1 μg of pCDH-EF1-DOA-MCS-IRES-mRuby and 1 μg of pEF1a-DOBMCS-IRES-AcGFP1 mixed with Lipofectamine 2000 (Thermo Fisher Scientific). HeLa.CIITA cells transfected with pCDH-EF1-DOA*0101- MCS-IRES-mRuby and pEF1a-MCS-IRES-AcGFP1 (empty vector) as well as pCDH-EF1-MCS-IRES-mRuby (empty vector) and pEF1a-DOB*0101- MCS-IRES-AcGFP1 were used as controls. Transfected cells were harvested 72 h later and analyzed by flow cytometry, immunoprecipitation, and/or Western blotting.

HeLa FACS analysis

MHCII was measured using an Ab specific for DR, DP, and DQ that was conjugated to PE-Vio770 (clone REA332; Miltenyi Biotec). MHCII–CLIP was measured using the mAb CerCLIP.1[57], and DM and DO levels were measured using the heterodimer-specific mAbs MaP.DM1[59] and Mags.DO5[39], respectively.

The MHCII–CLIP, DM-, and DO-specific Abs were purified from bioreactor supernatants using standard protein G chromatography and conjugated with Alexa Fluor 647 (Mags.DO5) or biotin (CerCLIP.1 and MaP.DM1).

Transiently transfected HeLa.CIITA cells were harvested and split for extracellular staining (MHCII–CLIP and MHCII) or for intracellular staining (DM and DO). For extracellular staining, HeLa.CIITA cells were blocked with normal mouse serum, incubated with Abs specific for MHCII–CLIP (CerCLIP.1–biotin) and MHCII at 4°C for 30 min, and washed. The cells were then incubated with streptavidin–Alexa Fluor 647 (Invitrogen) at 4°C for 30 min, washed, and analyzed by flow cytometry. DAPI was added prior to analysis for dead cell exclusion. For intracellular staining for DM and DO, transfected HeLa.CIITA cells were fixed and permeabilized using a Cytofix/Cytoperm Kit (BD Biosciences) for 30 min at 4°C. Cells were washed and blocked with normal mouse serum followed by incubation with Abs specific for DM (MaP.DM1–biotin) and DO (Mags.DO5–Alexa Fluor 647) for 30 min at room temperature (RT). After washing, cells were incubated with streptavidin–PE-Cy7 for 30 min at RT, washed, and analyzed. HeLa.CIITA were transfected individually with pCDH-EF1-DOA*0101-MCS-IRESmRuby or only pEF1a-DOB*0101-MCS-IRES-AcGFP1 were used as compensation controls for mRuby and AcGFP fluorescence. Data were acquired using a custom five-laser BD LSR II cytometer and analyzed using FlowJo software (BD Biosciences). Background fluorescence for MHCII–CLIP and DO expression was removed by subtracting the MHCII–CLIP and DO geometric mean fluorescent intensity (gMFI) values of

either the empty mRuby vector (EV-mRuby)/DOB*0101-AcGFP or the EV-mRuby/empty AcGFP vector (EV-AcGFP) controls from each sample.

Cell Sorting

HeLa.CIITA cells were transfected as described previously and harvested 72 h later. mRuby+ AcGFP+ cells were sorted, counted, and frozen for subsequent biochemical analysis.

Western blotting and quantification

Transiently transfected HeLa.CIITA cells were lysed for 30 min on ice in 20 mM Tris-HCl and 130 mM NaCl (pH 8) with 1% Triton X-100 and cOmplete Mini, EDTA-free Protease Inhibitor Cocktail Tablets (Roche Life Science). Nuclear material was removed by centrifugation, and supernatants were mixed with Laemmli sample buffer containing 20 mM DTT and incubated at 95˚C for 5 min. Protein samples were separated on 10–20% gradient SDS-PAGE gels (Criterion TGX; Bio-Rad Laboratories) and transferred to polyvinylidene fluoride membrane (MilliporeSigma). For analysis of DO immunoprecipitations, Laemmli sample buffer (without DTT) was added to the washed protein G bead pellets, and the samples were heated at 95°C for 5 min and analyzed by SDS-PAGE as above prior to transfer to polyvinylidene fluoride membranes for Western blot analysis. The membranes were blocked with 5% powdered milk for 30 min at RT, and the resulting membranes were incubated with an affinity-purified polyclonal rabbit Ab specific for the cytoplasmic tail of DOβ [R.DOB/c[25]] or a rabbit mAb specific for the cytoplasmic tail of DMβ (clone EPR7981; Abcam). After washing, the primary Abs were detected by the addition of HRP-conjugated donkey or goat anti-rabbit

Abs (Jackson ImmunoResearch Laboratories) followed by development with chemiluminescent peroxidase substrate (Pierce Biotechnology) and exposure to film.

To determine the relative amount of DO and DM that were recovered after coimmunoprecipitation, data were normalized to correct for differences in cotransfection efficiencies, using the following two strategies. For some experiments, the individual DOβ and DMβ band intensity values obtained after immunoprecipitation of DO were normalized based on the percentage of mRuby and AcGFP double-positive cells in each sample (as determined by flow cytometry prior to cell lysis). For other experiments, normalization was performed prior to cell lysis. The same number of mRuby and AcGFP double-positive cells in each sample as determined by flow cytometry were lysed prior to immunoprecipitation. In this case, the resulting uncorrected DOβ and DMβ band intensity values obtained were used for calculations. In both cases, the resulting values for DOβ and DMβ were subsequently normalized to the values obtained after expression of *DOA*0101*/*DOB*0101* in HeLa.CIITA cells to allow for comparison across independent experiments. Bands were quantified using ImageJ software.

DO immunoprecipitation and glycan digestion

HeLa.CIITA cells transiently transfected with plasmids encoding *DOB*0101* and the various *DOA* variants were lysed as described above. After removal of nuclear material by centrifugation, supernatants were precleared with 40 μL of Protein G Sepharose (GE Healthcare Life Sciences) and 5 μg of mouse IgG with

rotating for 30 min at 4°C. The samples were centrifuged, and the precleared supernatants were added to tubes containing 5 μg of Mags.DO5 and 30 μL of Protein G Sepharose to immunoprecipitate the DO–DM complex. After rotation at 4°C for 2 h, the beads were washed three times with 20 mM Tris-HCl and 130 mM NaCl (pH 8) containing 0.1% Triton X-100. Precipitated proteins were released from the beads by the addition of 105 μL of 0.5% SDS and 40mM DTT (NEB Biolabs) and heating for 10 min at 95ºC. Portions of each sample were either mock treated or treated with Endoglycosidase H (EndoH) (NEB Biolabs) according to the supplied protocol. Laemmli sample buffer containing 20 mM DTT was added to the digested or mock digested samples prior to SDS-PAGE and Western blotting as described above. To allow for the correct identification of glycosylated and de-glycosylated DOβ, total cell lysate from HeLa.CIITA cells transiently transfected with *DOA*0101* and *DOB*0101* expression plasmids were mock treated, treated with EndoH, or treated with Peptide-*N*-Glycosidase F (PNGaseF; cleaves all glycans) (NEB Biolabs) according to the supplied protocols and included in the analyses.

For the DO depletion studies, lysates from matched numbers of sorted cells were lysed and precleared as above. After preclearing, the lysates were split in two, and 5 μg of Mags.DO5 (DO precipitate) or 5 μg of mouse IgG (negative control precipitate) and 30 μL of Protein G Sepharose were added to the two tubes. The samples were rotated for 1 h, and each DO or control precipitation was repeated with the resulting supernatants two more times (for three total sequential precipitates) for 1 h each. The resulting Protein G bead pellets were washed

three times with 20 mM Tris-HCl and 130 mM NaCl (pH 8) containing 0.1% Triton X-100 prior to analysis by SDS-PAGE and Western blotting.

DM immunoprecipitation

DM was immunoprecipitated from HeLa.CIITA and T2.DM cells. Cell pellets were lysed, nuclear material was removed, and the samples were precleared as described previously. The samples were centrifuged, and the precleared supernatants were added to tubes containing 4 μL of MaP.DMB/c[57] ascites and 30 μL of Protein G Sepharose. After rotation at 4°C for 2 h, the beads were washed three times with 20 mM Tris-HCl and 130 mM NaCl (pH 8) containing 0.1% Triton X-100. Bead pellets were stored at -20˚C to be used later for peptide loading assays.

DR3-CLIP purification and peptide loading assay

DR3-CLIP was purified from frozen T2.DR3[68] cell pellets by lysing ~500 million cells for 60 min on ice in 25 mL of 20 mM Tris-HCl and 130 mM NaCl (pH 8) with 1.5% Triton X-100 and cOmplete Mini, EDTA-free Protease Inhibitor Cocktail Tablets (Roche Life Science). Nuclear material was removed via centrifugation, and the resulting supernatant was added to 1 mL of mouse Ig-beads and rotated at 4°C for 1-2 h. The precleared lysate was then centrifuged, and the supernatant was transferred to 1 mL of L243-beads. The sample was rotated overnight at 4°C to immunoprecipitate DR3-CLIP. The sample was centrifuged, and the supernatant was decanted. The L243-beads were washed with 3-5 mL of ice cold 0.1% Triton x-100 in Tris-buffered saline (TBS) and then spun down. The beads are washed once more with 3-5 mL 0.1% Triton x-100 in Tris-buffered

saline, then twice with 3-5 mL of 10mM Tris (pH 8) 300mM NaCl 0.1% SDS 0.05% Tx-100 buffer, once more with 3-5 mL 0.1% Triton x-100 in TBS, then twice with 3-5 mL 0.6% CHAPS in TBS. L243-beads were then transferred to a spin column and placed in a clean conical tube, washed with 0.6% CHAPS in TBS, and DR3 was eluted by adding 1 mL 0.1M Tris base (pH 11.5) in 0.6% CHAPS/TBS elution buffer. The column was then centrifuged, and the eluted fraction was neutralized to pH 7-7.5 with 1M acetic acid. This process was repeated until 12-15 fractions were collected. These fractions were checked for the presence of DR3 by performing SDS-PAGE and western blotting for DR3β (HB10A). Purity of each fraction was verified by performing SDS-PAGE with T2.DR3 total lysate as well as samples from each fraction collected. This gel was then silver stained to check for total protein content. Fractions containing purified DR3-CLIP were combined.

DM peptide loading assays were performed by resuspending pellets of immunoprecipitated DM in 50 μL of 0.6% CHAPS in 100 mM sodium acetate 100 mM NaCl (pH 5) with 10 μM MOMP-biotin and 4 μL of purified DR3-CLIP. The mixtures were incubated at 37°C for 2 h and then neutralized with 1M Tris. 12.5 μL of 5X Laemmli sample buffer was then added to each sample. SDS-PAGE was performed using 20 μL of each sample, followed by western blotting. Blots were blocked in 5% BSA, and stable DR3:MOMP-biotin complexes were detected with streptavidin-HRP. Blots were reprobed for DMβ (clone EPR7981; Abcam) and DR3β (HB10A).

Analysis of DO allotypes and linkage disequilibrium analysis

The association between *DOA* and *DOB* allelic variants was analyzed by retrieving all reference SNPs (rsSNPs) defining the corresponding alleles stated by the HLA-International ImMunoGeneTics Project (IMGT) database and then querying their pairwise combinations using Haploview 4.2. These queries were performed on the corresponding region chromosome 6:3300000-32000000 (GRCh38p12) of the human genome deposited in the 1000 Genomes Project (1000GP) dataset[63]. Furthermore, a Python script was written to retrieve the haplotype frequencies and their combinations at the individual level using the pLink and Haploview software packages. The script is available at https://github.com/e-morrison/dofreqs.

The LDpair tool from the LDlink Suite[71] was used to determine linkage disequilibrium between SNPs.

Statistical analysis

For Figs. 2.3C, 2.3D, 2.5, the average ± SD were calculated from the measured levels of *DOA*0101* combined with each of the five common *DOB* alleles (gray zones on bar graphs). In other experiments, significance was determined by performing Student unpaired t tests using Prism GraphPad.

Mice

C57BL/6J (B6) (The Jackson Laboratory), B6.*H2-Oa*$^{-/-}$[103], B6.*H2-Ob*$^{-/-}$[53], B6.B1-8[84], B6.B1-8 *H2-Oa*$^{-/-}$ CD45.1, B6.*H2-Ma*$^{-/-}$[104], B6.B1-8 CD45.1/.2, B6 mice chimeric for B6.B18 CD45.1/.2 and B6.B1-8 *H2-Oa*$^{-/-}$ CD45.1, and MMTV

infected B6 mice were maintained at the animal facility in the Child Health Institute of New Jersey.

TLR7 stimulation

Mice were intraperitoneally injected with 50 μg of the TLR7 agonist, R848 in saline.

Splenoctye chimeras

Splenocytes from B1-8 CD45.1/.2 and B1-8 *H2-Oa*$^{-/-}$ CD45.1 were stained for the frequency of NP-specific B cells. A 50/50 mix of NP-specific B cells (to a maximum of 20 million total cells) from WT and Oa$^{-/-}$ mice was then given to WT CD45.2 mice via intraocular injection. Chimeras were stimulated with 100 μg of NP-LPS via IP injection.

Peyer's patch isolation

Mouse small intestines were removed and placed in a small petri dish containing 5 mL of ice cold RPMI with 5% FBS. Small intestines were cut into 3 sections. One section at a time was removed from the dish and Peyer's patches were cut out and placed in a small petri dish containing 5 mL of ice cold RPMI with 5% FBS. Once all Peyer's patches were removed, Peyer's patches were homogenized between two frosted slides, and the cell suspension was applied to a 40 μm cell strainer over a 50 mL conical tube. Peyer's patch cells were then centrifuged at 1200 rpm for 20 min. Supernatant was carefully decanted by pouring, and cell pellets were resuspended in ice cold RPMI with 5% FBS and applied to a 96 well plate for FACS analysis.

Mouse FACS analysis

Mouse spleen and Peyer's patch cells were blocked with 100 μL Fcγ block and normal mouse serum in FACS buffer for 15 min at 4°C. Cells were then surface stained in 100 μL FACS buffer containing diluted antibodies for 30 min at 4°C. Samples were then washed twice with 200 μL FACS buffer. Intracellular staining was performed first by fixation and permeabilization using the BD Cytofix/Cytoperm kit. Nuclear fixation was performed using the eBioscience nuclear fixation/permeabilization kit. Fixed cells were blocked intracellularly with 100 μL Fcγ block and normal mouse serum in permeabilization buffer for 15 min at 4°C. Fixed cells were then intracellular stained in 100 mL permeabilization buffer containing diluted antibodies for 30 min at RT. Samples were then washed once with 200 μL permeabilization buffer, then once more with 200 μL FACS buffer.

Table 7.1 Flow cytometry panel used for analysis of TLR7 stimulation samples.

Antibody	Number[1]	Color	Dilution
B220	22	V450	1:400
CD11c	71	PE	1:300
CD8a	270	APC-Cy7	1:500
CD205	301	PE-Cy7	1:300
MHCII	434	AF594	1:1000
CD11b	62	A700	1:500

[1] Indicates the antibody tube number in the DenAngelo antibody database.

PDCA-1	828	PerCP-Cy5.5	1:600
2C3A	428	A488	1:500
Mags.Ob1	11	A647	1:500

Table 7.2 Flow cytometry panel used for analysis of splenocyte chimeras.

Antibody	Number	Color	Dilution
CD19	105	FITC	1:600
CD45.1	206	APC-Cy7	1:50
CD45.2	219	PerCP-Cy5.5	1:100
CD21	850	PE-Texas Red	1:3000
CD23	249	PE-Cy7	1:1000
NP	739	PE	1:3000

Table 7.3 B cell flow cytometry used for Peyer's patch analysis.

Antibody	Number	Color	Dilution
CD19	107	PE	1:300
CD38	244	A700	1:90
Fas	885	PE-Cy7	1:600
GL7	423	Biotin	1:2500
CD45.1	995	BV605	1:800
MHCII	537	BV650	1:1500
I-A(b)-CLIP	5	A488	1:400

Streptavidin	691	A647	1:3000

Table 7.4 T cell flow cytometry panel used for Peyer's patch analysis.

Antibody	Number	Color	Dilution
CD19	105	FITC	1:600
CD4	188	PerCP-Cy.5.5	1:500
PD-1	949	PE-Cy7	1:200
CXCR5	299	PE	1:100
CD45.1	995	BV605	1:800
CD62L	246	APC-780	1:500
CD44	978	BV650	1:2000
FoxP3	719	450	1:500

REFERENCES

1. Chaplin, D.D. Overview of the immune response. *J Allergy Clin Immunol* **125**, S3-S23 (2010).
2. Saleem, M.A., Arkwright, P.D., Davies, E.G., Cant, A.J. & Veys, P.A. Clinical course of patients with major histocompatibility complex class II deficiency. *Arch Dis Child* **83**, 356-359 (2000).
3. Matzaraki, V., Kumar, V., Wijmenga, C. & Zhernakova, A. The MHC locus and genetic susceptibility to autoimmune and infectious diseases. *Genome Biology* **18**, 76 (2017).
4. Marrack, P. & Kappler, J.W. Do MHCII-presented neoantigens drive type 1 diabetes and other autoimmune diseases? *Cold Spring Harb Perspect Med* **2**, a007765-a007765 (2012).
5. James, E.A., Pietropaolo, M. & Mamula, M.J. Immune Recognition of β-Cells: Neoepitopes as Key Players in the Loss of Tolerance. *Diabetes* **67**, 1035 (2018).

6. Marty Pyke, R. *et al.* Evolutionary Pressure against MHC Class II Binding Cancer Mutations. *Cell* **175**, 416-428.e413 (2018).

7. Roche, P.A. & Furuta, K. The ins and outs of MHC class II-mediated antigen processing and presentation. *Nat Rev Immunol* **15**, 203-216 (2015).

8. Gorer, P.A. The genetic and antigenic basis of tumour transplantation. *The Journal of Pathology and Bacteriology* **44**, 691-697 (1937).

9. Snell, G.D. & Higgins, G.F. Alleles at the histocompatibility-2 locus in the mouse as determined by tumor transplantation. *Genetics* **36**, 306-310 (1951).

10. Nakamura, T., Shirouzu, T., Nakata, K., Yoshimura, N. & Ushigome, H. The Role of Major Histocompatibility Complex in Organ Transplantation-Donor Specific Anti-Major Histocompatibility Complex Antibodies Analysis Goes to the Next Stage. *Int J Mol Sci* **20**, 4544 (2019).

11. Bach, F. & Hirschhorn, K. Lymphocyte Interaction: A Potential Histocompatibility Test in vitro. *Science* **143**, 813 (1964).

12. Bach, F.H. & Amos, D.B. Hu-1: Major Histocompatibility Locus in Man. *Science* **156**, 1506 (1967).

13. Dausset, J. Iso-leuco-anticorps. *Acta Haematologica* **20**, 156-166 (1958).

14. McDevitt, H.O. & Tyan, M.L. Genetic control of the antibody response in inbred mice. Transfer of response by spleen cells and linkage to the major histocompatibility (H-2) locus. *J Exp Med* **128**, 1-11 (1968).

15. McDevitt, H.O. & Chinitz, A. Genetic Control of the Antibody Response: Relationship between Immune Response and Histocompatibility (H-2) Type. *Science* **163**, 1207 (1969).

16. Kindred, B. & Shreffler, D.C. H-2 Dependence of Co-Operation Between T and B Cells in Vivo. *The Journal of Immunology* **109**, 940 (1972).

17. Ziegler, K. & Unanue, E.R. Identification of a macrophage antigen-processing event required for I-region-restricted antigen presentation to T lymphocytes. *The Journal of Immunology* **127**, 1869 (1981).

18. Shiina, T., Hosomichi, K., Inoko, H. & Kulski, J.K. The HLA genomic loci map: expression, interaction, diversity and disease. *Journal of Human Genetics* **54**, 15-39 (2009).

19. Unanue, E.R., Turk, V. & Neefjes, J. Variations in MHC Class II Antigen Processing and Presentation in Health and Disease. *Annual Review of Immunology* **34**, 265-297 (2016).

20. Watts, C. The endosome-lysosome pathway and information generation in the immune system. *Biochim Biophys Acta* **1824**, 14-21 (2012).

21. Blum, J.S. & Cresswell, P. Role for intracellular proteases in the processing and transport of class II HLA antigens. *Proc Natl Acad Sci U S A* **85**, 3975-3979 (1988).

22. Guce, A.I. *et al.* HLA-DO acts as a substrate mimic to inhibit HLA-DM by a competitive mechanism. *Nat Struct Mol Biol* **20**, 90-98 (2013).

23. Roche, P.A. & Cresswell, P. Invariant chain association with HLA-DR molecules inhibits immunogenic peptide binding. *Nature* **345**, 615-618 (1990).

24. Pos, W., Sethi, D.K. & Wucherpfennig, K.W. Mechanisms of peptide repertoire selection by HLA-DM. *Trends Immunol* **34**, 495-501 (2013).

25. Denzin, L.K. *et al.* Negative Regulation by HLA-DO of MHC Class II-Restricted Antigen Processing. *Science* **278**, 106 (1997).

26. Denzin, L.K. Inhibition of HLA-DM Mediated MHC Class II Peptide Loading by HLA-DO Promotes Self Tolerance. *Front Immunol* **4**, 465-465 (2013).

27. Nanaware, P.P., Jurewicz, M.M., Leszyk, J.D., Shaffer, S.A. & Stern, L.J. HLA-DO Modulates the Diversity of the MHC-II Self-peptidome. *Molecular & Cellular Proteomics* **18**, 490 (2019).

28. Trowsdale, J. & Kelly, A. The human HLA class II alpha chain gene DZ alpha is distinct from genes in the DP, DQ and DR subregions. *EMBO J* **4**, 2231-2237 (1985).

29. Inoko, H., Ando, A., Kimura, M. & Tsuji, K. Isolation and characterization of the cDNA clone and genomic clones of a new HLA class II antigen heavy chain, DO alpha. *The Journal of Immunology* **135**, 2156 (1985).

30. Tonnelle, C., DeMars, R. & Long, E.O. DO beta: a new beta chain gene in HLA-D with a distinct regulation of expression. *EMBO J* **4**, 2839-2847 (1985).

31. Karlsson, L., Surh, C.D., Sprent, J. & Peterson, P.A. A novel class II MHC molecule with unusual tissue distribution. *Nature* **351**, 485-488 (1991).

32. Hornell, T.M.C. *et al.* Human Dendritic Cell Expression of HLA-DO Is Subset Specific and Regulated by Maturation. *The Journal of Immunology* **176**, 3536 (2006).

33. Harton, J.A. & Ting, J.P. Class II transactivator: mastering the art of major histocompatibility complex expression. *Mol Cell Biol* **20**, 6185-6194 (2000).

34. Taxman, D.J., Cressman, D.E. & Ting, J.P.Y. Identification of Class II Transcriptional Activator-Induced Genes by Representational Difference

Analysis: Discoordinate Regulation of the DNα/DOβ Heterodimer. *The Journal of Immunology* **165**, 1410 (2000).

35. Nagarajan, U.M. *et al.* Class II Transactivator Is Required for Maximal Expression of HLA-DOB in B Cells. *The Journal of Immunology* **168**, 1780 (2002).

36. Fallas, J.L., Yi, W., Draghi, N.A., O'Rourke, H.M. & Denzin, L.K. Expression Patterns of H2-O in Mouse B Cells and Dendritic Cells Correlate with Cell Function. *The Journal of Immunology* **178**, 1488 (2007).

37. Chen, X. *et al.* Regulated expression of human histocompatibility leukocyte antigen (HLA)-DO during antigen-dependent and antigen-independent phases of B cell development. *J Exp Med* **195**, 1053-1062 (2002).

38. Chen, X., Reed-Loisel, L.M., Karlsson, L. & Jensen, P.E. H2-O Expression in Primary Dendritic Cells. *The Journal of Immunology* **176**, 3548 (2006).

39. Glazier, K.S. *et al.* Germinal center B cells regulate their capability to present antigen by modulation of HLA-DO. *J Exp Med* **195**, 1063-1069 (2002).

40. Porter, G.W., Yi, W. & Denzin, L.K. TLR agonists downregulate H2-O in CD8α(−) DCs. *Journal of Immunology (Baltimore, Md. : 1950)* **187**, 4151-4160 (2011).

41. Liljedahl, M. *et al.* HLA-DO is a lysosomal resident which requires association with HLA-DM for efficient intracellular transport. *EMBO J* **15**, 4817-4824 (1996).

42. van Lith, M. *et al.* Regulation of MHC Class II Antigen Presentation by Sorting of Recycling HLA-DM/DO and Class II within the Multivesicular Body. *The Journal of Immunology* **167**, 884 (2001).

43. Deshaies, F. *et al.* A point mutation in the groove of HLA-DO allows egress from the endoplasmic reticulum independent of HLA-DM. *Proc Natl Acad Sci U S A* **102**, 6443-6448 (2005).

44. Jiang, W. *et al.* pH-susceptibility of HLA-DO tunes DO/DM ratios to regulate HLA-DM catalytic activity. *Scientific Reports* **5**, 17333 (2015).

45. Pu, Z., Lovitch, S.B., Bikoff, E.K. & Unanue, E.R. T Cells Distinguish MHC-Peptide Complexes Formed in Separate Vesicles and Edited by H2-DM. *Immunity* **20**, 467-476 (2004).

46. Yi, W. *et al.* Targeted regulation of self-peptide presentation prevents type I diabetes in mice without disrupting general immunocompetence. *J Clin Invest* **120**, 1324-1336 (2010).

47. Gu, Y., Jensen, P.E. & Chen, X. Immunodeficiency and Autoimmunity in H2-O–Deficient Mice. *The Journal of Immunology* **190**, 126 (2013).

48. Acha-Orbea, H., Shakhov, A.N. & Finke, D. Immune response to MMTV infection. *Front Biosci*; 2007. pp. 1594-1609.

49. Golovkina, T.V. A Novel Mechanism of Resistance to Mouse Mammary Tumor Virus Infection. *Journal of Virology* **74**, 2752 (2000).

50. Purdy, A. *et al.* Unique Resistance of I/LnJ Mice to a Retrovirus Is Due to Sustained Interferon γ–dependent Production of Virus-neutralizing Antibodies. *Journal of Experimental Medicine* **197**, 233-243 (2003).

51. Case, L.K., Purdy, A. & Golovkina, T.V. Molecular and Cellular Basis of the Retrovirus Resistance in I/LnJ Mice. *The Journal of Immunology* **175**, 7543 (2005).

52. Case, L.K. *et al.* Replication of beta- and gammaretroviruses is restricted in I/LnJ mice via the same genetic mechanism. *Journal of virology* **82**, 1438-1447 (2008).

53. Denzin, L.K. *et al.* Neutralizing Antibody Responses to Viral Infections Are Linked to the Non-classical MHC Class II Gene H2-Ob. *Immunity* **47**, 310-322.e317 (2017).

54. Lek, M. *et al.* Analysis of protein-coding genetic variation in 60,706 humans. *Nature* **536**, 285-291 (2016).

55. Yoon, T. *et al.* Mapping the HLA-DO/HLA-DM complex by FRET and mutagenesis. *Proceedings of the National Academy of Sciences* **109**, 11276 (2012).

56. Sloan, V.S. *et al.* Mediation by HLA-DM of dissociation of peptides from HLA-DR. *Nature* **375**, 802-806 (1995).

57. Denzin, L.K., Robbins, N.F., Carboy-Newcomb, C. & Cresswell, P. Assembly and intracellular transport of HLA-DM and correction of the class II antigen-processing defect in T2 cells. *Immunity* **1**, 595-606 (1994).

58. Khalil, S. *et al.* Class II transactivator-induced expression of HLA-DO(beta) in HeLa cells. *Tissue antigens* **60**, 372-382 (2002).

59. Hammond, C. *et al.* The Tetraspan Protein CD82 Is a Resident of MHC Class II Compartments Where It Associates with HLA-DR, -DM, and -DO Molecules. *The Journal of Immunology* **161**, 3282 (1998).

60. Alfonso, C. & Karlsson, L. Nonclassical MHC Class II Molecules. *Annual Review of Immunology* **18**, 113-142 (2000).

61. Robinson, J. *et al.* The IPD and IMGT/HLA database: allele variant databases. *Nucleic Acids Res* **43**, D423-D431 (2015).

62. Sherry, S.T. *et al.* dbSNP: the NCBI database of genetic variation. *Nucleic Acids Res* **29**, 308-311 (2001).

63. Auton, A. *et al.* A global reference for human genetic variation. *Nature* **526**, 68-74 (2015).

64. Álvaro-Benito, M. *et al.* Distinct editing functions of natural HLA-DM allotypes impact antigen presentation and CD4+ T cell activation. *Cellular & Molecular Immunology* **17**, 133-142 (2018).

65. Schrodinger, LLC. The PyMOL Molecular Graphics System, Version 1.8. 2015.

66. Kropshofer, H. *et al.* A role for HLA-DO as a co-chaperone of HLA-DM in peptide loading of MHC class II molecules. *EMBO J* **17**, 2971-2981 (1998).

67. Deshaies, F. *et al.* A point mutation in the groove of HLA-DO allows egress from the endoplasmic reticulum independent of HLA-DM. *Proc Natl Acad Sci U S A* **102**, 6443-6448 (2005).

68. Denzin, L.K. & Cresswell, P. HLA-DM induces clip dissociation from MHC class II alpha beta dimers and facilitates peptide loading. *Cell* **82**, 155-165 (1995).

69. Yao, Y. *et al.* Association between human leucocyte antigen-DO polymorphisms and interferon/ribavirin treatment response in hepatitis C virus type 1 infection in Chinese population: a prospective study. *BMJ open* **8**, e019406-e019406 (2018).

70. Zhang, X.-L. *et al.* Association of the rs3077 and rs9277535 polymorphisms in HLA-DP with hepatitis B virus infection and spontaneous clearance: A meta-analysis. *Scandinavian Journal of Gastroenterology* **48**, 736-744 (2013).

71. Machiela, M.J. & Chanock, S.J. LDlink: a web-based application for exploring population-specific haplotype structure and linking correlated alleles of possible functional variants. *Bioinformatics* **31**, 3555-3557 (2015).

72. Alvaro-Benito, M., Morrison, E., Wieczorek, M., Sticht, J. & Freund, C. Human leukocyte Antigen-DM polymorphisms in autoimmune diseases. *Open Biol* **6**, 160165 (2016).

73. Álvaro-Benito, M., Wieczorek, M., Sticht, J., Kipar, C. & Freund, C. HLA-DMA Polymorphisms Differentially Affect MHC Class II Peptide Loading. *The Journal of Immunology* **194**, 803 (2015).

74. Duggal, P. *et al.* Genome-wide association study of spontaneous resolution of hepatitis C virus infection: data from multiple cohorts. *Ann Intern Med* **158**, 235-245 (2013).

75. Rehermann, B. & Nascimbeni, M. Immunology of hepatitis B virus and hepatitis C virus infection. *Nature Reviews Immunology* **5**, 215-229 (2005).

76. Waters, J., Pignatelli, M., Galpin, S., Ishihara, K. & Thomas, H.C. Virus-neutralizing Antibodies to Hepatitis B Virus: The Nature of an Immunogenic Epitope on the S Gene Peptide. *Journal of General Virology* **67**, 2467-2473 (1986).

77. Takeda, K., Kaisho, T. & Akira, S. Toll-Like Receptors. *Annual Review of Immunology* **21**, 335-376 (2003).

78. Trombetta, E.S. & Mellman, I. Cell Biology of Antigen Processing in vitro and in vivo. *Annual Review of Immunology* **23**, 975-1028 (2004).

79. Shin, J.-S. *et al.* Surface expression of MHC class II in dendritic cells is controlled by regulated ubiquitination. *Nature* **444**, 115-118 (2006).

80. Dudziak, D. *et al.* Differential Antigen Processing by Dendritic Cell Subsets in Vivo. *Science* **315**, 107 (2007).

81. Kane, M. *et al.* Innate immune sensing of retroviral infection via Toll-like receptor 7 occurs upon viral entry. *Immunity* **35**, 135-145 (2011).

82. Geahlen, R.L. Syk and pTyr'd: Signaling through the B cell antigen receptor. *Biochimica et Biophysica Acta (BBA) - Molecular Cell Research* **1793**, 1115-1127 (2009).

83. Draghi, N.A. & Denzin, L.K. H2-O, a MHC class II-like protein, sets a threshold for B-cell entry into germinal centers. *Proceedings of the National Academy of Sciences* **107**, 16607-16612 (2010).

84. Shih, T.-A.Y., Roederer, M. & Nussenzweig, M.C. Role of antigen receptor affinity in T cell–independent antibody responses in vivo. *Nat Immunol* **3**, 399-406 (2002).

85. Victora, G.D. *et al.* Germinal center dynamics revealed by multiphoton microscopy with a photoactivatable fluorescent reporter. *Cell* **143**, 592-605 (2010).

86. Victora, G.D. & Nussenzweig, M.C. Germinal Centers. *Annual Review of Immunology* **30**, 429-457 (2012).

87. Allen, C.D.C., Okada, T. & Cyster, J.G. Germinal-center organization and cellular dynamics. *Immunity* **27**, 190-202 (2007).

88. Kane, M. *et al.* Successful transmission of a retrovirus depends on the commensal microbiota. *Science (New York, N.Y.)* **334**, 245-249 (2011).

89. Tellier, J. & Nutt, S.L. Standing out from the crowd: How to identify plasma cells. *European Journal of Immunology* **47**, 1276-1279 (2017).

90. Ardavín, C. *et al.* B Cell Response After MMTV Infection: Extrafollicular Plasmablasts Represent the Main Infected Population and Can Transmit Viral Infection. *The Journal of Immunology* **162**, 2538 (1999).

91. Jung, C., Hugot, J.-P. & Barreau, F. Peyer's Patches: The Immune Sensors of the Intestine. *Int J Inflam* **2010**, 823710-823710 (2010).

92. Kobayashi, N., Takahashi, D., Takano, S., Kimura, S. & Hase, K. The Roles of Peyer's Patches and Microfold Cells in the Gut Immune System: Relevance to Autoimmune Diseases. *Front Immunol* **10**, 2345 (2019).

93. Gullberg, E. & SÖDerholm, J.D. Peyer's Patches and M Cells as Potential Sites of the Inflammatory Onset in Crohn's Disease. *Annals of the New York Academy of Sciences* **1072**, 218-232 (2006).

94. Monack, D.M. *et al.* Salmonella exploits caspase-1 to colonize Peyer's patches in a murine typhoid model. *J Exp Med* **192**, 249-258 (2000).

95. Ishii, H. *et al.* Peyer's Patches in the Terminal Ileum in Ulcerative Colitis: Magnifying Endoscopic Findings. *J Clin Biochem Nutr* **46**, 111-118 (2010).

96. Karapetian, O., Shakhov, A.N., Kraehenbuhl, J.P. & Acha-Orbea, H. Retroviral infection of neonatal Peyer's patch lymphocytes: the mouse mammary tumor virus model. *J Exp Med* **180**, 1511-1516 (1994).

97. Golovkina, T.V., Dudley, J.P. & Ross, S.R. B and T Cells Are Required for Mouse Mammary Tumor Virus Spread Within the Mammary Gland. *The Journal of Immunology* **161**, 2375 (1998).

98. Victora, G.D. Clonal and Cellular Dynamics in Germinal Centers. *Gene Expression and Signaling in the Immune System*. Cold Spring Harbor Laboratory; 2020.

99. Miles, B. & Connick, E. Control of the Germinal Center by Follicular Regulatory T Cells During Infection. *Front Immunol* **9**, 2704-2704 (2018).

100. Daft, J.G., Ptacek, T., Kumar, R., Morrow, C. & Lorenz, R.G. Cross-fostering immediately after birth induces a permanent microbiota shift that is shaped by the nursing mother. *Microbiome* **3**, 17 (2015).

101. Cullum, E. *et al.* Genetic Control of Neonatal Immune Tolerance to an Exogenous Retrovirus. *Journal of Virology* **94**, e01608-01620 (2020).

102. Mohan, J.F., Petzold, S.J. & Unanue, E.R. Register shifting of an insulin peptide-MHC complex allows diabetogenic T cells to escape thymic deletion. *J Exp Med* **208**, 2375-2383 (2011).

103. Liljedahl, M. *et al.* Altered Antigen Presentation in Mice Lacking H2-O. *Immunity* **8**, 233-243 (1998).

104. Miyazaki, T. *et al.* Mice Lacking H2-M Complexes, Enigmatic Elements of the MHC Class II Peptide-Loading Pathway. *Cell* **84**, 531-541 (1996).